Final Report – November 2005

Early Sinkhole Detection and Verification Using Airborne Laser and Infrared Technologies

BC-354-54

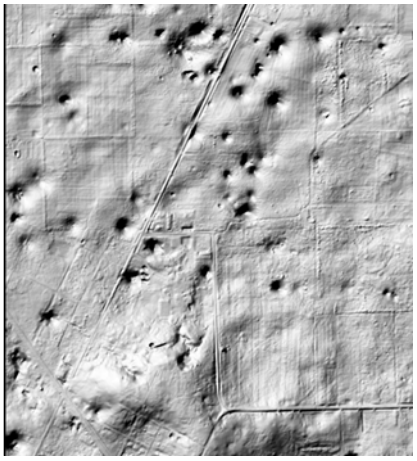

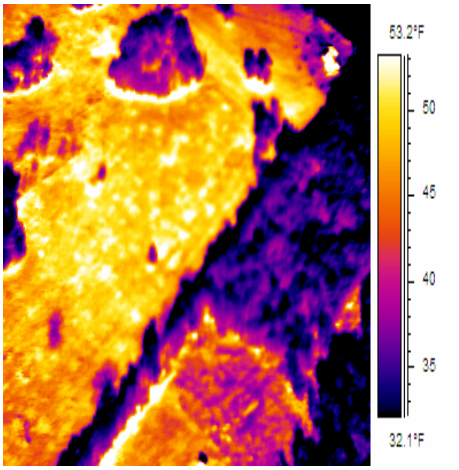

Submitted to:

Peter W. Lai, P.E.
Assistant State Geotechnical Engineer
Department of Transportation
605 Suwannee Street, MS 33
Tallahassee, FL 32399-0450

Submitted by:

David Bloomquist, P.E.
Ramesh L. Shrestha
Clinton Slatton
Department of Civil & Coastal Engineering
365 Weil Hall, P.O. Box 116580
University of Florida, Gainesville, FL 32611

Disclaimer

The opinions, findings, and conclusions expressed in this publication are those of the author and not necessarily those of the State of Florida Department of Transportation."

SI (MODERN METRIC) CONVERSION FACTORS (from FHWA)

APPROXIMATE CONVERSIONS TO SI UNITS

SYMBOL	WHEN YOU KNOW	MULTIPLY BY	TO FIND	SYMBOL
LENGTH				
in	inches	25.4	millimeters	mm
ft	feet	0.305	meters	m
yd	yards	0.914	meters	m
mi	miles	1.61	kilometers	km

SYMBOL	WHEN YOU KNOW	MULTIPLY BY	TO FIND	SYMBOL
AREA				
in^2	square inches	645.2	square millimeters	mm^2
ft^2	square feet	0.093	square meters	m^2
yd^2	square yard	0.836	square meters	m^2
ac	acres	0.405	hectares	ha
mi^2	square miles	2.59	square kilometers	km^2

SYMBOL	WHEN YOU KNOW	MULTIPLY BY	TO FIND	SYMBOL
VOLUME				
fl oz	fluid ounces	29.57	milliliters	mL
gal	gallons	3.785	liters	L
ft^3	cubic feet	0.028	cubic meters	m^3
yd^3	cubic yards	0.765	cubic meters	m^3
NOTE: volumes greater than 1000 L shall be shown in m^3				

SYMBOL	WHEN YOU KNOW	MULTIPLY BY	TO FIND	SYMBOL
MASS				
oz	ounces	28.35	grams	g
lb	pounds	0.454	kilograms	kg
T	short tons (2000 lb)	0.907	megagrams (or "metric ton")	Mg (or "t")

SYMBOL	WHEN YOU KNOW	MULTIPLY BY	TO FIND	SYMBOL
TEMPERATURE (exact degrees)				
^oF	Fahrenheit	5 (F-32)/9 or (F-32)/1.8	Celsius	^oC

SYMBOL	WHEN YOU KNOW	MULTIPLY BY	TO FIND	SYMBOL
ILLUMINATION				
fc	foot-candles	10.76	lux	lx
fl	foot-Lamberts	3.426	candela/m^2	cd/m^2

SYMBOL	WHEN YOU KNOW	MULTIPLY BY	TO FIND	SYMBOL
FORCE and PRESSURE or STRESS				
lbf	pound force	4.45	newtons	N
lbf/in^2	pound force per square inch	6.89	kilopascals	kPa

APPROXIMATE CONVERSIONS TO SI UNITS

SYMBOL	WHEN YOU KNOW	MULTIPLY BY	TO FIND	SYMBOL
		LENGTH		
mm	millimeters	0.039	inches	in
m	meters	3.28	feet	ft
m	meters	1.09	yards	yd
km	kilometers	0.621	miles	mi

SYMBOL	WHEN YOU KNOW	MULTIPLY BY	TO FIND	SYMBOL
		AREA		
mm^2	square millimeters	0.0016	square inches	in^2
m^2	square meters	10.764	square feet	ft^2
m^2	square meters	1.195	square yards	yd^2
ha	hectares	2.47	acres	ac
km^2	square kilometers	0.386	square miles	mi^2

SYMBOL	WHEN YOU KNOW	MULTIPLY BY	TO FIND	SYMBOL
		VOLUME		
mL	milliliters	0.034	fluid ounces	fl oz
L	liters	0.264	gallons	gal
m^3	cubic meters	35.314	cubic feet	ft^3
m^3	cubic meters	1.307	cubic yards	yd^3

SYMBOL	WHEN YOU KNOW	MULTIPLY BY	TO FIND	SYMBOL
		MASS		
g	grams	0.035	ounces	oz
kg	kilograms	2.202	pounds	lb
Mg (or "t")	megagrams (or "metric ton")	1.103	short tons (2000 lb)	T

SYMBOL	WHEN YOU KNOW	MULTIPLY BY	TO FIND	SYMBOL
		TEMPERATURE (exact degrees)		
^oC	Celsius	1.8C+32	Fahrenheit	^oF

SYMBOL	WHEN YOU KNOW	MULTIPLY BY	TO FIND	SYMBOL
		ILLUMINATION		
lx	lux	0.0929	foot-candles	fc
cd/m^2	candela/m^2	0.2919	foot-Lamberts	fl

SYMBOL	WHEN YOU KNOW	MULTIPLY BY	TO FIND	SYMBOL
		FORCE and PRESSURE or STRESS		
N	newtons	0.225	pound force	lbf
kPa	kilopascals	0.145	pound force per square inch	lbf/in^2

*SI is the symbol for the International System of Units. Appropriate rounding should be made to comply with Section 4 of ASTM E380.
(Revised March 2003)

Technical Report Documentation Page

<table>
<tr><td colspan="2">1. Report No.</td><td colspan="2">2. Government Accession No.</td><td colspan="2">3. Recipient's Catalog No.</td></tr>
<tr><td colspan="4" rowspan="2">4. Title and Subtitle

Early Sinkhole Detection and Verification
Using Airborne Laser and Infrared Technology</td><td colspan="2">5. Report Date
November 2005</td></tr>
<tr><td colspan="2">6. Performing Organization Code</td></tr>
<tr><td colspan="4">7. Author(s)
David Bloomquist, Ramesh Shrestha, Clinton Slatton, Michael Sartori, Jeff Brown, M.. Starek, Brian. Luzum</td><td colspan="2">8. Performing Organization Report No.</td></tr>
<tr><td colspan="4" rowspan="2">9. Performing Organization Name and Address
Department of Civil and Coastal Engineering
365 Weil Hall
University of Florida
Gainesville, Florida 32611</td><td colspan="2">10. Work Unit No. (TRAIS)</td></tr>
<tr><td colspan="2">11. Contract or Grant No.
BC 354 RPN05</td></tr>
<tr><td colspan="4" rowspan="2">12. Sponsoring Agency Name and Address
Florida Department of Transportation
605 Suwannee Street, MS 30
Tallahassee, FL 32399</td><td colspan="2">13. Type of Report and Period Covered
Final Report
8/2003 – 10/2005</td></tr>
<tr><td colspan="2">14. Sponsoring Agency Code</td></tr>
<tr><td colspan="6">15. Supplementary Notes</td></tr>
<tr><td colspan="6">16. Abstract</td></tr>
<tr><td colspan="3">17. Key Word
Laser, LIDAR, IR, Sinkhole</td><td colspan="3">18. Distribution Statement
No restrictions.</td></tr>
<tr><td>19. Security Classif. (of this report)
Unclassified.</td><td colspan="2">20. Security Classif. (of this page)
Unclassified.</td><td>21. No. of Pages
114</td><td colspan="2">22. Price</td></tr>
</table>

Executive Summary

Objectives

The major objectives of this research include:

A. To utilize airborne laser technology (ASLM) in an attempt to identify potential sinkhole activity. This includes conducting multiple overflights, extensive data processing and analysis. The rationale was that these temporal over-flights of suspect areas, would allow engineers to observe if quantitative topographical changes had occurred over time.

B. Conduct preliminary tests using an aerial Infrared Camera system to locate surficial anomalies that could then be interpreted as potential sinkholes. The underlying concept is that the moisture content of soil varies as a function of its geomorphology. Hence, it may be possible to identify dissimilar soils via surface temperatures resulting from the relative amounts of entrapped water.

Findings and Conclusions

Based on the research the following conclusions can be made:

1. While it is indeed possible to create a DEM (digital terrain model) of sinkhole prone areas, the necessary resolution and accuracy provided by airborne LIDAR does not lend itself to monitoring small vertical/lateral displacements over time. The plethora of input parameters required to compare successive DEMs and draw statistically valid conclusions about differences, induces excessive variability. This comparison difficulty is compounded by the presence of dense, near-surface vegetation (e.g., thick grasses), which prevents laser pulses from reaching the actual ground surface. Thus, observed differences could manifest themselves solely through changes in vegetation and conceal actual ground subsidence, if indeed, present.

2. The most important and positive aspects of this research clearly shows that ALSM can identify suspect areas that merit future investigation. This has clearly been documented in this research report. Thus, as newer software and faster ALSM pulse rate systems become available, it is probable that this technology will prove beneficial in actual monitoring ground movements.

3. The use of airborne IR (infrared) thermography to characterize subsurface activity through surface expression was another very beneficial attribute of the research. Since IR thermography is only capable of monitoring the surface temperature of an object, the technique is usually limited to situations where defects are located near the surface. As defect depth increases and defect size decreases, assessment becomes more difficult. Fortunately, the near surface moisture retained in fine-grained soils, meets this requirement. In addition, capillary action in silt size material signifies that the IR technique indeed can be used to penetrate deeper into the surface. Several attempts to utilize this technology were made by over flying an area (void of recent rains) and then identify zones of different types soils simply by their thermal signatures. If there is a supply of subsurface water/moisture, capillary rise would maintain a constant migration of water upwards thereby indirectly indicating subsurface conditions. This technology showed substantial promise and more work is currently in progress to perfect the technique.

Benefits

The benefits of utilizing airborne based devices to investigate potential sinkhole activity is very high. If suspect areas are identified prior to their impacting Florida's infrastructure (highways in particular) proactive remediation is the most cost effective option. This research has clearly shown that ALSM and IR technologies have the potential to locate suspect areas. However, they are not sensitive enough to monitor long-term changes. Nevertheless, based on this research, additional aerial surveys have been conducted for FDOT and more are planned in the future.

TABLE OF CONTENTS **Page**

CHAPTER 1. PROBLEM STATEMENT AND OVERVIEW OF PROJECT

Background

Sinkholes are a common, naturally occurring geologic feature and a predominant landform of Florida. The subsurface is noted for a predilection to the formation of sinkholes due to its karst (limestone) topography. Chemical dissolution and mechanical erosion of these thick carbonate deposits by groundwater movement as well as large fluctuations in phreatic surfaces induce geostatic stresses that frequently exceed the soil's structural resistance.

The peninsula has experienced thousands of sinkholes over the years and the majority appears to concentrate in the central Florida area. Here, the overlying insoluble siliciclastic sediments (sands and clays) are relatively thin (0 to 30 feet thick) and coupled with rain exacerbates the dissolution and weathering process.

Another factor that contributes to sinkhole formation is large fluctuations in rainfall amounts. First, periods of drought can significantly increase the propensity for development. This is due to an excessive removal (pumping) of groundwater, which in turn increases the effective overburden pressures as the water table is lowered. However, even more crucial are conditions in which prolonged droughts are followed by wetter than normal climatological periods. Here, the additional weight of the excess surficial water (temporarily perched) creates higher vertical pressures which when transmitted to the underlying limestone can induce downward raveling of the material. Since it is appears that the current drought (on-going for 3+ years) has begun to abate, it is problematic that we will likely observed substantial sinkhole activity during the next 24 months.

There are three primary types of sinkholes and each has its own distinct characteristics. The ones that garner the most publicity are the cover collapse type, since a hole (some of which can be quite large) appears very suddenly. However, cover-subsidence sinkholes are of particular interest due in part to their gradual developmental process. These typically occur where sand overlies the limestone and once a solutional opening in the karst surface appears, it allows the sand and clay above to slowly migrate into it. These are quite common in the State and hence frequent monitoring of a particular region and or highway corridor over time can be extremely

valuable, since disruption of traffic is costly - both time wise and fiscally. Thus, the focus of this research was to determine if an airborne laser system is sensitive and accurate enough to observe temporal topographic surficial changes. This would allow FDOT to proactively mitigate impending damage. However, dependant on the results of the laser in terms of quantitative assessment, a novel use of infrared technology was also examined on a cursory basis.

Project and System Overview

UF's $1.3 million laser system is installed in a Cessna 337 in-line twin aircraft. The laser pulses are directed through an access hole in the bottom of the fuselage. A photograph of the interior of the aircraft and system is shown below.

Figure 1-1. Cessna 337 with laser equipment installed.

As the aircraft flies over the designated target area, the operator turns on the pulse generator, emitting 33,000 laser pulses per second towards the ground surface in an oscillating saw tooth pattern. The pattern geometry varies, based primarily on the altitude and ground speed of the aircraft during the data collection.

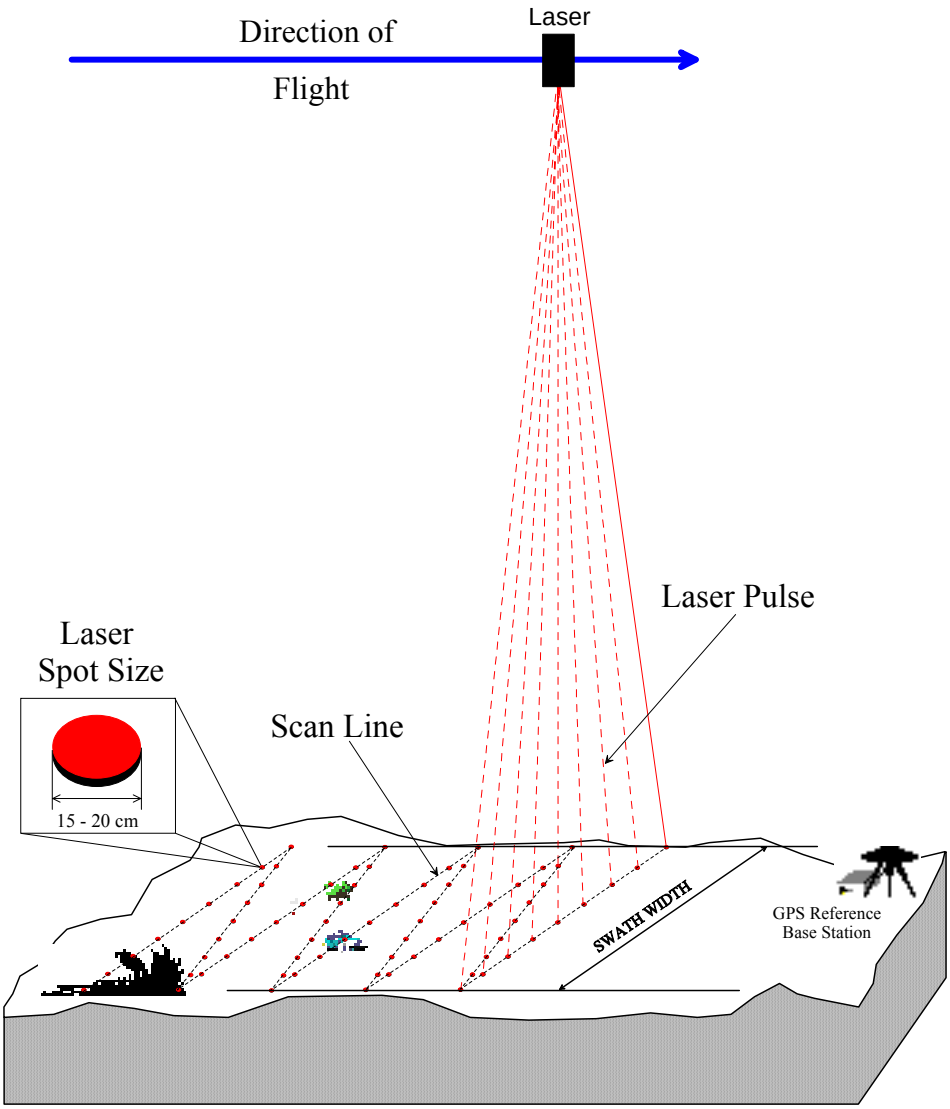

Figure 1-2. Saw tooth shaped laser pulse pattern

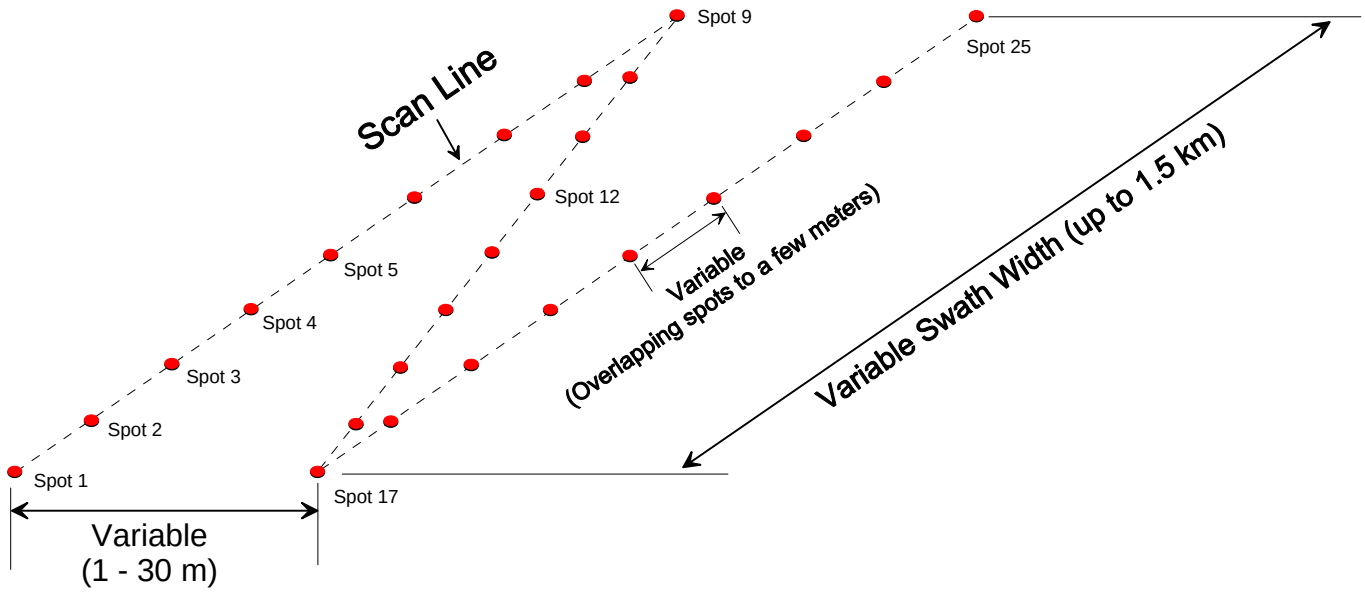

Figure 1-3. The spot locations are dependant on the aircraft speed and altitude.

In order to maintain the highest accuracy of the point locations, a ground GPS station is set up in the vicinity of the site (typically within 40 km) and simultaneously collects GPS satellite data while positioned over an identifiable location (a surveying benchmark, for example). This information is then used to "correct" the GPS data that the aircraft also acquires during the flight. This data is then processed using various computer programs. It bears mentioning that typically for each hour of data collection (laser on time), 40 hours of processing is required. Hence while a large amount of data can be collected very rapidly (2 million points per minute), it lengthens the final product delivery time.

The research consisted of overflights at several locations to see if changes in topography were evident. The time lapse between flights varied from 6 months to 8 months. Hence, the primary objective was to evaluate ALSM technology in terms of identifying potential sinkholes. A complimentary task (not included in the original scope) was to attempt to utilize infrared photography to distinguish soil type (primarily as a function of moisture content), thereby identifying suspect or problematic areas for further study.

Flight Operations

Since it is extremely costly for sinkhole damage remediation – especially when they occur along Florida's major roadway corridors, advanced warning of subtle changes in topography is particularly useful in planning proactive corrective actions. Hence, the project's scope was to fly along the aforementioned corridors using UF's Airborne Laser System and collect topographical data. Three series of over flights were conducted and the data processed. These data serve as a baseline from which subsequent data collect flights were compared. Several sites identified by FDOT engineers are in Osceola and Alachua Counties and include:

- I-75 beginning at SW 38th Ct. and ending at SSR 484.
- W. Maitland starting at HW 441 and ending at SR 434.
- HW 27 starting at CR S 634 A and ending at Country Club Rd.

In addition, a site in High Springs Florida (Alachua County) was identified as a prime target due to the numerous depressions located in the area. Each site consists of 10 miles in length and a swath width of approximately 1200 feet. This width ensures that the shoulders and right of way are included in the data collection. All of the above areas were mapped using two passes to obtain closely spaced laser data points.

Processing of ALSM Data

While Chapter 2 delves into the pre and post processing procedures in more detail, it would be of reader interest to provide an overview of the processes.

The raw data set collected by the ALSM laser is in the form of a text document containing the millions of x-y-z coordinates from all returned laser pulses. Typically over 90% of the transmitted pulses return to the aircraft and include each and every surface that can reflect the pulses. For this reason, clouds, birds, trees, buildings, etc. are typically contained within the data files, thereby complicating the processing. (Note of interest: very still water – i.e., no ripples, does not return pulses since they reflect off the water surface at various incident angles and hence do not return to the photo diode collectors in the aircraft.).

The first step in data processing involves the accurate determination of the aircraft's flight trajectory. Unfortunately GPS alone, even with ground GPS correction, is insufficient, since the airplane also continuously rotates (to varying degrees) about its' three orthogonal axes - pitch, yaw and roll. As this motion occurs, each laser point then exits the aircraft in a direction distinct from what the aircraft's on board computer assumes is the actual flight path. Fortunately included in the laser equipment is an IMU (inertial measurement unit), which contains three sensitive accelerometers. By continuously recording the readouts of each, a double integration can generate angular displacements of the aircraft and ultimately its' three dimensional orientation. This data is then reconciled with the GPS information providing the data processor with accurate point trajectories (i.e., the distance the pulse traveled and its location on the surface.

The next processing effort involves using ***Surfer 8***, an analysis program, to view the data simply as a shaded relief map that uses each of the laser pulses' GIS coordinates. As mentioned above, this data is considered unfiltered, signifying that all vegetation and man-made features are contained in the file and hence are depicted in the shaded relief map. Because of this "noise", it is difficult to identify salient topographical features and track their spatial characteristics over time. Due to the program's inability to distinguish between the natural ground surface and all of the aboveground features, the data is then subjected to a tedious filtering process, which attempts to remove the noise. This filtered data can then be viewed again as a shaded relief map or to produce more useful products, e.g., a bare earth contour map and 3D topographic map. The bare earth map is also referred to as a Digital Elevation Model or DEM. A Digital Elevation Model consists of a sampled array of elevations for ground positions (laser points) that are normally spaced at regular intervals.

Once the data is in its final format, the DEM can be examined manually to search for low-lying circular depressions that may be possible sinkholes. Of course, this is a very subjective process, but when subsequent data sets are obtained, the software is capable of determining elevation differences. In addition, the volume of the depressions can be calculated using one of ***Surfer8's*** software application modules. In order to confirm or dismiss the evidence of a sinkhole, subsequent flights over the areas in question were be conducted on a regular basis to collect time-dependent data. This data will be subjected to the same filtering process and the suspected

sinkholes' volume and spatial geometry measured to determine if any reasonable differences have occurred.

While not a part of the scope of work, once a possible sinkhole is identified, a more accurate scan could be employed. This can be performed using an ILRIS laser scanner. This device (similar to but without the GPS/IMU features of the airborne system) can provide a more accurate DEM and hence dimensions of the depression. (For example, for a single laser point, the airborne accuracy of its location is 3-6 inches vertical and 6-8 inches horizontal, while the land laser is 0.2-0.5 inches vertical and horizontal respectively). By setting up the land laser at various points around the target, the data sets can then used to create a 3D image of the area of interest. Each of the data sets images must first be aligned or merged together using Polyworks™ software and a module ***IMAlign*** that utilizes common features visible in the various scans. For example a distinct part of a tree limb or stake placed in the ground by the laser operator. These merged images can then be processed through another Polyworks™ program called ***IMMerge*** that uses the millions of data points and creates a three dimensional surface. Finally, this 3D model can then be manipulated in Polyworks™ ***IMEdit*** program to compute geometric changes if they do occur. This process is expanded upon in Chapter 3.

The following chapters provides the reader with details on the data collection and processing requirements of ALSM, ILRIS and IR data.

Chapter 2. BASIC ALSM DATA COLLECTION

Introduction

ALSM data collection consists of four basic components: mission planning, setup of GPS base stations, onboard setup and monitoring of IMU and GPS, data retrieval and format.

Mission Planning

During mission planning, client requirements are determined and a flight plan is developed. From client requirements, the boundaries of the survey area are delineated and the spatial resolution is determined. Calculations are performed to determine flight and onboard setup parameters to obtain the desired resolution.

To develop a viable flight window, the number of available GPS constellations, PDOP levels, and weather are analyzed. At a minimum, 6 GPS satellites must be within range for a viable flight window; however, the target range is 9 or more satellites. The target level for Precision Dilution of Position (PDOP) is 3 or less, but levels in the range of 3 to 4 can be functional. The flight window is selected based upon the time range availability for GPS satellites and functional PDOP levels. Additional components of mission planning include an initial site visit and topography review, personnel requirements, and weather considerations. When the window is open and weather permitting, "you fly." Refer to chapter 7.0, "Survey Planning," in the ALTM Training Manual for an in-depth review of mission planning and utilization of GPS software for determination of flight windows .

GPS Base Station Receivers and Setup

Receivers:

Ashtech Z-12 (company renamed Thales)

5mb and 10mb of built-in memory

Onboard GPS = 10mb

*Note: 10mb of plane memory will fill up in about 6 hours.

Micro Z-Extreme

20mb flash cards

The receivers log both L1 and L2 frequencies. All receivers log at 1-second intervals, both the plane and ground station receivers and operate in conjunction with choke ring antennas.

Operating Procedures:

At a minimum, two GPS base stations should be running on the ground within the project site or as close to the project area as possible. Dependent upon project size, three or more receivers may be necessary to cover the range of the survey area. Offsets (instrumental height) must be computed from ground control point to static ground GPS antenna, and a minimum of 3-hours should be logged on static base stations to get good positions. In addition, the offset from the sensor head to the aircraft GPS antenna must be determined. Furthermore, at some point during the survey, ground truthing is performed within the project area to obtain accurate, hard surface coordinates of the ground for accuracy assessment of the laser data. Careful survey planning is crucial to the success of data collection flights.

Onboard Setup and Flight

Onboard Components:

The laser system calculates in real-time, and the GPS system interfaces directly with the laser computer system. The IMU consists of 3 gyros and accelerometers and cycles at ~ 50hz. The standard setup for the scanning mirror is 28hz at 20° half-angle. The laser pulse frequency is calibrated at 33khz and cannot be changed.

Flight Plan:

The Optech ALTM NAV software is utilized for planning and plane navigation and is monitored on the laptop. The pilot follows the flight plans that are setup with the software, and 50% overlap is flown between flight paths to correct for the poor data that occurs at the edges of the scan. The laser is turned on and off before and after each flight line.

Flight Protocol:

Standard flight altitude is 600m with a speed of 110 knots for a 1-meter ground resolution cell. Scans should not be performed when flying through clouds, and the max-angle for recording of

water is 8 to 10 degrees due to reflectance problems at more extreme angles. The plane is flown at least once over the base station/s to allow initialization of the kinematic solution, and it is flown perpendicular to the flight paths to allow scale calibration for each flight and to check swath-to-swath vertical agreement. Additionally, 3 to 5 minutes of level flight are recorded before and after the survey to stabilize the IMU and simplify processing.

Data Retrieval

The onboard hard drive utilized with the laser system records IMU and laser data. The hard drive is removable and allows downloading of the laser data. The RAW format of the laser data is an Optech proprietary format. Once the survey is completed, the following data sets are retrieved: laser data from the hard drive, base station GPS data, and onboard GPS data. The data is then processed and a 9-column output format is obtained:

[time stamp, x2, y2, z2, last return intensity, x1, y1, z1, first return intensity]

where the xyz-values are in UTM coordinates. The processed data can then be further processed and refined to generate project deliverables such as bare earth digital elevation models (DEMs). *Note: 9-column output is the traditional data form; however, a paradigm shift is manifesting which will provide an alternative processing output format.

Chapter 3. ALSM POST FLIGHT DATA PROCESSING

Introduction

During a survey the following data sets are collected: multiple base station GPS data, onboard GPS data, laser and IMU data. After the data sets are retrieved from the GPS units and the laser system, ALSM data processing is conducted. ALSM processing consists of the following basic steps:

1. Process the plane navigation data relative to multiple base station references
2. Combine the navigation data with the IMU data and process
3. Combine the navigation-IMU data with the laser data and process to output format
4. Post process to create project deliverables (e.g. DEM)

Processing of Navigation Data

The initial step in processing ALSM observations is to compute points along the trajectory of the aircraft using phase-differenced kinematic techniques to determine the aircrafts position during the survey [2]. First, a reference coordinate is processed for the ground station/s relative to a control reference. The desired reference control is something local from the region. Published coordinates are normally not utilized. Rather, the project GPS receivers are generally processed to the CORS reference stations, often 50-200km distant, utilizing NOAA's on-line processor, OPUS.

CORS and OPUS

The National Geodetic Survey (NGS), an office of NOAA, coordinates a network of Continuously Operating Reference Stations (CORS) that provide GPS carrier phase and code range measurements in support of three-dimensional positioning activities throughout the US and its territories. CORS data can be applied to position points where GPS data have been collected enabling positioning accuracies that approach a few centimeters relative to the National Spatial Reference System, both horizontally and vertically [5].

The On-line Positioning User Service (OPUS) is an on-line processing system developed by NGS and NOAA that allows users to upload their GPS data files via the Internet to NGS, where the data is processed to determine a position using NGS computers and software. Each data file

that is submitted is processed with respect to 3 CORS sites that are selected based upon distance from the station, number of observations, site stability, and other criteria. OPUS is an automatic system and requires the following information from the user [6]:

- The email address where you want the results sent
- The data file that you want to process
- The antenna type used to collect this data file (selected from a list of calibrated GPS antennas)
- The height of the Antenna Reference Point (ARP) above the monument or mark that you are positioning
- As an option, you may also enter the state plane coordinate code if you want SPC northing and easting.
- As an option, up to 3 base stations may be selected for use in determining your solution.

The data file to be processed is uploaded to OPUS in RINEX format. Multiple files may be submitted in a zip archive, but your selected options will be applied to all of the files in the archive. OPUS will only process dual-frequency, carrier-phase data (L1 & L2). Only data from a dual-frequency receiver may be submitted. Single frequency data (L1 only) will not be processed. The data must have been collected from a stationary receiver and for a minimum of 2 hours [6].

After the data file is uploaded, OPUS will process it and provide a solution file for the position of your receiver via email in both ITRF and NAD83 coordinates as well as UTM, USNG and State Plane Coordinates (SPC) northing and easting [6]. The NAVD88 (GEOID99) datum is probably utilized most often, and occasionally, the NAD83 datum is utilized where the vertical datum is ellipsoid height based upon the NAD83 ellipsoid, WGS84 (i.e. GRS80). However, the datums utilized vary and are dependent on the project.

Aircraft Trajectory

After a reference coordinate has been determined, the precise plane trajectory is computed by processing the onboard kinematic (moving) GPS data relative to the static base station's reference coordinate using the *KARS* program developed by Dr. Gerry Mader of NOAA [4]. One should try and utilize the precise orbits for the GPS satellites for processing of the trajectory

solution rather than the broadcast orbit, which is a predicted orbit. Agencies that provide precise orbit values for the GPS satellites include JPL and the Naval Observatory.

For each reference base station, the trajectory of the plane is processed relative to that station to perform QA/QC analysis of the trajectory. The trajectories relative to each base station are differenced and compared to determine if essentially the same trajectories were computed. Large differences between the trajectories indicate a potential problem and/or error in the processing and corrections must be implemented.

Error targets are in the range of less than 1 to 2 cm horizontally and 2 to 3 cm vertically on a second by second basis. Generally, one strives for 90% of differenced values to be less than + or – 5 cm vertically and + or – 2 cm horizontally. If the ranges are within acceptable limits and one is confident in the quality of the trajectories, a trajectory for the plane can then be selected. Usually the trajectory relative to the base station with the minimum baseline to the aircraft is selected; however, the selected trajectory can change dependent upon survey characteristics and changes in the current region of interest.

Essentially, the entire processing sequence for determining the plane trajectory is computed utilizing NOAA software. The CORS network and the OPUS system are used to process reference coordinates for each static base station, and the *KARS* program is utilized to process the kinematic GPS solution relative to each static base station's reference coordinate.

Processing of IMU Data

After determining a high-confidence trajectory, the next phase in ALSM processing is to combine the trajectory data with the IMU data utilizing the Applanix *POSProc* tools to determine the position and orientation of the sensor.

Description of POSProc

POSProc stands for Position and Orientation System post-PROCessing. It comprises a set of software tools that interact together to compute an optimally blended navigation solution of the planes trajectory from inertial data and aiding sensor data . The inertial data comes from the

ALSM onboard IMU system and the onboard firmware designed by Optech. The aiding sensor data for this discussion refers to the GPS trajectory solution from section 2.0 above.

The *POSProc* system architecture consists of an integrated inertial navigation module (*iin*) and a smoother module (*smth*) that work symbiotically to produce a Best Estimate of Trajectory. The most widely used *iin* configuration is a closed-loop aided inertial navigation architecture that consists of a feedback error controller, strapdown navigator, and Kalman filter. The Kalman filter processes measurements that match the strapdown navigation solution with the aiding sensor data to obtain estimates of the significant errors in the navigation instruments .

Typical error characteristics of the inertial navigator are Schuller oscillations and a position error that grows linearly with time, compared to the GPS receiver with error characteristics indicative of broadband noise. The low frequency error of the IMU data and the broadband errors of the aiding sensor GPS data are complementary. The Kalman filter uses the complementary nature of these error characteristics to calibrate the inertial errors and aiding sensor errors against each other .

iin computes an optimally accurate navigation solution at each time point based on the information provided for all past and current input data. The closed-loop error control algorithm utilizes the estimated errors generated by the Kalman filter to control the errors internal to the strapdown navigator so that the strapdown navigator output is the blended navigation solution. The inertial navigator is continuously aligned and its position and velocity errors are regulated to impose consistency with the accuracies of the aiding sensor data .

The smoother module (*smth*) is a recursive modified Bryson-Frazier smoother that operates on the Kalman filter data generated by *iin* and calculates smoothed navigation error estimates that are more accurate than the navigation error estimates computed by *iin*. The smoother then uses the smoothed error estimates to correct the strapdown navigation solution from the *iin* to which the Kalman filter's estimated errors apply thereby generating the Best Estimate of Trajectory (BET) for the given suite of navigation sensors. This is the most accurate navigation solution obtainable from the processed IMU and aiding GPS trajectory data .

It is important to note that there are several *POSProc* processing configurations other than the closed-loop error control configuration that can be implemented dependent upon processing requirements including the feedforward error control configuration and the free-inertial INS configuration. For an in depth review on *POSProc* architecture and configuration setups refer to the *POSProc* User Manual .

Processing with POSProc

In order to combine the trajectory data with the IMU data in *POSProc,* the trajectory data must be reformatted into an Applanix binary format. Each trajectory record is formatted to an 80-byte record based on C-language language data types. Each IMU record can be formatted to either a 32-byte integer type record or a 56-byte floating-point type record, both of which are based on C-language data types.

After the data is properly formatted, the files are input into *POSProc* for processing. The generated output is a 50hz position and orientation "sbet" file containing the blended navigation solution for the trajectory based on the IMU and aiding sensor data.

Validating the Navigation Solution

POSProc essentially acts as a black box processor where the user provides the IMU and GPS differential specifications and the software outputs a solution. *POSProc* provides tools to analyze errors generated during the Kalman filtering process. These tools allow one to validate results and compare differences in output dependent upon the Kalman filter mode selected. When the "sbet" file is validated and determined acceptable, the processing of the aircraft navigation is completed.

Processing of Navigation Solution and Laser Data

After processing of the navigation and IMU data is completed and a high-confidence position and orientation solution for the sensor is determined, the final step is to combine and process the navigation solution and laser data with *REALM* to determine the ground position of each laser range measurement. *REALM* is the main laser-processing software developed by Optech. The "sbet" file containing the navigation solution is imported into *REALM* along with the laser range-file. The laser range-file contains the scanner mirror angles, laser ranges, and time stamps. The

range-file is downloaded from the onboard removable hard drive and imported directly into the *REALM* software.

Description of REALM

REALM (Results of Airborne Laser Mapping) is a modular survey software suite for processing of the raw laser data derived from the Optech ALTM sensor. *REALM* was designed to work with the complete range of ALTM systems, and it enables one to download, convert, and manipulate airborne laser data. The processed data files can then be brought into an "off-the-shelf" visualization package for graphic representation and product output .

REALM produces three-dimensional point data acquired by the ALTM. These are processed from various inputs including: laser ranges, intensity values, scan angles, differential GPS data, inertial navigation data, and system calibration data. Classification and output algorithms allow for the controlled output of the 3D point data into different types including ground or vegetation only, time sequential, flight line, comprehensive format output, patches (input for DEM generation), buildings (3D city modeling), and power lines .

REALM provides a graphical user interface to interact with different tool components of the software (e.g. Geodetic tools, GPS tools, INS tools, ALS tools). The modular structure ensures that the various tools are connected to each other providing controlled process flow. Figure 3-1 below displays the basic processing steps of *REALM*. Figure 3-2 on the following page displays the processing flow among the various modules in *REALM* .

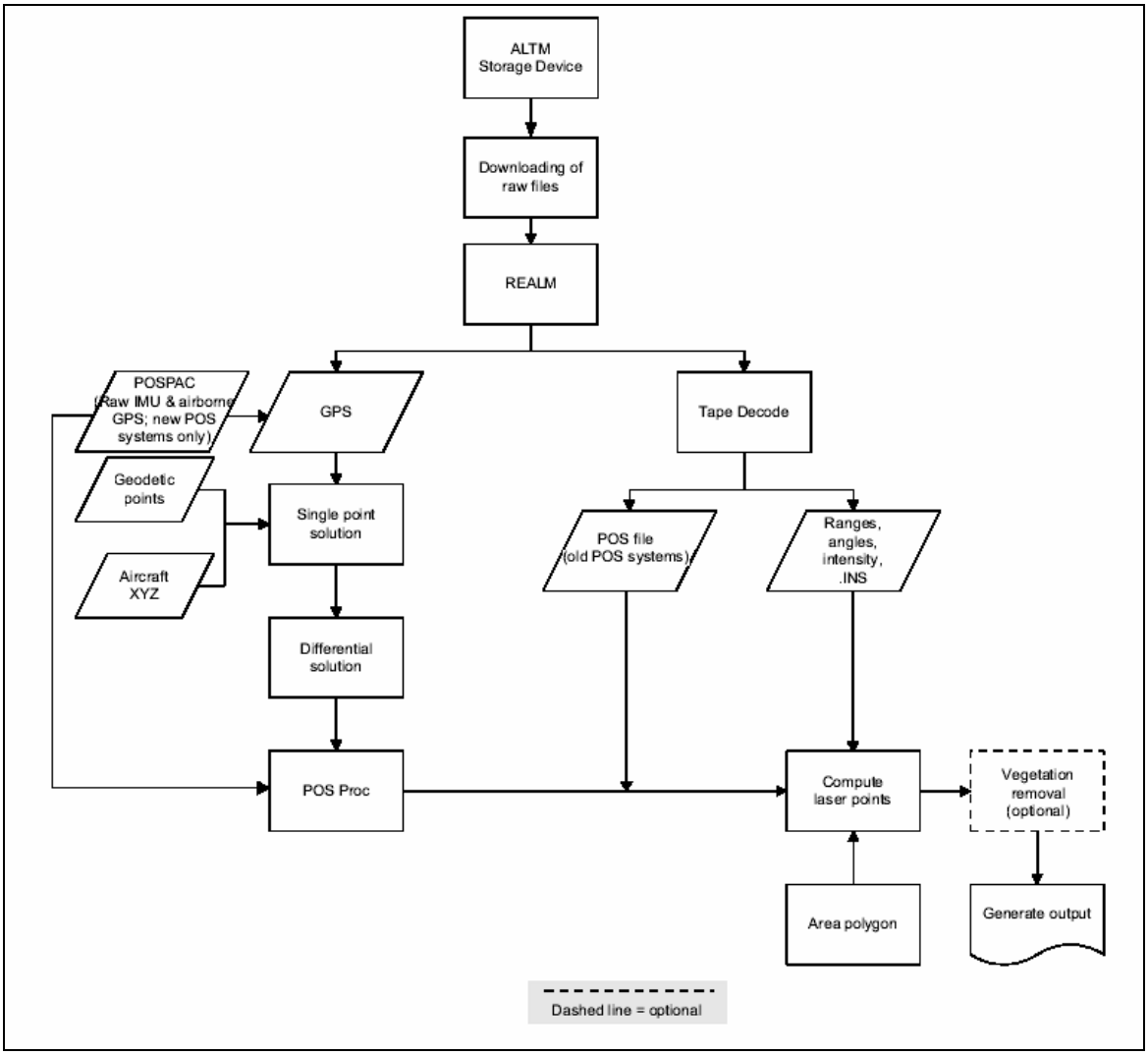

Figure 3-1: *REALM* Basic Processing

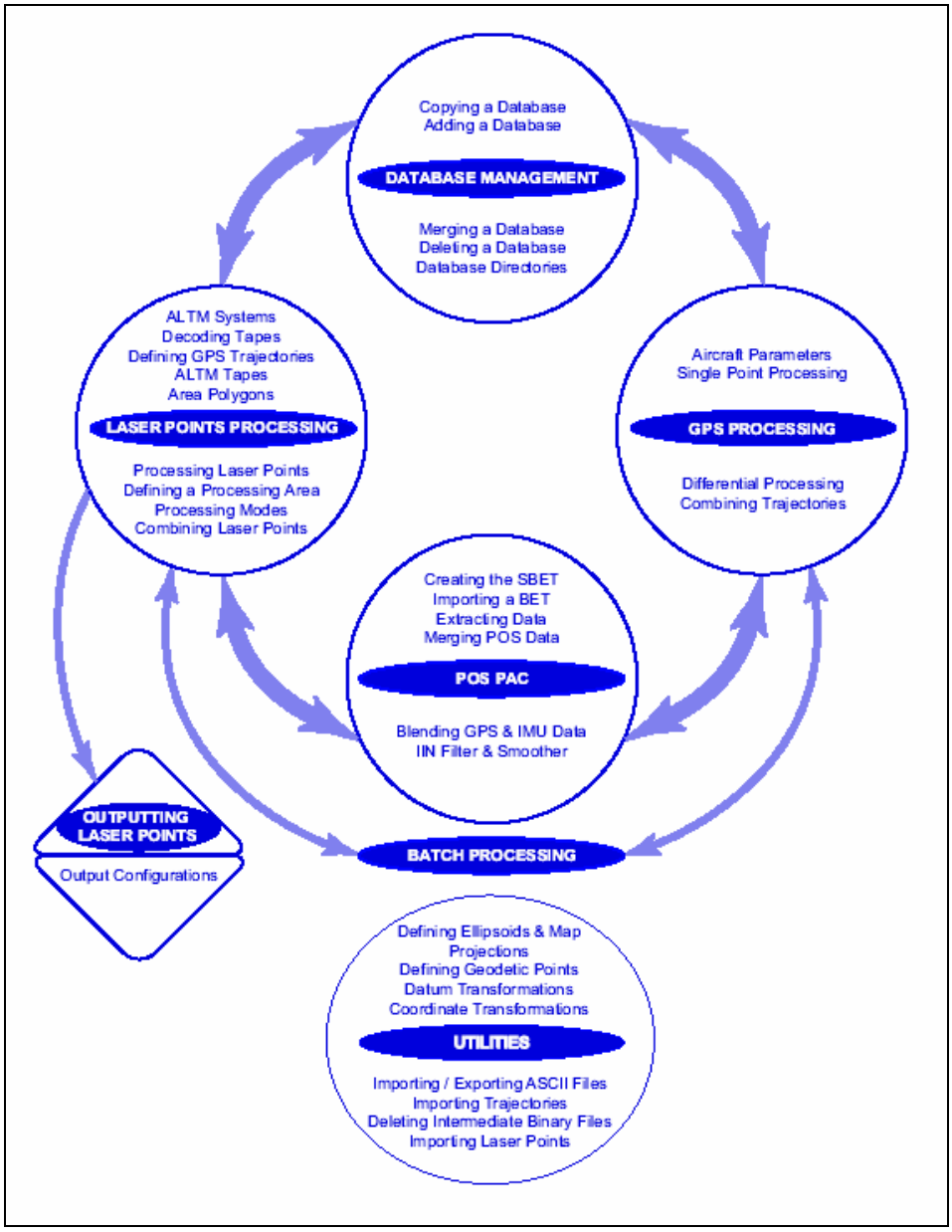

Figure 3-2: *REALM* Processing Flow

REALM Processing

Laser processing in *REALM* is based upon area-polygons defined by the user. *REALM* provides a graphical representation of the flight lines for the survey area thereby allowing the user to select a given region for processing by highlighting the region with a user-defined polygon. This functionality allows the user to group areas of close spatial proximity together for processing rather than having to process the entire survey region as a whole; however, if desired, the entire survey area can be processed by defining a polygon to encompass all flight lines. Polygons are selected dependent upon project requirements and characteristics of the survey region such as spatial proximity of flight lines, size of the survey area, specific regions of interests defined by the client, etc.

Comprehensive Output Format

After selecting a region for processing by defining an area-polygon, *REALM* processes the region and outputs a final output format. In the past, the most used output format provided by *REALM* was a 9-column format as follows:

[time stamp, x2, y2, z2, last return intensity, x1, y1, z1, first return intensity]

where the xyz-values of the 9-column format are in UTM coordinates. However, a paradigm shift is occurring. *REALM* provides a new data format called the **comprehensive format**, and the paradigm shift is towards the utilization of this new comprehensive format. The user can select *REALM* to have the data processed and output with the "comprehensive" computing mode. The data will be output to a file with a ".CMP" extension. The file name is automatically assigned by *REALM*. The comprehensive format requires an extensive amount of disk space: for example, over 9 mb/sec for a 50khz ALTM system . The header format is presented in Figure 3-3 and the record format is presented in Figure 3-4.

Header: 718 Bytes

Description	Type	Size
Record Type	int16	2 bytes
Number of Record	int32	4 bytes
GPS Week Number	int16	2 bytes
Min Time	double	8 bytes
Max Time	double	8 bytes
UtmZone	int16	2 bytes
Min LP	3 x double	24 bytes
Max LP	3 x double	24 bytes
Number of Strips	int16	2 bytes
List of Strip Numbers	256 x int16	512 bytes
Filling Space	130 x char	130 bytes

Figure 3-3: Comprehensive Header Format

Record: 207 Bytes

Description	Type	Size
GPS Time	double	8 bytes
Pulse Count	int8	1 byte
Last Pulse - ENH	3 x double	24 bytes
Third Pulse - ENH	3 x double	24 bytes
Second Pulse - ENH	3 x double	24 bytes

Figure 3-4: Comprehensive Record Format

First Pulse - ENH	3 x double	24 bytes
Last pulse intensity	int16	2 bytes
Third pulse intensity	int16	2 bytes
Second pulse intensity	int16	2 bytes
First pulse intensity	int16	2 bytes
Last Pulse calibrated range	double	8 bytes
Third Pulse calibrated range	double	8 bytes
Second Pulse calibrated range	double	8 bytes
First Pulse calibrated range	double	8 bytes
Calibrated angle in radians	double	8 bytes
Roll in radians	double	8 bytes
Pitch in radians	double	8 bytes
Heading in radians	double	8 bytes
Plane position - ENH	3 x double	24 bytes
Strip number	int16	2 bytes
Reserved	int32	4 bytes

Figure 3-4 (cont): Comprehensive Record Format

From the above it is apparent that the comprehensive format provides return intensities for intermediate values as well as the first and last return; however, the GEM ALTM system only provides 1st and last return intensities. Intermediate returns are only provided by the latest Optech systems. Refer to the *REALM* data processing manual for an in-depth discussion on the comprehensive format and software utilization .

Post Processing

Processing of the navigation solution and laser data within *REALM* renders the data into a usable, "final" format, which then can be directly utilized or further processed. Depending on the application and project requirements, the data can be post processed for creation of specific project deliverables. In most instances, the required project deliverable for the client is a bare earth digital elevation model (DEM).

Gridding with Surfer

The generation of DEMs is accomplished with *Surfer*. *Surfer* is a contouring and 3D surface visualization and mapping program that can convert XYZ data files into contour, surface, wireframe, vector, image, shaded relief, and post maps. The most common application of *Surfer* and the importance of *Surfer* for this example is its ability to create a grid-based data file from an irregular spaced XYZ data file [3].

Gridding methods produce a regularly spaced, rectangular array of Z-values (heights) from irregularly spaced XYZ data. The term "irregularly spaced" means that the points follow no particular pattern over the extent of the region, resulting in many "holes" where data are missing. Gridding fills in these holes by interpolating Z-values at those locations where no data exist. The grid that is formed is a rectangular region comprised of evenly spaced rows and columns. The intersection of a row and column is called a grid node, and gridding generates a Z-value at each grid node by interpolation [3].

Surfer provides many different gridding methods for interpolation of the data. Different gridding methods provide different interpretations of the data because each method calculates grid node values using a different algorithm. Some methods are better than others in preserving the data, and sometimes some experimentation is necessary before one can determine the optimal method for the data. Gridding methods provided by *Surfer* include Inverse Distance to a Power, Kriging, Minimum Curvature, Modified Shepard's Method, Natural Neighbor, Nearest Neighbor, Polynomial Regression, Radial Basis Function, Triangulation with Linear Interpolation, Moving Average, Data Metrics, and Local Polynomial [3].

Kriging

The method utilized for gridding of the processed ALTM laser data is **Kriging**. Kriging is a geostatistical gridding method that can produce accurate, optimally gridded data points from irregularly spaced data. The statistical properties of Kriging attempt to model trends suggested in the data, so that, for example, high points might be connected along a ridge rather than isolated by bull's-eye type contours [3].

Kriging is a very flexible interpolation method that can be custom-fit to a data set by specifying an appropriate variogram model within *Surfer*. Kriging incorporates anisotropy and underlying trends, and the user can adjust the anisotropy parameters to better suit the data. In addition, Kriging can operate as either an exact or a smoothing interpolator depending on the parameters selected by the user in *Surfer* [3].

Creating a DEM in Surfer

The following is an example workflow of the steps taken within *Surfer* to create a DEM utilizing the Kriging interpolation method. It is important to note that this example assumes that the data has been completely processed and filtered before importing into *Surfer*. Therefore, any filtering such as vegetation and structure removal for generation of bare earth DEMs must be completed prior to conducting the gridding process in *Surfer* outlined below. Refer to the GEM report on "filtering" for details.

In *Surfer*:

1. Click on **Grid | Data** from the file menu.
2. In the **Open** dialog, select the data file containing the XYZ values of the processed laser data and then click the *Open* button. A **Grid Data** dialog display will open similar to below.

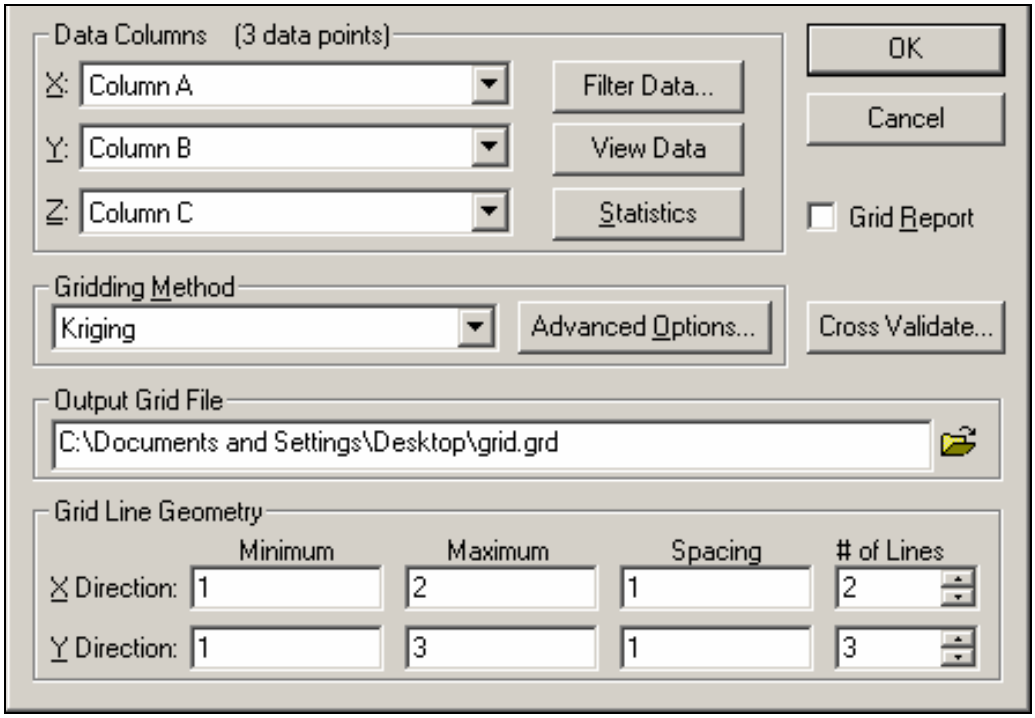

Figure 3-5: Grid Data Dialog [3]

3. In the **Grid Data** dialog, select the appropriate columns for the X, Y, and Z-values from the data file. Select *Kriging* in the *Gridding Method* group, select the desired spacing, range, and size of the grid in *Grid Line Geometry* fields, and select a location for the *Output Grid File*.

4. Next, click on **Advanced Options** and select the **General** tab on the Kriging advanced options window. Click the *Add* button to add variogram components. Select the *Linear* variogram, adjust the *slope* and *anisotropy* parameters if need be, and click *OK* to add it.

5. Click *Add* again and select the *Nugget Effect.* Set the *variance* to 0 (standard configuration but can be adjusted) and click *OK* to add the Nugget Effect. The display should now be similar to below.

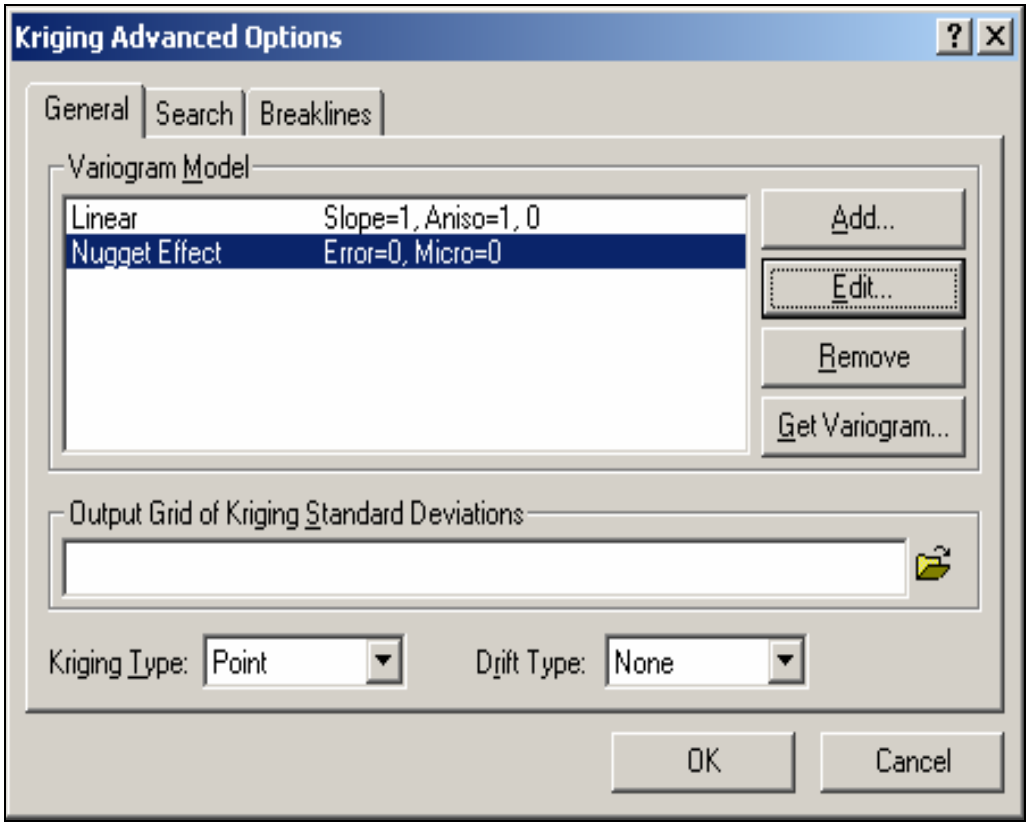

Figure 3-6: Krigging Advanced Options [3]

6. Next, select the **Search** tab to adjust the search capabilities of the Kriging algorithm. To utilize all of the data, make sure the *No Search* box is checked. Otherwise, uncheck the *No Search* box and enter the search parameters. Figure 3-7 below displays a standard format for the search parameters. Click *OK* to return back to the **Grid Data** dialog box.

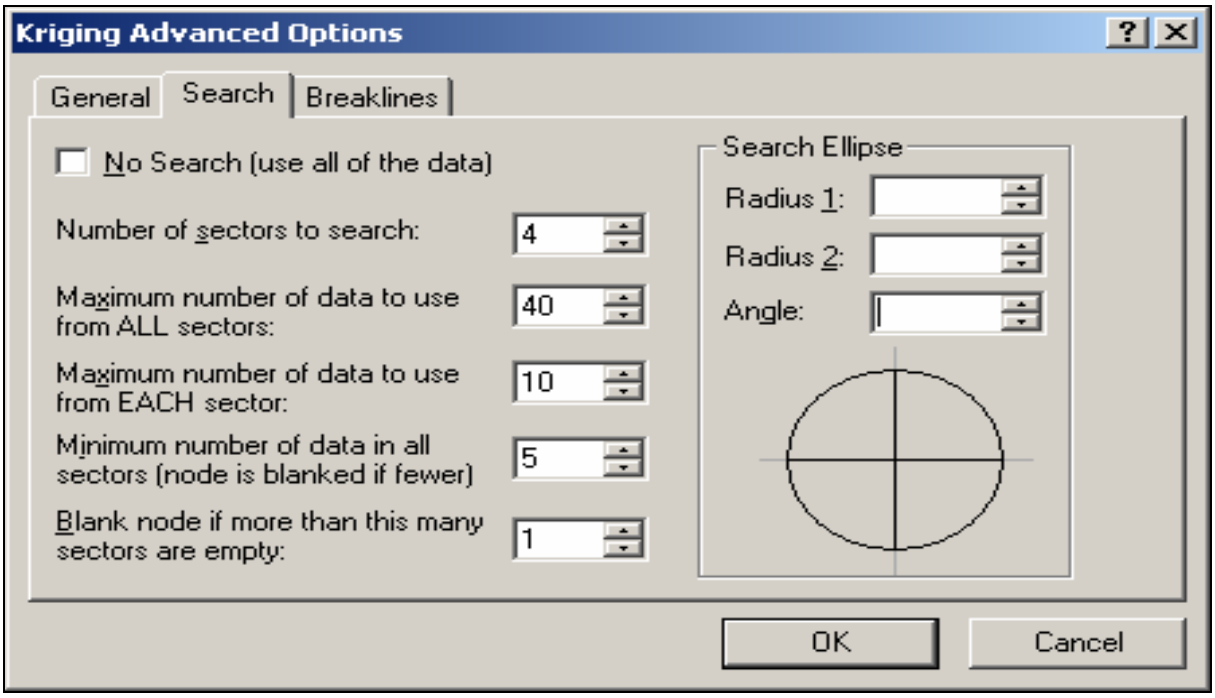

Figure 3-7: Standard Values for Search Parameter [3]

7. After the advanced options and parameters have been set, click *OK* on the **Grid Data** dialog box and the DEM will be generated utilizing the defined Kriging parameters.

The above is only a general outline of the steps in *Surfer* to generate a DEM and may vary dependent upon the data being processed and the parameters utilized. There are numerous Kriging parameters that can be adjusted or refined and it may be necessary to experiment with different settings until a desired result is found. Most gridding is automated within *Surfer* performed by scripts. Refer to the *Surfer* User Manual for further detail [3].

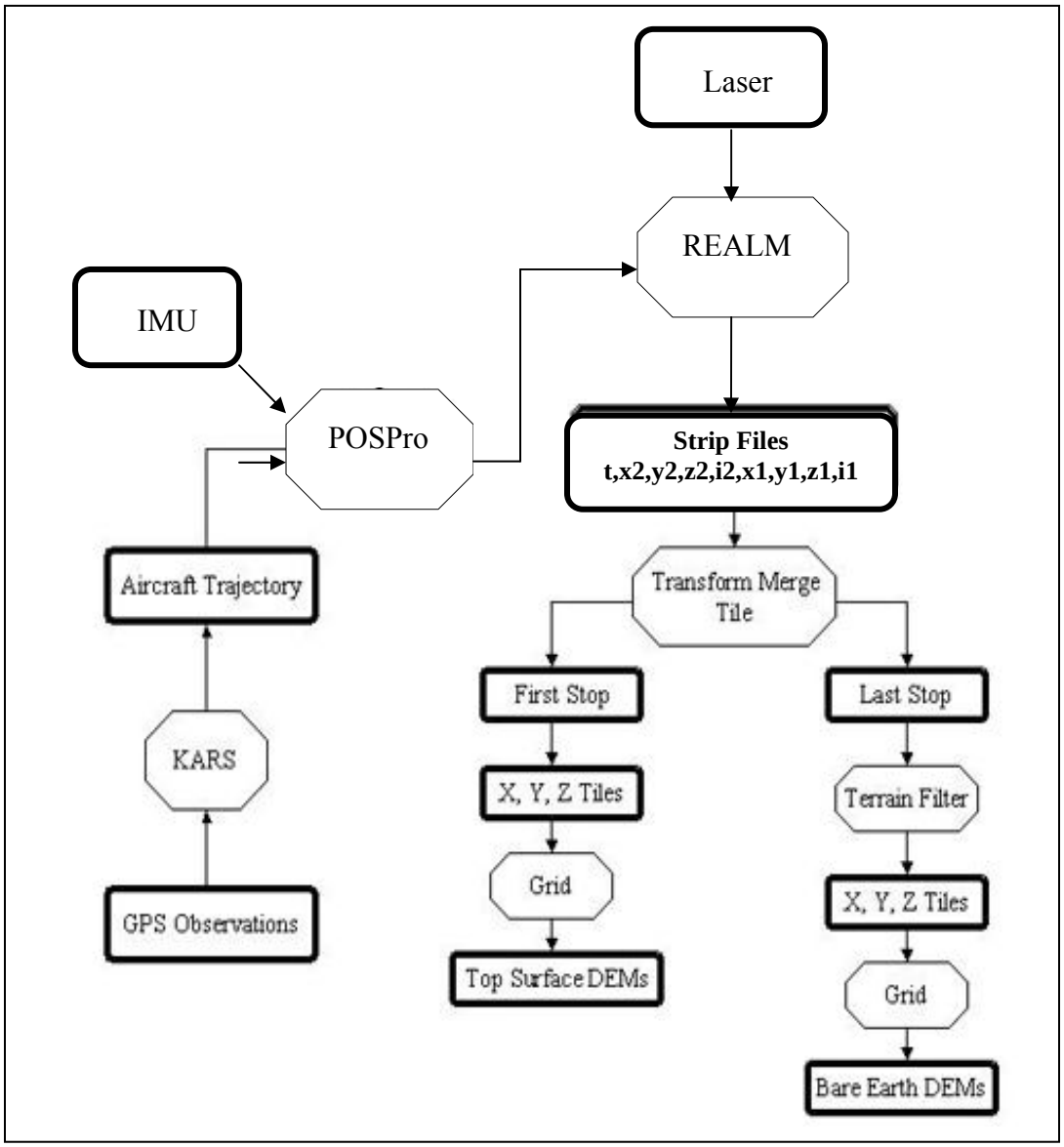

Figure 3-8: Outline of Data Processing Flow

Table of Software:

Software	Maker	Application
Online Positioning User System (OPUS)	NOAA – NGS - 2004	Processing of GPS base stations with CORS
POSPac version 4.02	Applanix – 2002	Processing of IMU and trajectory with POSProc module contained in POSPac 4.02
REALM version 3.2	Optech – 2003	Processing of navigation and ALTM laser data
Surfer version 8.03	Golden Software, Inc. – 2003	Generation of DEMs

As can been inferred from the above, it is a very labor intensive process to create a workable DEM. It should also be apparent that there are numerous opportunities to induce "noise" into the results. This noise will affect the relative resolution of data collected and in turn could limit the ability to ascertain small topographic changes.

Normalizing ALSM Intensities

The intensities of reflected laser returns detected by the ALSM system are affected by the following factors: variations in path length, surface roughness and orientation, beam divergence, object composition, object density, saturation from background reflections, and attenuation of the signal through the atmosphere.

Surface roughness and orientation, composition, and density are fundamental components of the spectral reflectivity properties of the observed surface/object. Furthermore, laser measurements are usually not affected by background reflections such as reflections due to ambient sunlight. The Optech ALTM 1233 system utilized in this research scans laser pulses within a preferred range of angles and is designed to operate in daylight. The system implements a narrow band-pass filter to prevent light from entering that does not fall within a few Angstroms +/- of the 1064 nm sampling wavelength. This prevents extraneous light from saturating the sensor and producing spurious results. In addition, atmospheric conditions, and thus effects on intensity values due to atmospheric extinction, are likely to be similar throughout the entire data collection

as long as the data are collected within a relatively short period of time (i.e. a few days). Therefore, intensity values sampled across a region within a small temporal range can be considered to be influenced by the same atmospheric extinction values. Note that this assumption may not be valid if intensity data with significant temporal displacement are being compared.

The effects on intensity due to the previously discussed factors are considered intrinsic components of the surface/object and survey environment and generally do not require compensation within the intensity data. However, variations in path length of the laser return result in unwanted weakening or strengthening of the intensities. Therefore, these effects must be corrected for in the ALSM intensity data. Factors that influence path length, and consequently intensity, include changes in ground topography, variations in flying height, and variations in scan angles. To observe how these factors affect the path length and result in brighter or dimmer returns, refer to Figure 3-9 below.

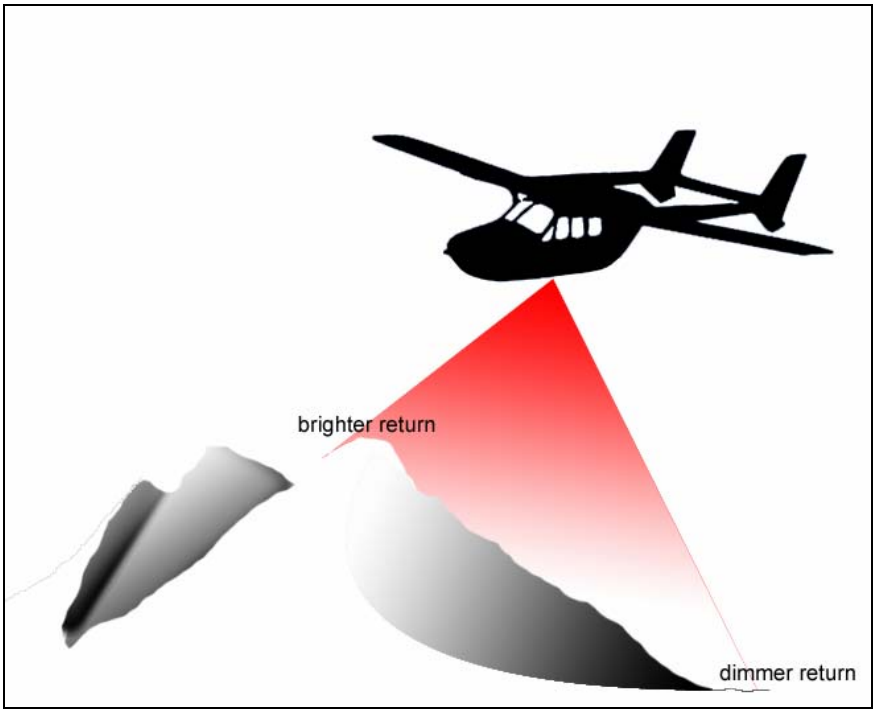

Figure 3-9: Changes in Path Length Due to Elevation [A. Mamatas, GEM Center]

As can be observed in the above figure, the path length changes dramatically due to the drastic variations in ground topography, resulting in dimmer returns from the lower elevations on the right side of the figure and brighter returns from the higher elevations on the mountain, assuming the reflectivity properties of the surfaces are similar. The same effects occur as the path length varies due to changes in scan angles (e.g. –20 deg to +20 deg) and differences in flying heights. To correct for these effects, the intensity values must be normalized. If the ALSM intensity data are not normalized to correct for varying path length, comparison of intensity values and display of intensity images across and between scans and different scan regions cannot be properly conducted. Figure 3-10 below displays an intensity image that combines three adjacent scan regions where the middle region was created from non-scaled (non-normalized) intensity values. As can be observed in the image, the middle region's intensities differ from the neighboring regions, which results in a non-uniform, unrealistic intensity image. Figure 3-11 demonstrates the same image with the intensities normalized for all three regions.

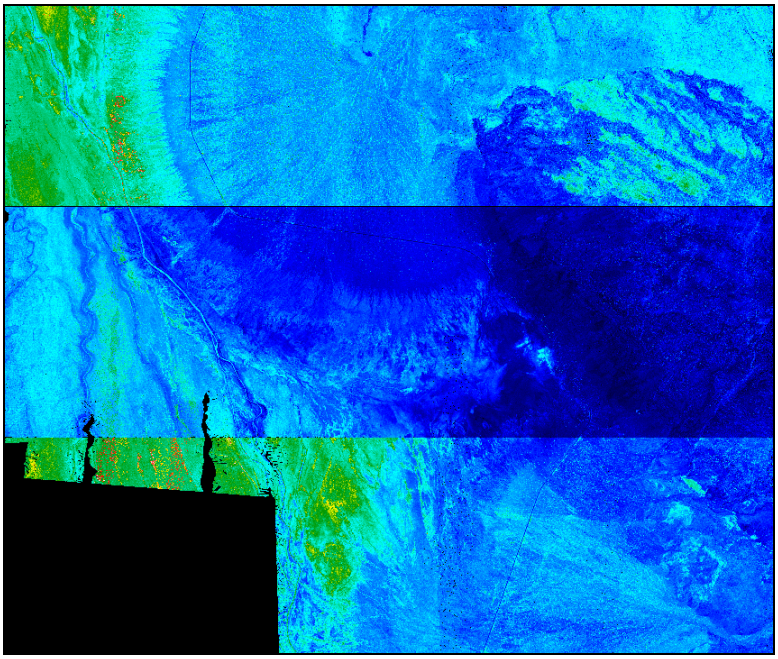

Figure 3-10: Intensity Image - Middle Region Non-Scaled [Gem Center]

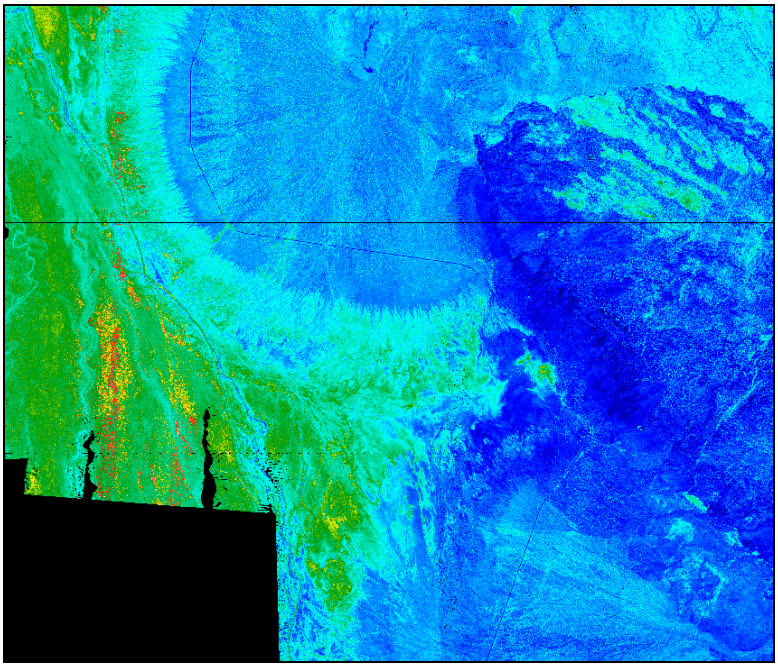

Figure 3-11: Intensity Image - All Regions Scaled [Gem Center]

Normalization Routine

The intensities are normalized by an in-house routine developed in C called *norm_intensity*. The program compensates for the one over distance squared (geometric) fall-off of electromagnetic signal. Using the square of the range, the intensities are normalized to a user-defined standard range. This correction should compensate for differences in flying height, changes in ground topography, and other variations in path length such as from observations taken at different scan angles. The algorithm executed by the program does not correct for effects due to beam divergence as well as the other factors that affect reflectivity as explained in section 1.0 above. The algorithm only corrects for the effects on intensity caused by variations in path length.

Algorithm Description

1. Utilizing the 9-column ALSM data file and the trajectory file for the aircraft, the GPS time tag available in both files is used to determine the two trajectory points that are closest in time to the ALSM laser shot.
2. Next, the estimated position of the aircraft at the exact time the laser shot was fired is computed by linear interpolation based on the two closest trajectory points.
3. Then, using the coordinates of the interpolated position of the aircraft and the reflected ground coordinates, the range is determined by computing the three dimensional Euclidean distance between the two.
4. Finally, the intensity is normalized by the square of the standard range as follows: intensity value of laser shot * (square of computed range / square of standard range)

5. The above steps are repeated for every laser shot.

Program Execution

To run the program, the **norm_intensity** executable is called from the *MS Windows* command prompt supplied with the required inputs as follows:

norm_intensity *trajectory_file laser_file output_file [std range]*

trajectory_file is the corrected aircraft trajectory file obtained after processing with the *KARS* program. It is in the format ASCII *[time, x, y, z]*. The x,y,z values must be in UTM coordinates due to the 9-column x,y,z values being in UTM. The location of the trajectory file is usually found in the working directory for the project region determined by the person or persons that processed the data. In general, it is located under the following folders in the project directory: "kars"→ "sol". If the trajectory coordinates have been converted to UTM, the file will often have an ".utm" extension. However, this is only a general rule of thumb and the actual person or persons that processed the data should be contacted if the file location is unknown. *laser_file* is the ALSM data file in ASCII 9-column format *[time, 2nd x, 2nd y, 2nd z, 2nd intensity, 1st x, 1st y, 1st z, 1st intensity]*, *ouput_file* is the output file name, which will be output in the same 9-column

format as the ALSM input file except that the intensities will be normalized, and *[std_range]* is an optional user-defined input for the standard range to normalize the intensities; 600m is the default and the value entered must be an integer.

The trajectory file and ALSM 9-column data file must be located in the same working directory as the executable. The output file will be output to the same directory.

C source code for *norm_intensity* program developed by Mark Lee, formerly of the GEM Center.

```
#include <stdio.h>
#include <math.h>
#include <stdlib.h>
#include <string.h>
#include <search.h>

#define MAXLINE              200
#define MAXNAME              257
#define STD_RANGE            600
#define LONG_STRING_MINIMUM  80
#define NUM_X_CHARS          9

int main(int argc, char *argv[])
{

        FILE    *trajfileptr;
        FILE    *laserfileptr;
        FILE    *outfileptr;

        char    trajfilename[MAXNAME];
        char    laserfilename[MAXNAME];
        char    outfilename[MAXNAME];

        char    laserstring[MAXLINE], trajstring[MAXLINE], x1string[20], x2string[20];

        double  lasertime, laser1x, laser1y, laser1z, laser1i, laser2x, laser2y, laser2z, laser2i;
        double  trajtime, trajx, trajy, trajz, prevtime, prevx, prevy, prevz;
        double  matchx, matchy, matchz, difftime, range1sq, range2sq;
        double  std_range, std_range_squared, epoch;

        int     norm1i, norm2i, numcols, offset, length;

        printf("\nThis program normalizes laser intensity data to a standard range, using the\n"
               "square of the laser range.\n\n");

        if (argc < 4)
        {
               printf("\n\tUsage: norm_intensity trajectoryfile laserfile outfile [std range]"
               "\n\nthe trajectory file has time, X, Y, Z of aircraft"
               "\n\nthe laser file has time, X, Y, Z, intensity of laser"
               "\n\nthe out file will be same as laser file, but with normalized intensities"
                      "\n\nthe standard range, which is optional, set to %d if left blank.\n\n",
        STD_RANGE);
               exit(0);
        }

        strcpy(trajfilename, argv);
        strcpy(laserfilename, argv[2]);
        strcpy(outfilename, argv[3]);

        std_range = STD_RANGE;
        if (argc > 4) {
               std_range = atof(argv[4]);
        }

        printf("\nStandard range is %.1lf\n", std_range);

        std_range_squared = pow(std_range,2);

        if ((trajfileptr = fopen(trajfilename, "rt"))==NULL)
```

```
        {
                printf("\nFile %s could not be opened\n",trajfilename);
                exit(1);
        }

        if ((laserfileptr = fopen(laserfilename, "rt"))==NULL)
        {
                printf("\nFile %s could not be opened\n",laserfilename);
                exit(1);
        }

        if ((outfileptr = fopen(outfilename, "wt"))==NULL)
        {
                printf("\nFile %s could not be opened\n",outfilename);
                exit(1);
        }

        fscanf(trajfileptr, "%lf%lf%lf%lf", &trajtime, &trajx, &trajy, &trajz);

        while ((fgets(laserstring, MAXLINE, laserfileptr)) != NULL)
        {
numcols = sscanf(laserstring,"%lf%s%lf%lf%lf%s%lf%lf%lf",
&lasertime, x1string, &laser1y, &laser1z, &laser1i, x2string, &laser2y, &laser2z, &laser2i);

                while( lasertime > trajtime ) {

                        prevtime = trajtime;
                        prevx = trajx;
                        prevy = trajy;
                        prevz = trajz;

                        if (fgets(trajstring, MAXLINE, trajfileptr) != NULL) {

                        sscanf(trajstring, "%lf%lf%lf%lf", &trajtime, &trajx, &trajy, &trajz);
                                printf("\rTrajectory time: %.1lf", prevtime);

                        }
                        else {

                        printf("\nEarly end of trajectory file!  Need more trajectory data!");
                                fclose(outfileptr);
                                exit(1);
                        }
                }

                difftime = lasertime - prevtime;
                epoch = trajtime - prevtime;
                matchx = prevx + (trajx - prevx) * (difftime / epoch);
                matchy = prevy + (trajy - prevy) * (difftime / epoch);
                matchz = prevz + (trajz - prevz) * (difftime / epoch);

                length = strlen(x1string);
                offset = length - NUM_X_CHARS;
                laser1x = atof(x1string + offset);

                range1sq = pow(matchx-laser1x,2) + pow(matchy-laser1y,2) + pow(matchz-laser1z,2);
                norm1i = (int) floor(laser1i * (range1sq / std_range_squared) + 0.5);

                if ( strlen(laserstring) < LONG_STRING_MINIMUM ) {

                        fprintf(outfileptr, "%15.6lf %11.2lf %10.2lf %7.2lf %5d\n",
                                        lasertime, laser1x, laser1y, laser1z, norm1i);
                }

                else if (numcols == 9) {

                        length = strlen(x2string);
                        offset = length - NUM_X_CHARS;
                        laser2x = atof(x2string + offset);

                range2sq = pow(matchx-laser2x,2) + pow(matchy-laser2y,2) + pow(matchz-laser2z,2);
                norm2i = (int) floor(laser2i * (range2sq / std_range_squared) + 0.5);
```

```
fprintf(outfileptr, "%15.6lf %11.2lf %10.2lf %7.2lf %5d %11.2lf %10.2lf %7.2lf %5d\n",
        lasertime, laser1x, laser1y, laser1z, norm1i, laser2x, laser2y, laser2z, norm2i);
        }

        else if (numcols == 5) {

fprintf(outfileptr, "%15.6lf %48.2lf %10.2lf %7.2lf %5d\n",lasertime, laser1x, laser1y,
laser1z, norm1i);
        }

        else {

                printf("\nError in data at time %lf\n", lasertime);
        }


}

fclose(outfileptr);
fclose(laserfileptr);
fclose(trajfileptr);
```

As mentioned previously, FDOT also has at its disposal, a land-based laser system, the ILRIS 3D imager. While not a part of this particular project, it could be used in the future to further evaluate potential areas of concern. Hence, the following is a brief overview of the system.

Chapter 4. ILRIS-3D GROUND BASED LASER AND POLYWORKS

Introduction

Intelligent Laser Ranging and Imaging System (ILRIS)-3D is a tripod-mounted, 3-dimensional, terrain laser scanner developed by Optech for high-resolution engineering and mapping applications. The system is designed for static, ground perspective surveys, not flight surveys, and the data can be fused with other data sets such as airborne laser survey data for high-resolution analysis shown in Figure 4-1 below. The following is a basic overview on ILRIS including system specifications, scanner control and operation, data retrieval and processing, and the *PolyWorks* software.

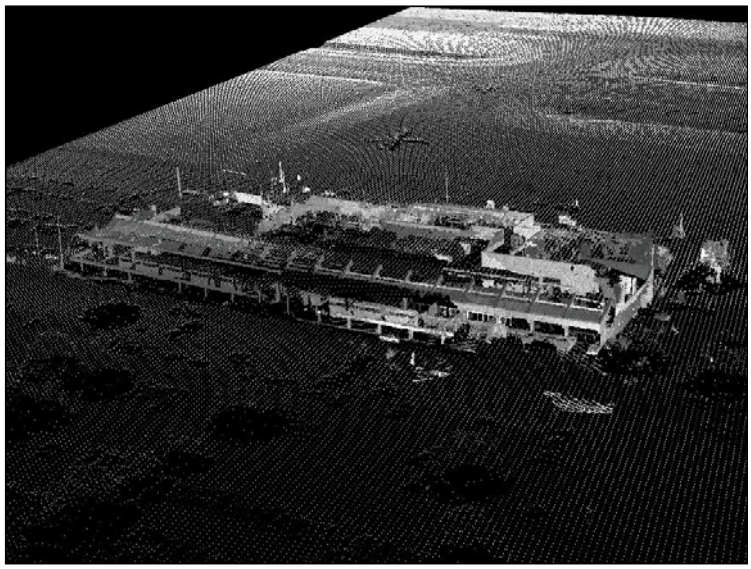

Figure 4-1: Fusion of ILRIS and Airborne Laser Data

ILRIS Features

Key specifications include [2]:

- Scanning range of 3m to >1000m
- 2,000 pulse-per-second scan rate
- 1,547 nm laser (eyesafe at all distances including binoculars)
- Max field-of-view is 40˚ horizontal and vertical (20˚ half angle)
- Spot size 29mm @ 100m
- Modeled output accuracy in the range of 5 mm
- 640 x 480 pixel color digital camera
- 17cm VGA viewfinder for targeting
- Power: 24 VDC battery; 24 V rechargeable
- Control interface: palm pilot, laptop, or compatible PDA

- Scan size: range from a few megabytes to 10+ megabytes in size
- Memory: ATA flash cards (128mb PCMCIA flash cards in current use by GEM)

Key benefits include [2]:
- Resolves small features at long range
- Short scan time: scene with 1.2 to 1.8 million points can be fully captured in 10-15 minutes
- Easy to use, no extensive training, easy to set up
- No leveling, retro-reflectors, or mirrors required
- Portable and compact, deployed by a single operator
- Battery-operated
- Edit out intermittent objects during data processing
- Digital data directly compatible with GIS programs

Figure 4-2: View of FDOT's ILRIS

ILRIS Control and Operation

Scanner control and setup is managed by control software that is stored either on a palm pilot, laptop, or compatible PDA. Currently, GEM utilizes a palm pilot for set up and operation of the ILRIS via control software developed by Optech to run on *Palm OS* (i.e. the palm pilot's operating system). The palm pilot can be operated in wireless infrared mode or directly connected to the scanner. Figure 4-3 displays a standard operating mode utilizing the palm pilot.

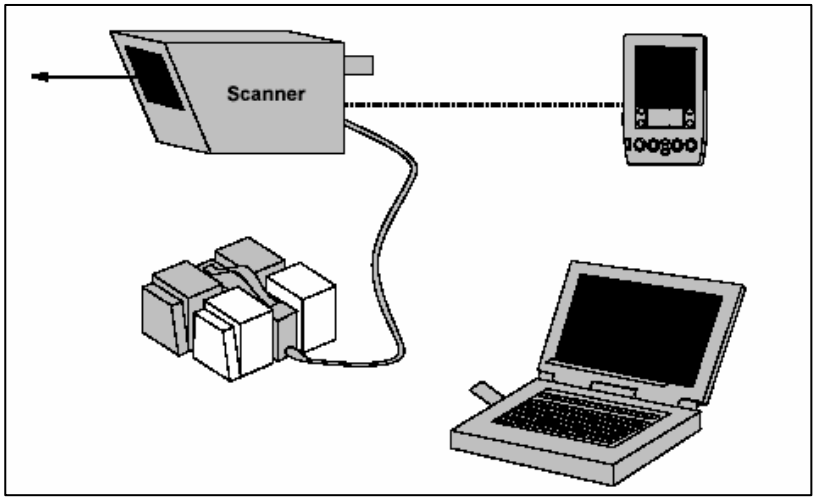

Figure 4-3: ILRIS Working Setup

Basic fundamental camera settings such as contrast, brightness, etc. are controlled via the control software. In addition, the control software allows one to see the camera's field-of-view (FOV) through the viewfinder and select regions to scan. The maximum range for the FOV is 40˚ horizontal x 40˚ vertical, and for a specific FOV, a single region or multiple regions can be selected to scan. The actual area of the FOV is slightly narrower than the scan region because the camera is not bore sighted and parallaxed is introduced between the camera and scanner. This difference is small and only noticeable at very close distances.

Adjustment of Point Spacing

The point spacing of the laser can be controlled and adjusted by the control software. During scanner setup, the control software computes the mean range for the selected scan region. It then calculates a theoretical plane orthogonal to the laser pulse at 0˚ and 0˚ to provide an estimate of the point spacing for that particular scene. Based on this estimate, adjustments to point spacing can be made to achieve desired resolution. However, it is important to indicate that this mean theoretical range for point spacing is simply a rough estimate and should serve only as a guideline for adjusting the point spacing. The actual point spacing will vary across each scan and from region to region.

Operating Procedures

The following is a simplified outline of steps taken to perform a scan with ILRIS:

1) Turn on the system by plugging in the battery power; there is no "on" switch
2) Connect the palm pilot, laptop, or PDA to the scanner and run control software
3) Position scanner to obtain desired FOV for scan object.
4) Select target/s to scan within the FOV
5) Determine mean range for point spacing
6) Adjust point spacing to achieve desired resolution for the scan
7) Start scan and wait to complete
8) Turn off ILRIS
9) Remove flash card and download scan data to desktop or laptop

Data Retrieval and Processing

The following data items are recorded during an ILRIS scan: raw survey metafile consisting of XYZ and laser intensity data (0-255), digital photo data, and a log file. The log file contains operator setup parameters and notes from the control unit (i.e. palm pilot) for the specific scan. This includes parameters such as point spacing, time of day the scan was recorded, etc.

All the data items recorded are integrated and stored into a single file format with a ".i3d" extension. ".i3d" is an Optech proprietary data format, and the file must be downloaded off the scanner flash card and parsed to a useable format before the survey data can be incorporated into *PolyWorks*, discussed in below, and/or other third-party software or applications.

ILRIS Parser

Optech provides standard software, the *ILRIS Parser*, to parse the ".i3d" data file into a useable format. With this software, the data can be parsed into a variety of formats including "PIF" and ASCII XYZ. For GEM purposes, "PIF" is the standard file format selected for export because this format is utilized by *Polyworks*. However, it is important to realize that the "PIF" file will be exported to a file with a ".pf" extension, not ".PIF". Furthermore, there are many other software formats available for export with the *ILRIS Parser*.

Operation of the software is straightforward and simply entails selecting the ".i3d" file to parse and the desired export format, which is generally "PIF" for GEM applications. Once the file is exported to "PIF" format, it can then be incorporated into *PolyWorks* for further processing.

Polyworks

PolyWorks is a software package designed by InnovMetric for survey and manufacturing applications. It is a powerful point cloud software solution that processes data obtained from any short-range, mid-range, or long-range 3D scanner. *PolyWorks* provides scan alignment, geo-referencing, measurement, feature extraction, and visualization capabilities to produce survey-accurate results and extracted elements for downstream software suites such as AutoCAD and MicroStation .

The main utilization of *PolyWorks* for GEM Center applications is the registering of multiple scans together to produce one, large scene. Within *PolyWorks,* a single scan or multiple scans can be georeferenced and registered. For georeferencing, three points in the scan that are easily identifiable and presurveyed are required to reference the scan.

In addition to registering scans together and georeferencing, *PolyWorks* provides measurement tools for measuring within models, and it provides tools for fitting primitive shapes to point clouds. A triangulated irregular network (TIN) can be generated to fit the surface of a point cloud. The TIN can then be exported for use in other applications.

PolyWorks is not a single program; it is composed of several modules including IMAlign, IMInspect, and IMCompress. IMAlign is the module used to register scans and georeference. Additionally, IMAlign provides statistics on the processes. IMInspect is the module used to perform measuring tasks, and IMCompress is the module used to make a triangulated irregular network (TIN) surface of a point cloud.

Table of Software:

Software	Maker	Application
Palm OS	Optech	Control software for operation of the scanner.
ILRIS Parser	Optech	Parsing of ".i3d" file into a useable format; usually parsed to "PIF" for incorporation into PolyWorks
PolyWorks	InnovMetric	Registering of multiple scans together for generation of a large scene, georeferencing, measurement, and generation of TINs

CHAPTER 5. RESULTS OF ALSM DATA ANALYSIS

This chapter provides the results of the various overflights at suspect sinkhole locations. The data, predominately DEM figures (Digital Elevation Models) are self explanatory. First however, a brief review of the vetting process required to obtain the various figures is provided below.

Data Filtering Explanation

Filtering the data collected for the FDOT ALSM project is a crucial step in the analysis process. If the filtering is not accurate, valuable artifacts (e.g., slope or elevation changes) may be lost. Hence, removing artificial structures (autos) and/or vegetation covering an area of interest is critical. This processing produces a digital elevation model (DEM) that represents the actual topographic features of the land – within a variable confidence interval. There are several different filtering methods available. Of these methods, the two used for this project include the DEM filter and the HTF filter.

The DEM filter is based off existing topographic data available from USGS. This process involves indexing a USGS digital elevation model in order to filter out any structures or vegetation above the DEM's surface. This filter is primarily used to remove large structures from the data before filtering it using the HTF.exe filter.

The HTF filter is a sorting and indexing program and basically has two filters built in to it. It requires the user input of several parameters specific to a given set of data. The first parameter the user is prompted to specify is the "floor." This parameter is the lowest possible elevation of the topographic features in a given set of data. The second parameter the user is prompted to specify is the "ceiling." This parameter is the highest possible elevation of the topographic features in a given set of data. The third, fourth, and fifth parameters the user is prompted to specify, all pertain the second filtering element of the program. These parameters are the "length," the "width," and the "tolerance."

The first process the HTF filter goes through is that it sorts all of the data points by their Northing coordinate. It then uses its primary filtering element using the user specified "floor" and "ceiling." All data points with elevations below the "floor" and all data points with

elevations above the "ceiling" are filtered out. The program then proceeds to process the data using the second filtering element. It breaks the data down into sectors according to the "length" and "width" parameters. It then sorts the data in the x-direction from low to high according to the data points' elevations. The program then uses the "tolerance" parameter to determine where the slope, or change in elevation of the sorted data exceeds the user specified parameter and filters out all of the data beyond that point; usually around 35% of the data points within that sector. It then sorts the data in the y-direction the same way and then follows the same procedure, filtering out another 5% of the data points within that sector. The values of the "length" and "width" parameters are dependent on the type of area you wish to filter. For example, in urban areas with large artificial structures, a large "length" and "width" may be specified, such as 30 meters by 5 meters, such that they cover the size of an entire structure. For more rural areas, where only vegetation needs to be removed, smaller "length" and "width" parameters may be used. The "tolerance" parameter should be chosen such that it represents the expected maximum slope, or change in elevation from data point to data point, of the topography.

Summary of Data from I-75 overflights

- 8,058,237 total unfiltered data points
    - Install *TextPad* to view and print raw data if desired
- 5,174,676 total filtered data points
- No significant topographic change observed (signifying an active sinkhole)
- Recommendation
    - Collect data using ALSM of a known, existing sinkhole.
    - Compare topographic results with data collected using other methods
        - Traditional surveying (grid)
        - ILRIS, Lidar Imaging System
    - Determine if change in sinkhole topography as collected using ALSM is the same as that using other methods.
    - If effective, then use ALSM to find other sinkholes and measure topographic changes.
- See *HTF Filtering Process Parameters below* for a expanded explanation on HTF parametric values.

HTF Filtering Process

Estimation of HTF Parameters

- Open 3-D text file (*.txt) in ***Surfer 8*** as a worksheet.
- Highlight the "elevation column" and go to **Data → Statistics…**
- Use the **Statistics** function to find the:
    - Minimum
    - Maximum
    - Mean
    - First Quartile
    - Third Quartile
- Use these values for estimates of the floor and ceiling in the **HTF.exe** filtering program.

Filtering Data Using HTF.exe

- Create a file called **filelist.txt** in your working directory (same directory containing HTF.exe) using Notepad containing the list of all the files you wish to filter at one time (i.e. have similar parameters).
    - Example: arialscan1
      arialscan2
- Open up the **DOS command prompt**.
- Change directory to that containing both **HTF.exe** and **filelist.txt**
    - (ex. cd filter).
- Type in:
    - HTF floor ceiling length width tolerance
    - Where:
        - ***Floor*** is the minimum elevation found in your statistical analysis.
        - ***Ceiling*** is an estimated value of what you think the highest ground elevation should be (look at mean, first/third quartiles). This may take several tries to get the gridded data to look correctly.
        - ***Length*** is the length of the rectangular area in which you wish to filter at one time. Consider the shape of the scan: if the scan is wider than it is tall, make the length parameter smaller than the width parameter and vice versa if the scan is taller than it is wide. (2)
        - ***Width*** is the width of the rectangular area in which you wish to filter at one time. (50)
        - ***Tolerance*** is the expected change in slope over the rectangular area you wish to filter at one time. This value is objective in that one would expect a greater increase in slope in an area with more relief. For Florida, a value of **around 0.30** is accepted.
- Press **enter** and let the long filtering process run.

Gridding and Analyzing the Data

Gridding the Data

- Before gridding the data, open the data as a *Post Map* and overlay it over the unfiltered *Shaded Relief Map* to see what data you have filtered out.
- If there are large holes, open up the gridded unfiltered data as a grid map and click the cursor over the missing area to find the elevation (and possibly change the ceiling value).
- If the elevation seems to be correct, try changing the tolerance.
- Open up a new plot document using ***Surfer 8***.
- Go to menu option **Grid → Data…**
- Select the 3-D text data file which you wish to grid.
- Make sure the X, Y, and Z selection match the corresponding columns.
- Select the ***Kriging*** gridding method.
- Select the **Advanced Options** button:
    - On the **General** tab:
        - Add → Linear → Slope = **0.5**
    - On the **Search** tab:
        - No. sectors = **4**
        - Max No. Data from all sectors = **28**
        - Max No. Data from each sector = **7**
        - Min No. Data from all sectors = **5**
        - Blank Node = **1**
        - Radius 1 = **30** (var.)
        - Radius 2 = **30** (var.)
        - Angle = **0**
    - Press **OK**.
- Adjust **Grid Line Geometry** such that minimum and maximum are whole numbers so the spacing can be divided into the space specified evenly (i.e. # of lines is a integer value).
- Name your output file accordingly.
- Press **OK** to start gridding process.
- View by using **Map → Shaded Relief Map…**
    - Adjust **Z-scale** by right clicking on the image and selecting **Properties**.
    - If there are holes or uncharacteristic flat areas - need to adjust **Tolerance**, **Ceiling**, and/or **Radius 1(2)** values and repeat above process.

Measuring Sink Hole Volume

- Zoom in on a possible sinkhole.
- Use the **Digitize** command (right click on image) to find the upper-left and lower-right boundaries of the rectangular area containing the possible sinkhole.
- Go thru the gridding process again, but this time, enter the upper-left and lower-right boundaries in the **Grid Line Geometry**.
- Also, use a smaller value of **Spacing** for higher accuracy (ex. 0.3333).
- Open the newly gridded sinkhole file as a grid file in ***Surfer 8***.

- Left click around the perimeter of the sinkhole to find a reasonable value for the elevation (Z-value) around the top of the sinkhole.
- Open up gridded file again as a Plot Document.
- Use the menu function **Grid → Volume…**
    - Select sinkhole file you wish to measure.
    - Set the **Upper Surface** as the elevation (Z-value) you found in the previous step.
    - Set the **Lower Surface** as the grid file of the sinkhole you wish to measure.
    - Press **OK**.
    - Analyze cut and fill volumes accordingly (i.e. fill volume is volume of sinkhole).

As can be seen from the above narrative, the data collection (flying a particular site and activating the laser) is the unproblematic part of the overall process. It is estimated that for every 1 hour of data collection, upwards of 40 hours are needed to filter and analyze the information. Unfortunately, the task is very user sensitive, i.e., for a given set of data, 5 data processors will produce 5 different products – albeit similar. Thus, until the software becomes more robust, attempting to discern temporal changes in topographic features is difficult.

During the course of the project, several Progress Reports were prepared and presented at various venues. Hence, the following plots are extracted from these presentations with a brief summary of each.

- Four Sebring project areas were chosen and one Gainesville location. Unfortunately, two of the four sites had excess vegetation covering the ground surface. These heights alternated between tall grass, 14 inches tall and mowed or cut (3 inches - ostensibly from the public works department). Hence, the data was corrupted such that no meaningful analysis was possible. There were however three very interesting areas that did produce quantitative data amenable to analysis.

Project: I-75 starting from SW 38th Ct. and ending at SSR 484.

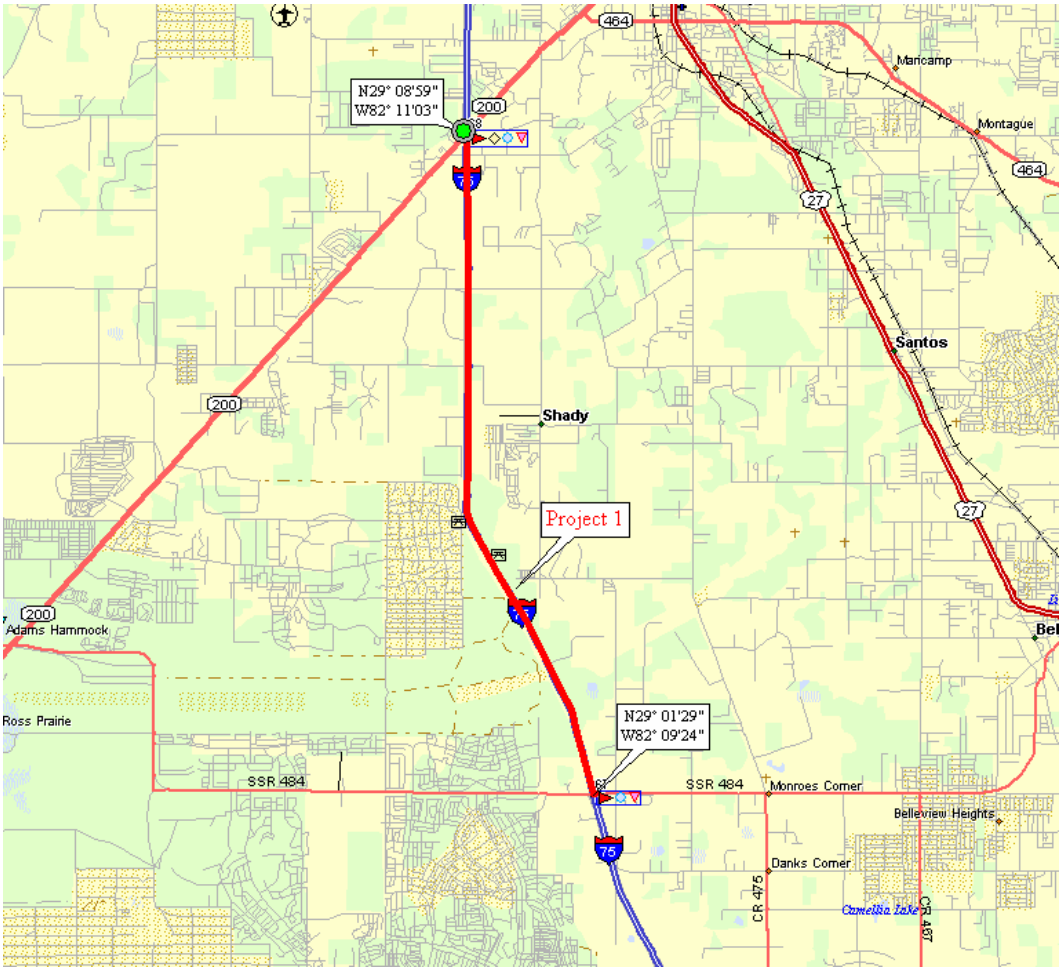

Figure 5-1. I-75 Project location at SSR 484 overpass

Raw Data

- Airborne laser collected millions of data points. (33,000 points per second)
- Each point has:
  - A Northing
  - An Easting
  - An Elevation
  - An Intensity

The data was saved as a text or Excel file for processing

	A	B	C	D
1	387032.91	3213000.0	-7.52	45
2	387033.04	3213000.1	-7.56	35
3	387033.03	3213000.1	-7.55	43
4	387033.06	3213000.1	-7.65	42
5	387033.03	3213000.1	-7.56	48
6	387033.14	3213000.1	-7.54	46
7	387033.04	3213000.1	-7.59	49
8	387033.04	3213000.1	-7.61	44
9	387033.02	3213000.1	-7.54	41
10	387033.03	3213000.1	-7.58	42
11	387033.01	3213000.1	-7.5	41
12	387033.02	3213000.1	-7.54	43
13	387032.97	3213000.1	-7.4	52
14	387032.92	3213000.1	-7.22	62
15	387032.88	3213000.0	-7.1	62
16	387032.93	3213000.1	-7.25	72
17	387032.89	3213000.1	-7.14	68
18	387032.81	3213000.0	-7.26	72
19	387032.8	3213000.0	-7.23	70
20	387032.8	3213000.0	-7.23	64
21	387032.81	3213000.0	-7.27	70
22	387032.83	3213000.0	-7.34	60
23	387032.84	3213000.0	-7.37	67
24	387032.8	3213000.0	-7.24	65
25	387032.78	3213000.0	-7.2	66
26	387032.78	3213000.0	-7.2	59
27	387032.8	3213000.0	-7.27	66
28	387032.79	3213000.0	-7.25	62
29	387032.79	3213000.0	-7.27	64
30	387032.77	3213000.0	-7.19	64
31	387032.76	3213000.0	-7.17	65
32	387032.76	3213000.0	-7.17	60

Figure 5-2. Typical ALSM Data Set

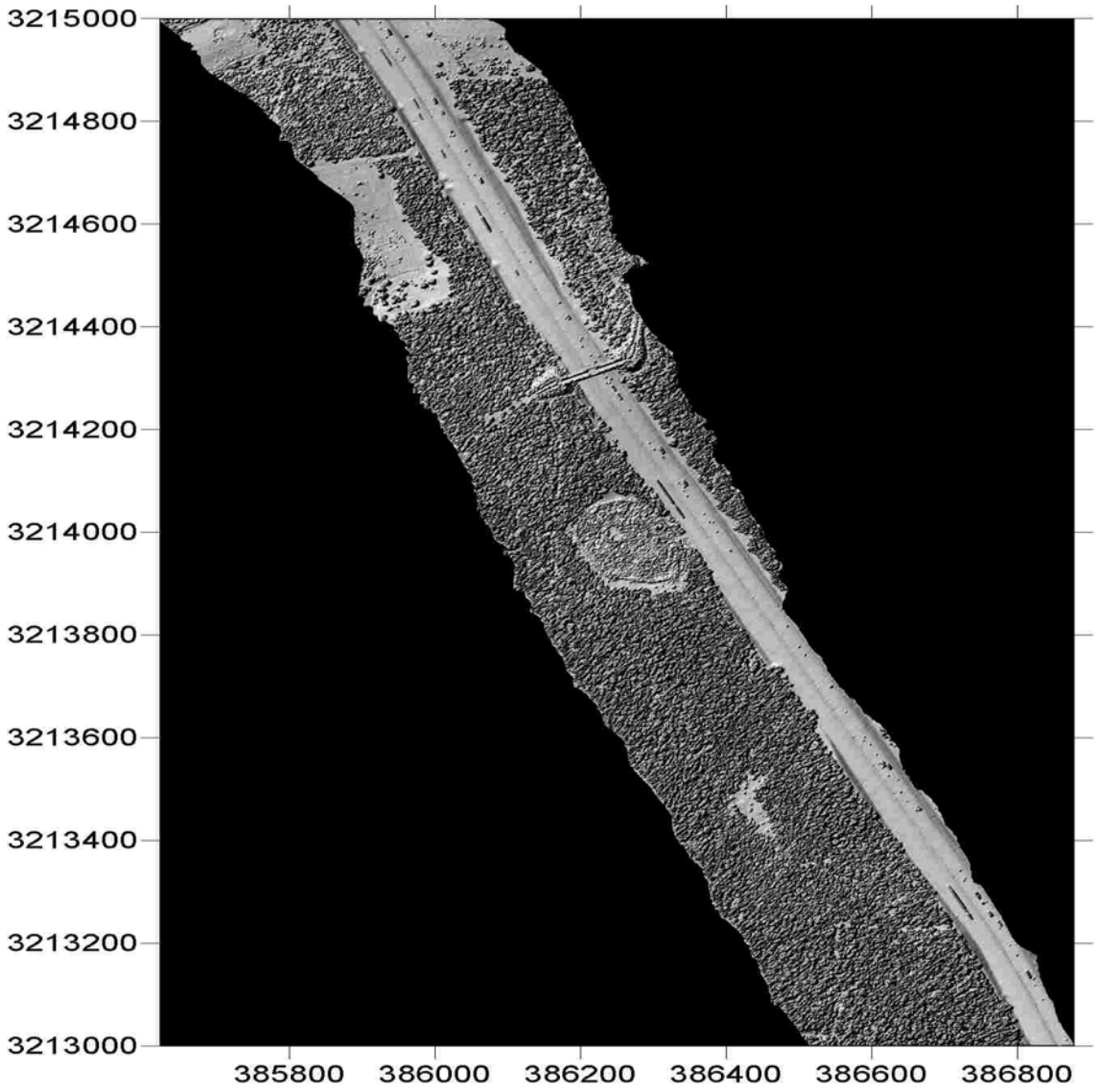

Figure 5-3. I-75 Project ALSM Raw Data (note overpass and vehicular traffic)

Grid Volume Computations

Fri Jul 12 09:25:46 2002

Upper Surface

Level Surface defined by Z = 6

Lower Surface

Grid File Name:	C:\Sebring\Project_4\Sinkholes\452.grd
Grid Size:	319 rows x 349 columns
X Minimum:	452784
X Maximum:	452900
X Spacing:	0.3333333333333
Y Minimum:	3032070
Y Maximum:	3032176
Y Spacing:	0.3333333333333
Z Minimum:	5.3190330589379
Z Maximum:	6.9677626215808

Volumes

Z Scale Factor: 1

Total Volumes by:

Trapezoidal Rule:	1768.8902453643
Simpson's Rule:	1769.1437525078
Simpson's 3/8 Rule:	1768.6825357976

Cut & Fill Volumes

Positive Volume [Cut]:	2564.1549109239
Negative Volume [Fill]:	795.26350573905
Net Volume [Cut-Fill]:	1768.8914051849

Areas

Planar Areas

Positive Planar Area [Cut]:	9052.241284172
Negative Planar Area [Fill]:	3243.7587158279
Blanked Planar Area:	0
Total Planar Area:	12296

Surface Areas

Positive Surface Area [Cut]:	9159.9279110309
Negative Surface Area [Fill]:	3275.5546111335

Figure 5-4. Surface Computations

	Sinkhole ID	Upper Surface (UTM elev)	X Minimum (UTM coord)	X Maximum (UTM coord)	X Spacing	Y Minimum (UTM coord)	Y Maximum (UTM coord)	Y Spacing	Z Minimum (UTM elev)	Z Maximum (UTM elev)	Volume (m^3)	Surface Area (m^2)
	384_3217	0.75	384426	384644	0.333333	3218537	3218749	0.333333	-6.535240205	2.247882967	75614.8798	21917.846
	384_3221	3	384842	384896	0.333333	3221120	3221163	0.333333	-0.091128425	3.649152651	1194.9807	1752.0876
Project 1	384_3223	-3	384618	384676	0.333333	3223915	3223978	0.333333	-5.229806354	-1.764895678	2526.57122	3299.5249
	385_3215	0.5	385813	385897	0.333333	3215224	3215305	0.333333	-1.622715909	2.006179891	4147.45791	5668.36
	387_3211	-3.5	387318	387531	0.333333	3211606	3211815	0.333333	-7.676085569	-2.974648776	86213.7545	38469.865
	457_6	-2	457379	457405	0.333333	3168112	3168135	0.333333	-3.498042174	-1.368803112	187.908982	387.60033
Project 2	457_6b	0.5	457483	457500	0.333333	3168230	3168244	0.333333	-5.060430233	1.609766266	225.91748	180.00651
	459_5	0	459292	459308	0.333333	3168045	3168059	0.333333	-1.775328474	0.588362576	77.7560912	152.36254
	451_8a	17.5	451515	451530	0.333333	3041984	3041997	0.333333	16.21728304	17.9551923	66.3408679	153.14609
Project 3	451_8b	17.5	451496	451513	0.333333	3042042	3042060	0.333333	16.33744206	17.83491047	115.865424	275.5425
	451_8c	17	451521	451542	0.333333	3042074	3042090	0.333333	14.81506357	17.6825201	51.2518457	119.5433
	451_8d	15	451652	451671	0.333333	3042146	3042161	0.333333	14.46005803	15.45933074	41.3546024	164.34626
	444_444_11	3	444438	444504	0.333333	3032057	3032125	0.333333	1.166033532	4.147152269	1594.95469	2169.0644
	446_446_11	0	446267	446293	0.333333	3032262	3032285	0.333333	-0.851733936	0.708286933	160.822914	384.24474
	447_446_11	2	447049	447085	0.333333	3032037	3032070	0.333333	1.202140919	2.230320561	457.7493	1118.1076
	447b_446_11	2.2	447296	447362	0.333333	3032056	3032119	0.333333	1.347945086	2.276217036	1663.14193	4144.5519
	448_448_11	1	448221	448269	0.333333	3032115	3032156	0.333333	-0.154447926	1.982032202	963.574429	1668.151
	448b_448_11	0	448390	448420	0.333333	3032127	3032153	0.333333	-0.654025795	0.781887835	154.409973	448.24393
Project 4	450_450_10	9	450711	450784	0.333333	3032160	3032196	0.333333	8.3156437	9.226778196	697.484394	2292.2753
	451_450_10	9.5	451216	451235	0.333333	3032261	3032289	0.333333	8.376635302	9.901903735	141.228986	284.97552
	451b_450_10	8.8	451365	451464	0.333333	3032086	3032181	0.333333	7.968019401	9.293546714	3151.14482	8372.3439
	451c_450_10	9.1	451136	451149	0.333333	3032301	3032316	0.333333	8.810731089	9.224461041	16.1956776	157.87619
	452_452_11	6	452784	452900	0.333333	3032070	3032176	0.333333	5.319033059	6.967762622	2564.15491	9159.9279
	453_452_11	6	453358	453418	0.333333	3032058	3032102	0.333333	4.798402197	6.45254468	1185.06871	2006.2163
	454_454_11	1.5	454414	454422	0.333333	3032110	3032118	0.333333	0.92230822	1.617549993	12.079993	56.66211
	457_456_11	4.2	457907	457951	0.333333	3033846	3033868	0.333333	3.130406846	5.877494849	220.207447	606.95666

Figure 5-5 Tabulated Data

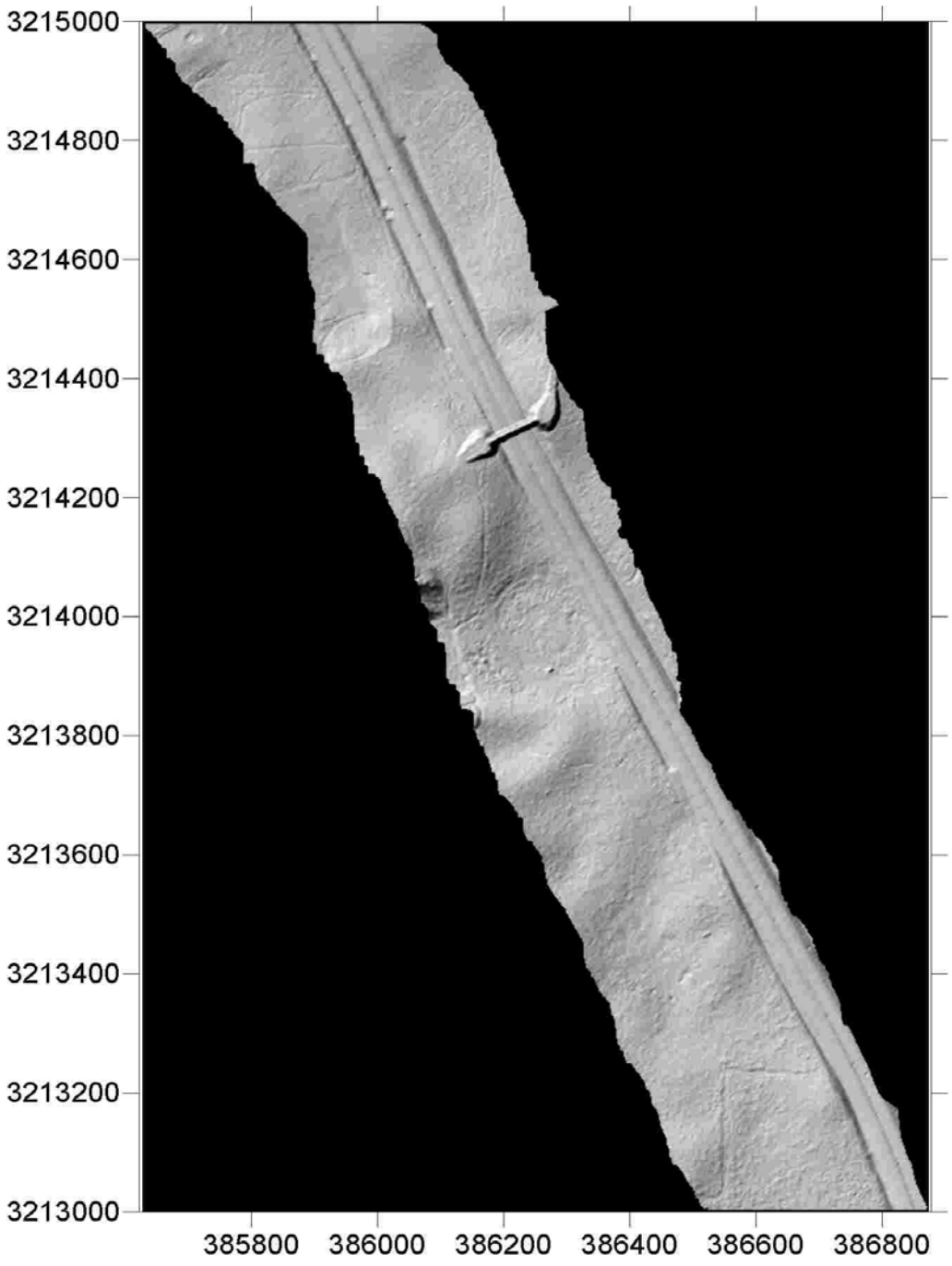

Figure 5-6. Bare Earth DEM

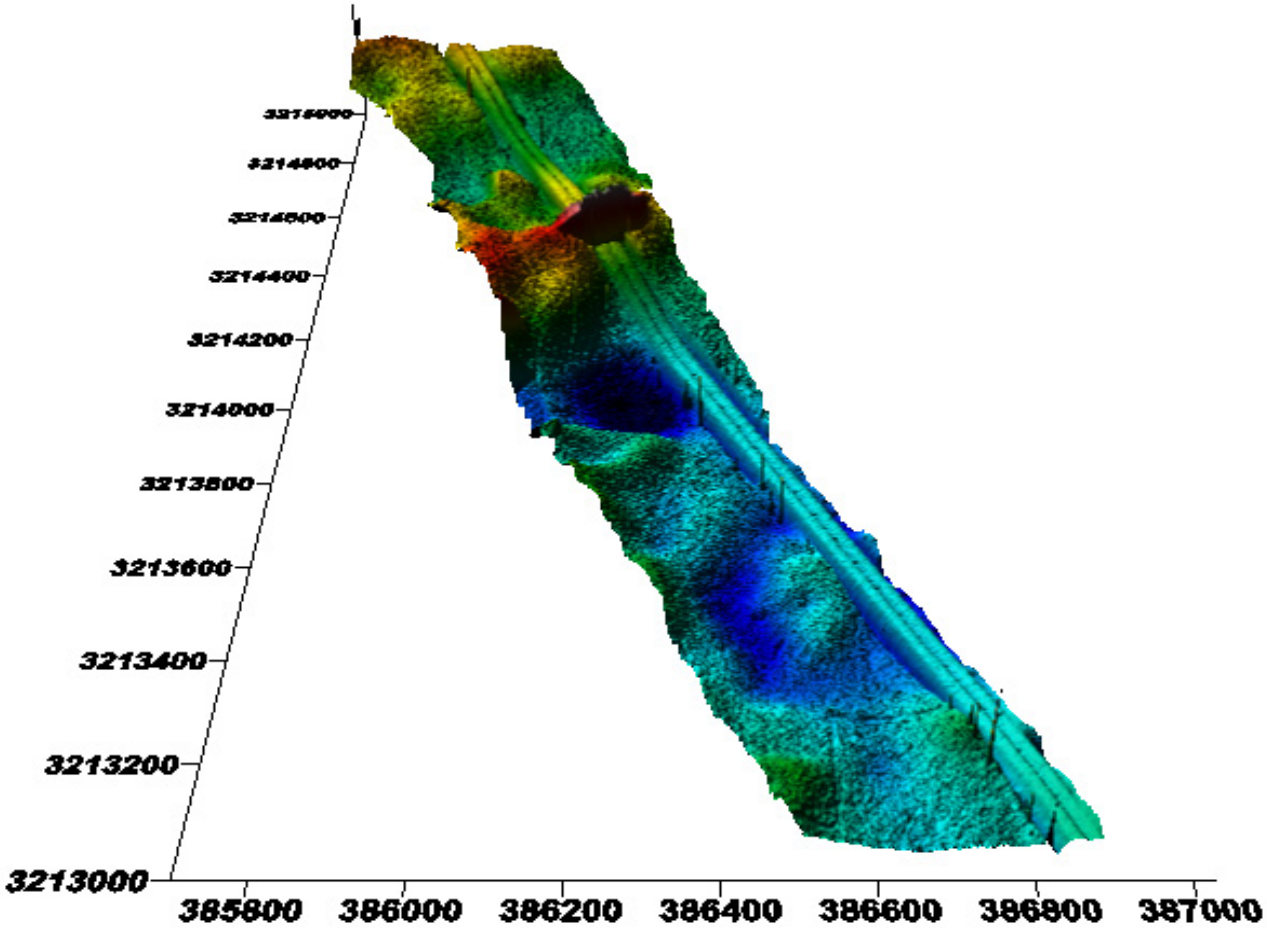

Figure 5-7. False Color Image. Blue indicates negative elevation (from an arbitrary datum, red above)

Once the data collect and analysis was completed, a second overflight was performed 8 months later to note any substantive differences.

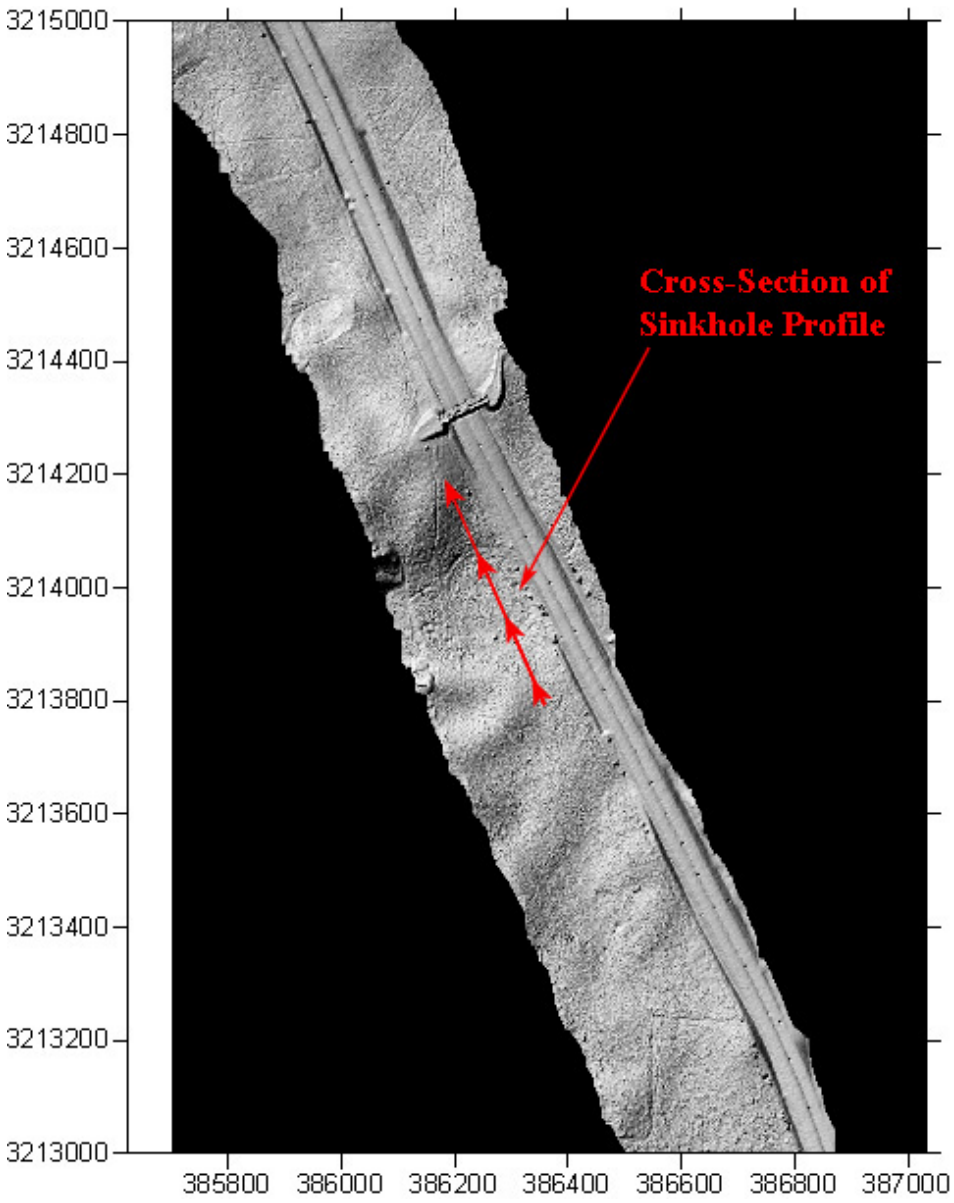

Figure 5-8. Cross Sectional cut along depression, i.e., a “Sinkhole”

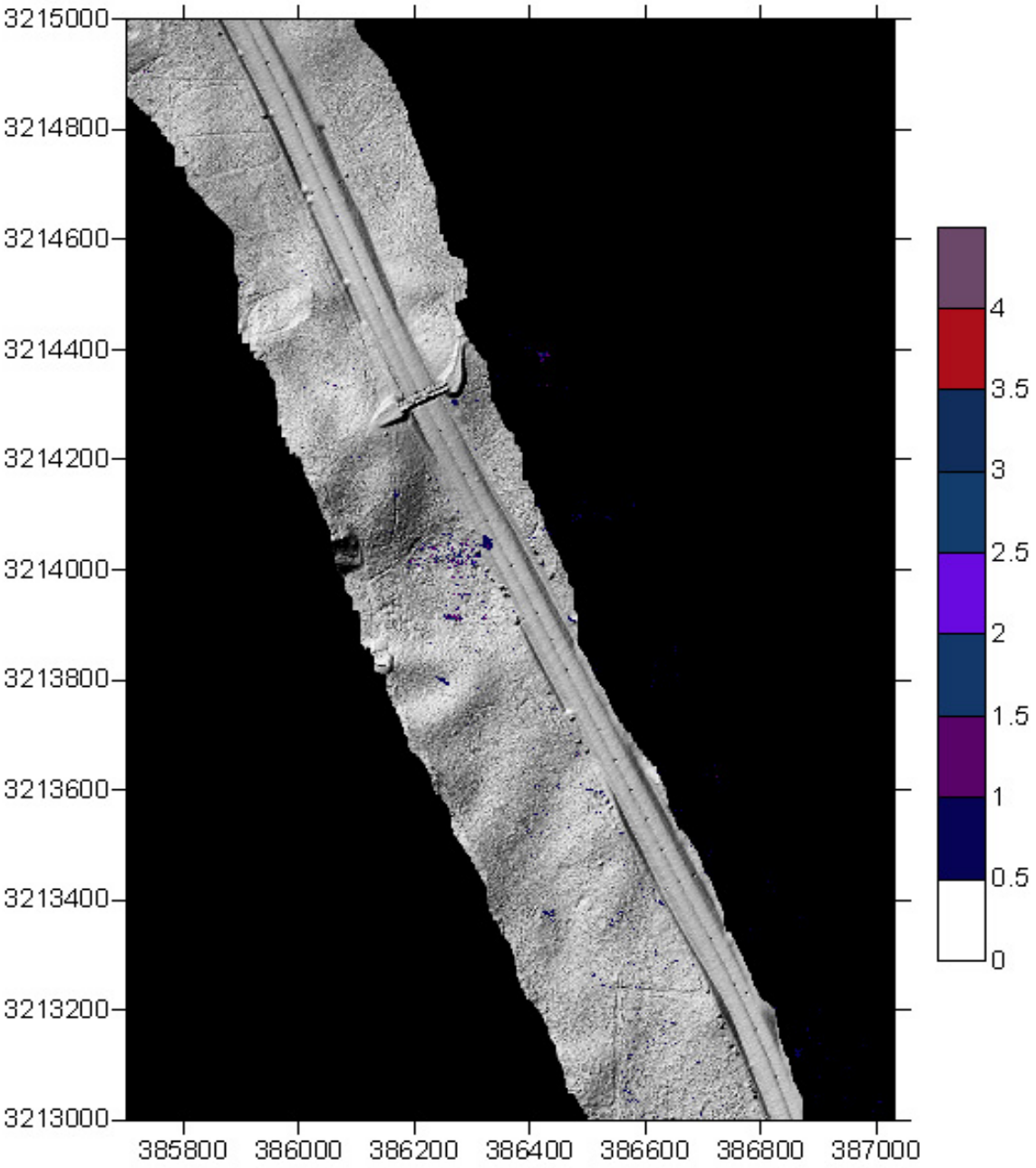

Figure 5-9. Difference between 1st and 2nd overflights

As can be seen in the figure above, there are several distinct blue areas that show a difference in elevation between flights.

A third flight was conducted 12 months after the second. The figure below indicates that very little elevation change has occurred. There is some difference, but as previously mentioned, data

“noise” could be corrupting the observed changes.

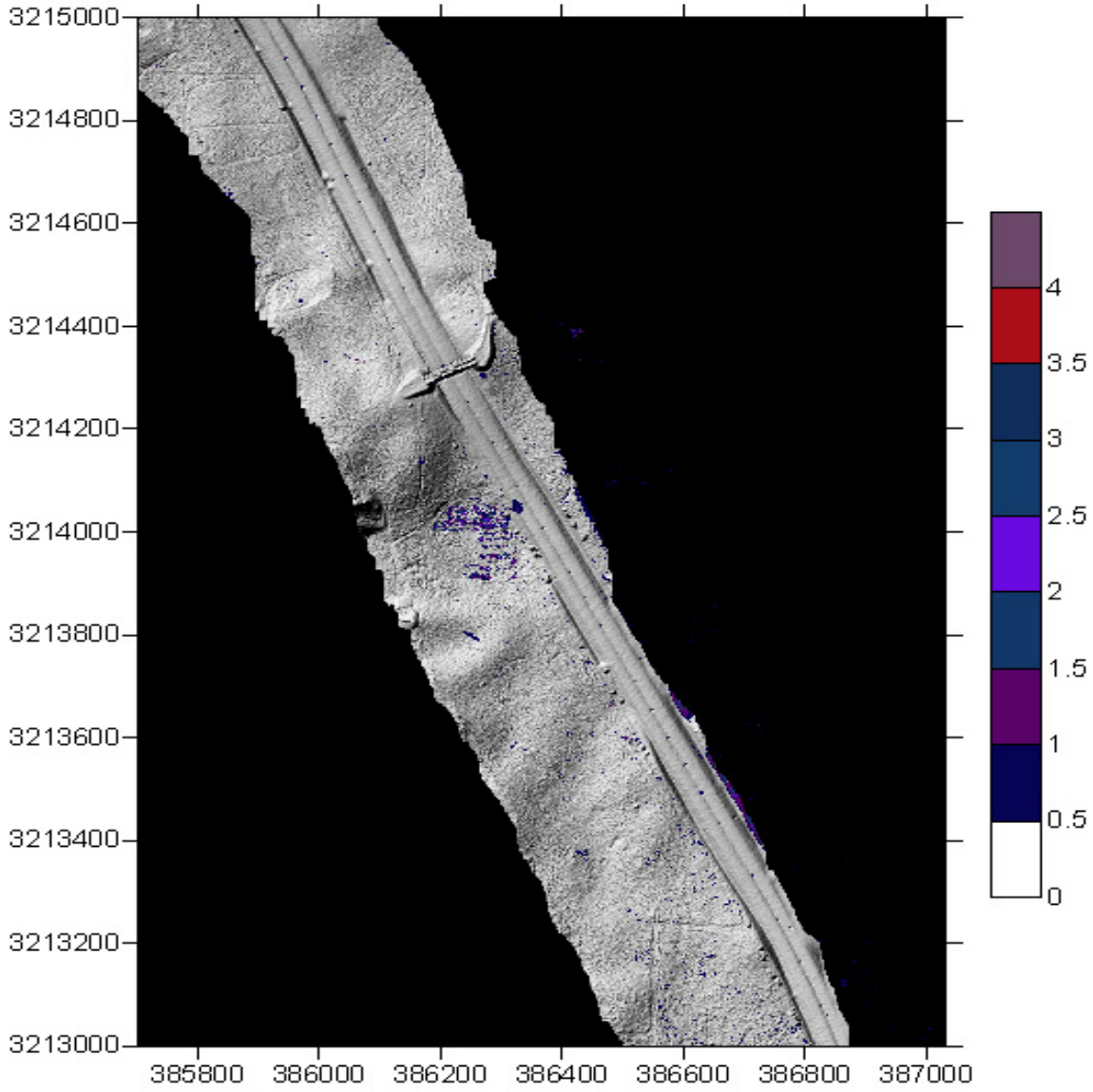

Figure 5-10. Difference between 1st and 3rd overflights

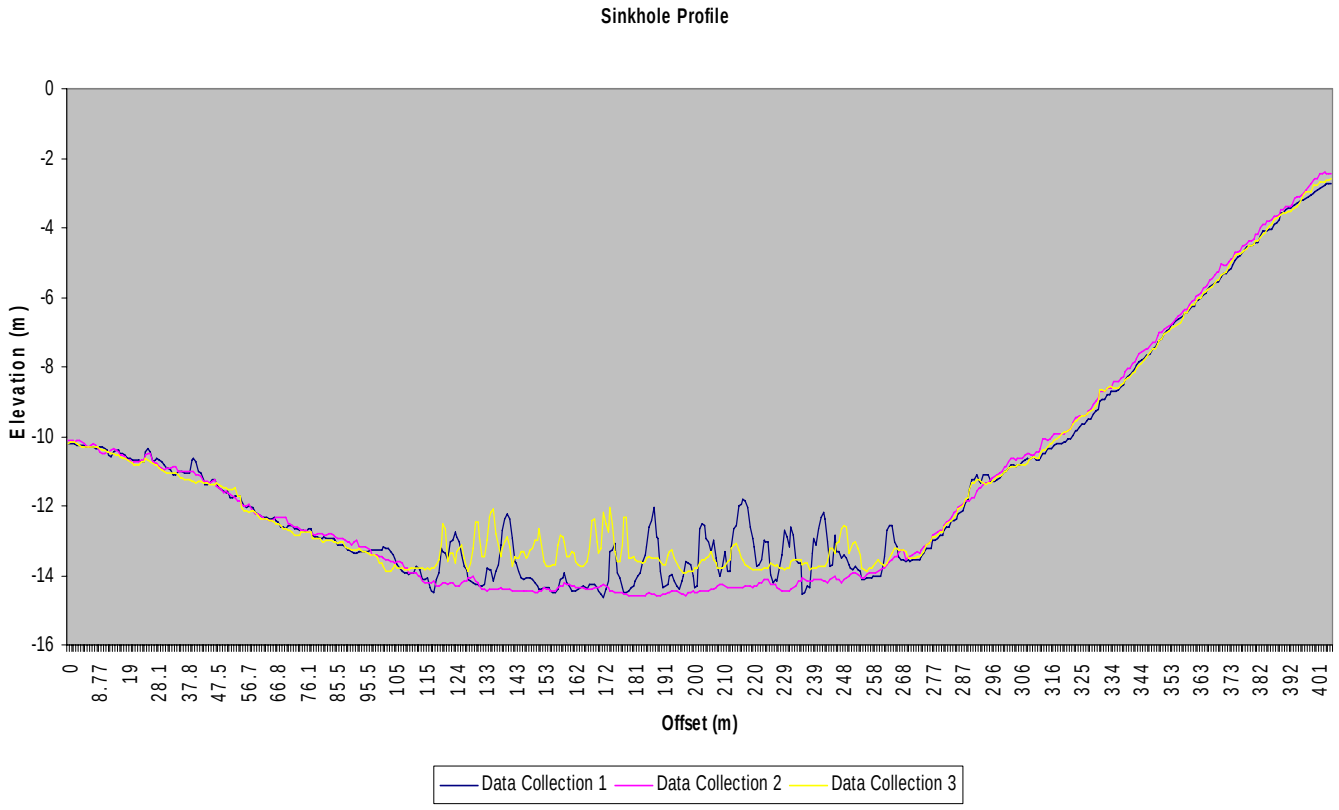

Figure 5-11. Cross sectional view of depression.

As can be seen from the above figure, the changes are affected by relatively high frequency scatter in the data. It is interesting to note that data collections 1 and 3 occurred during the spring and summer months, while flight 2 was performed during the winter. Thus it is a reasonable supposition that ground cover or vegetation is the culprit. The side slope differences are very similar, indicating that the bottom of the depression collects or provides additional moisture for the vegetation to flourish.

The next site of interest is located in the same vicinity, i.e., along SR 66. Below is the raw DEM of the roadway and a circled area of interest.

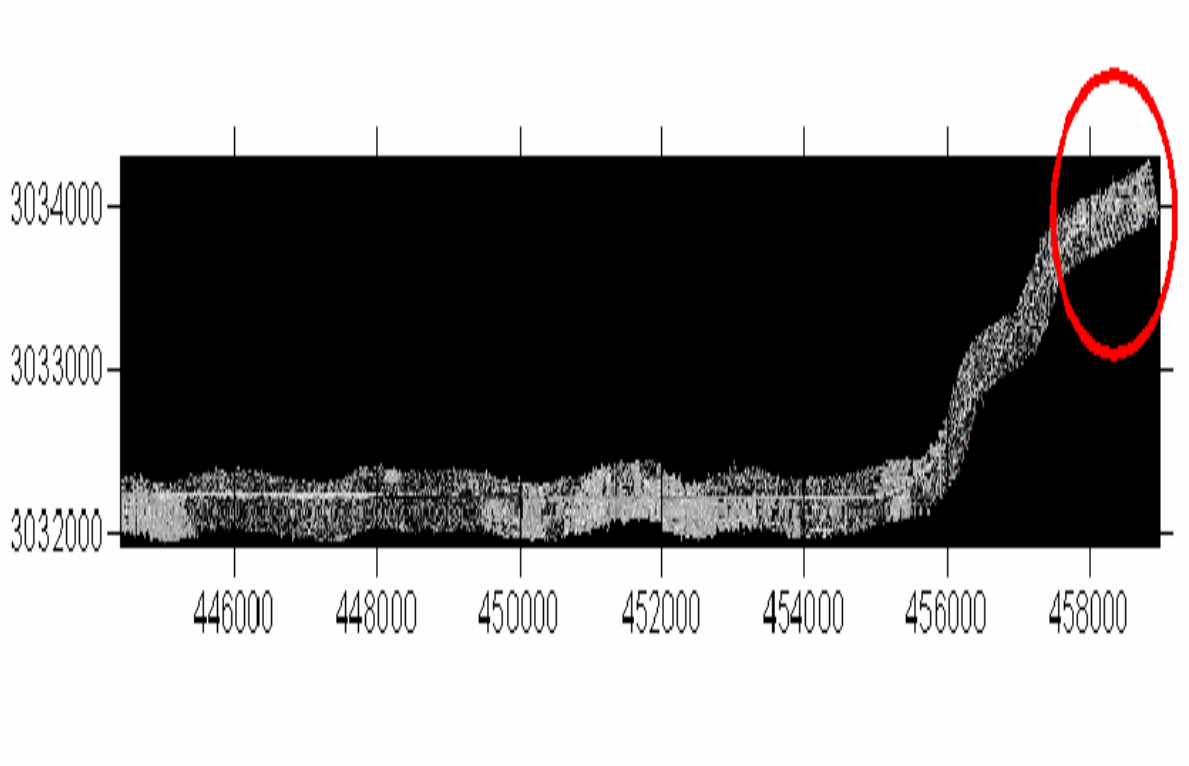

Figure 5-12.SR 66 - Second Area of Interest – the targeted zone is just off the right side of the figure, but zoomed in Figure 5-13 below.

Figure 5-13. Close up DEM of area of interest.

Figure 5-13. Bare Earth DEM of SR 66. Area of interest is 458200 east, 3033850 North.

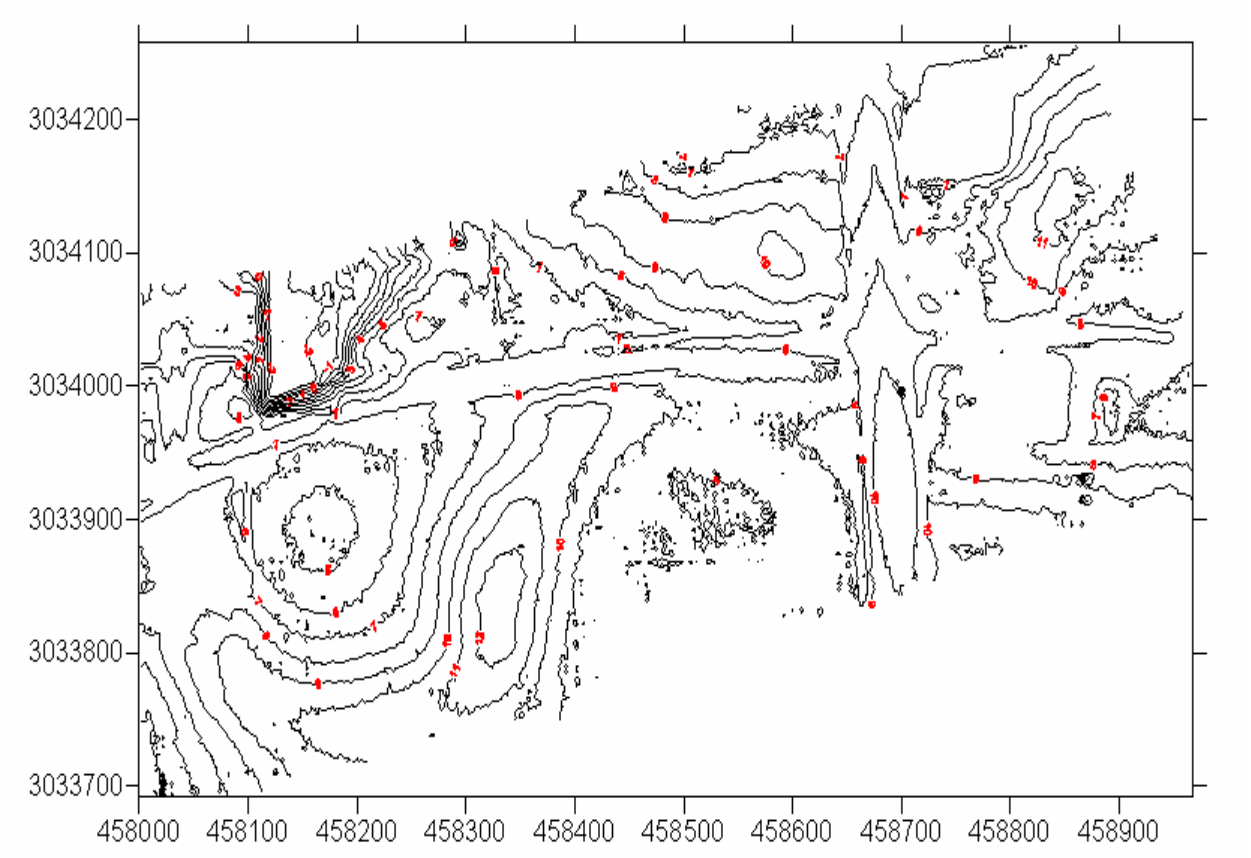

Figure 5-14. Bare Earth DEM Contour Map. Note circular contours at the lower left of the figure.

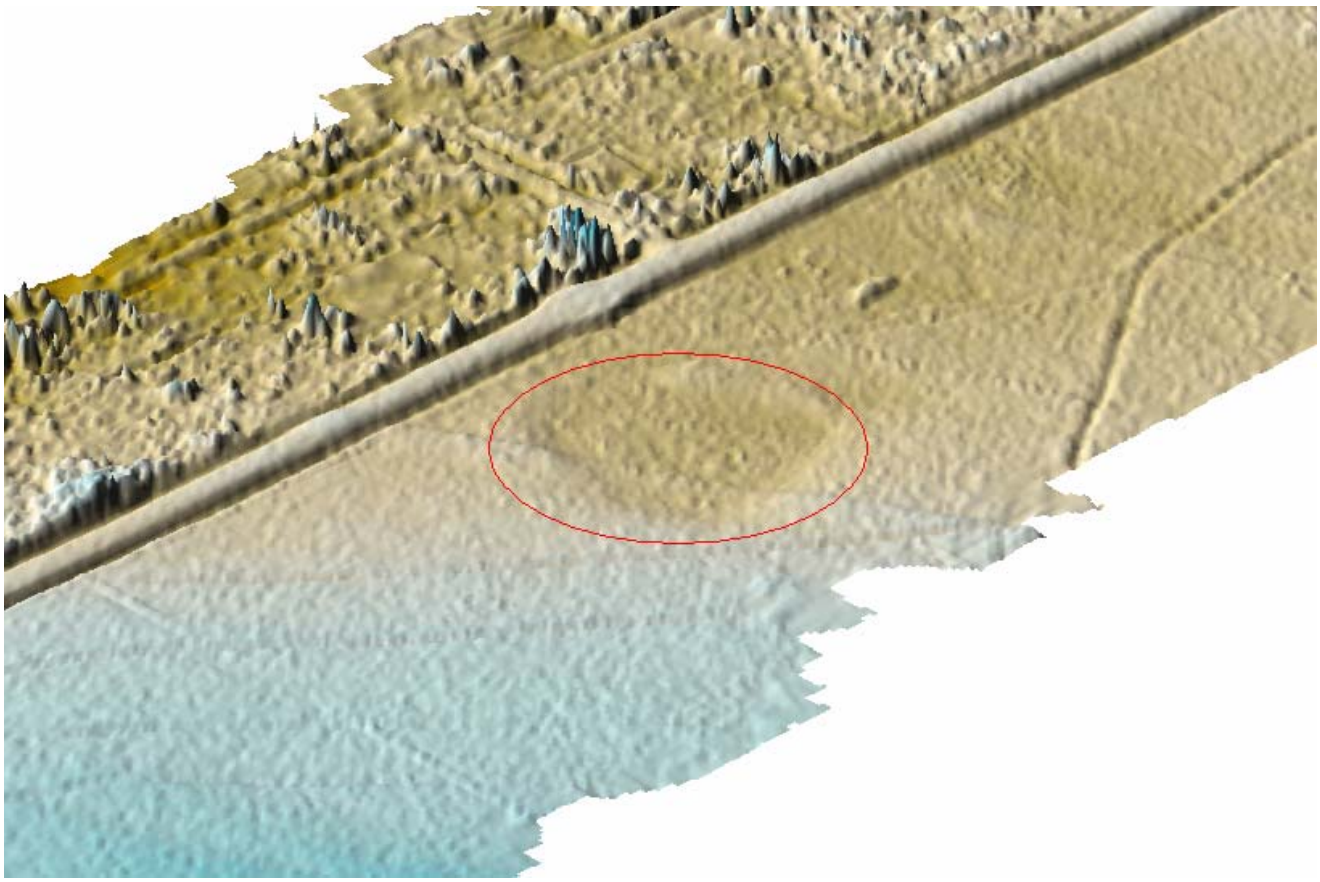

Figure 5-15. False color image of targeted area.

A second flight was performed 10 months after the initial overflight. A comparison was then made between the two and the differences computed as shown in figure 5-16.

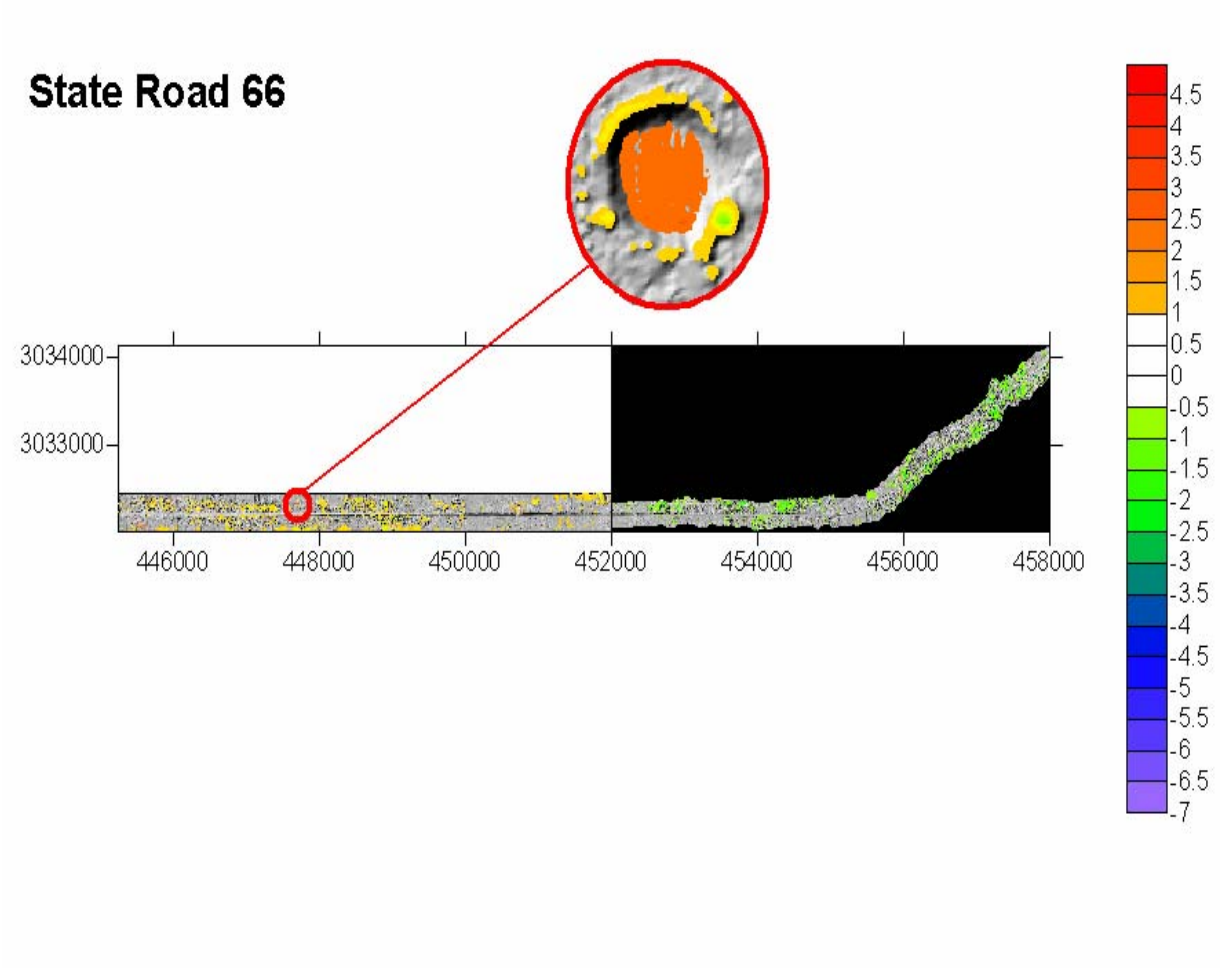

Figure 5-16. False Color Image showing elevation differences between successive flights.

While the striking differences were apparent, after observing the regular geometry of the changes, it was obvious that this was caused by human activity. In fact, one can see that the excavated material was stockpiled along the perimeter of the depression.

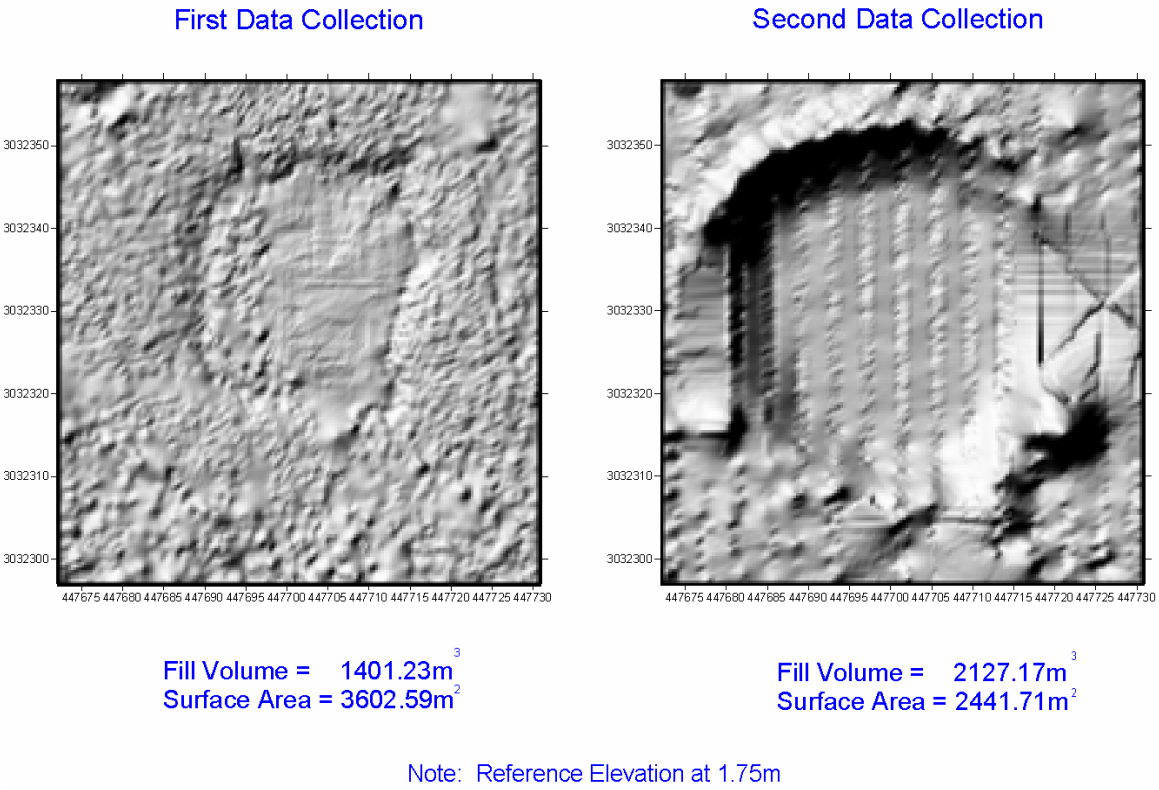

Figure 5-17. DEM indicating volumetric changes.

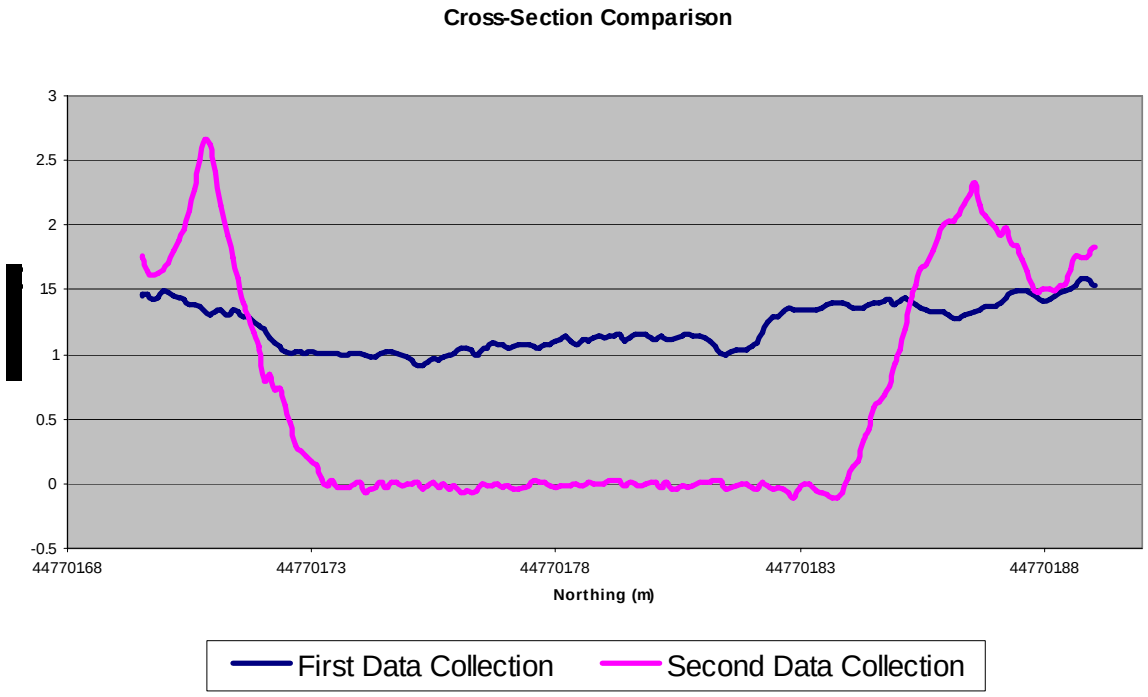

Figure 5-18. Cross Section View of successive overflights.

The most interesting site is located near High Springs, Florida. As can be seen by comparing the topographic and laser shaded relief maps, there are numerous depressions located near a secondary highway. (Upper part of figure). It is interesting to note the large number of changes that have occurred since the USGS map was produced. It appears that the area has experienced a large number of new small depressions. Hence, this area was chosen as the area in which the IR camera was also utilized and is discussed in Chapter 6.

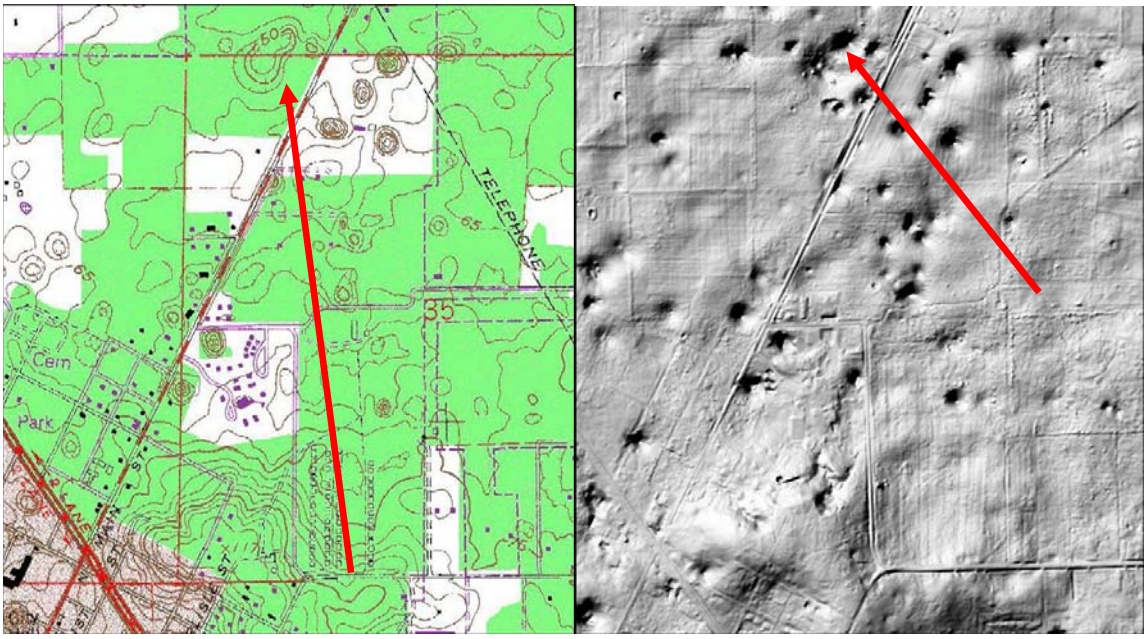

Figure 5-19. High Springs, Florida FDOT research area of interest.

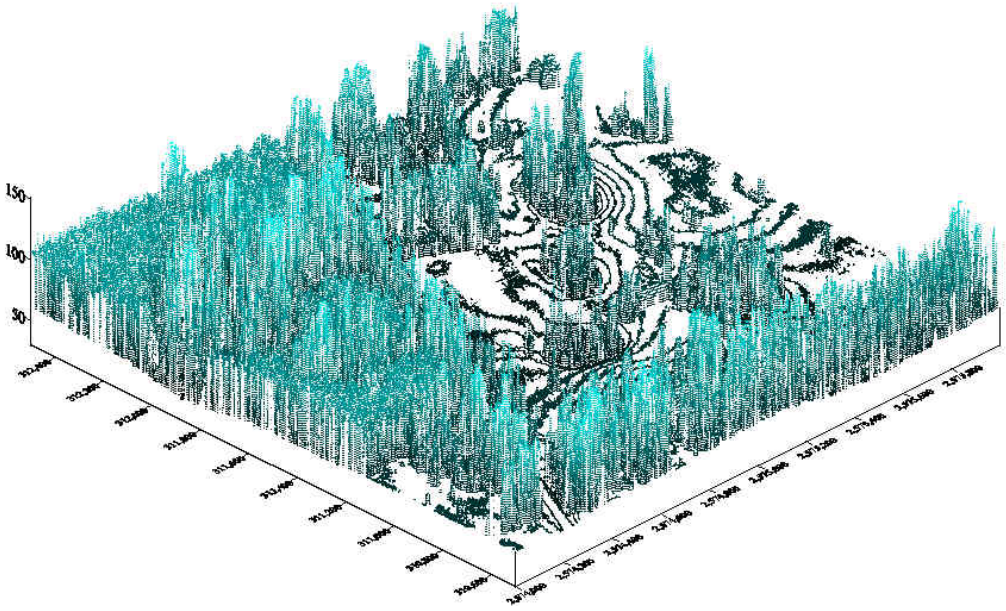

Figure 5-20. Pre filtered 3D DEM of area of interest.

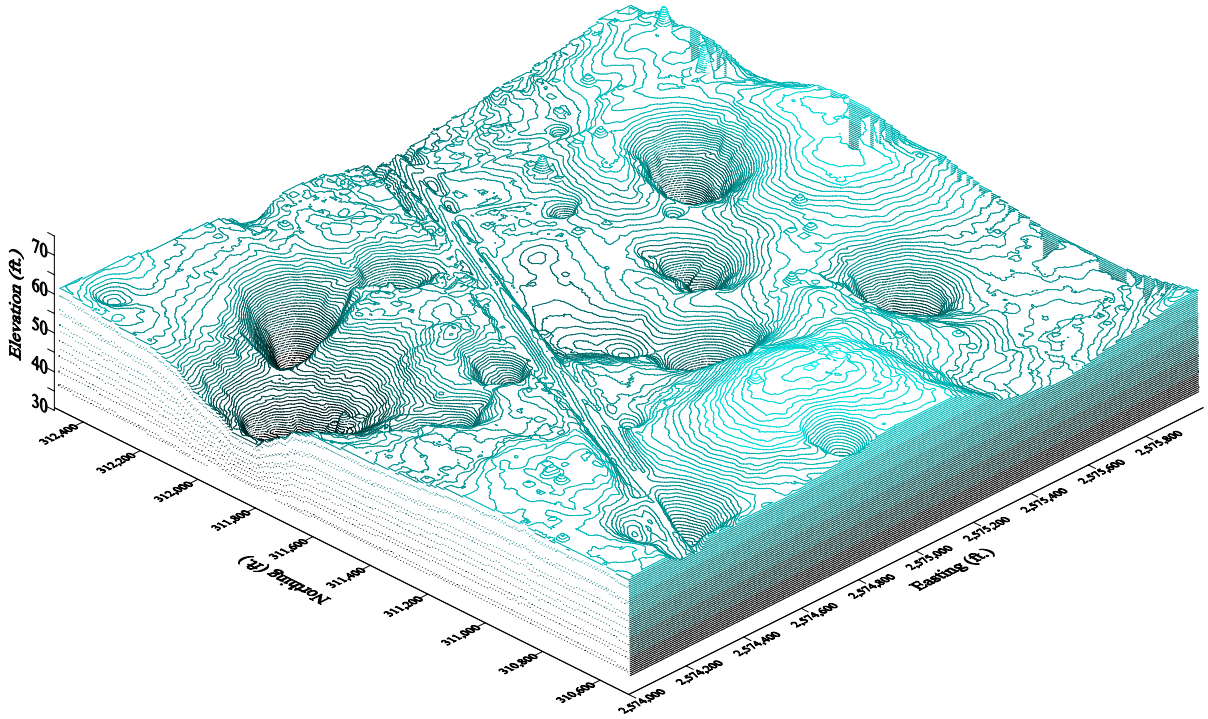

Figure 5-23. Post filtered 3D DEM

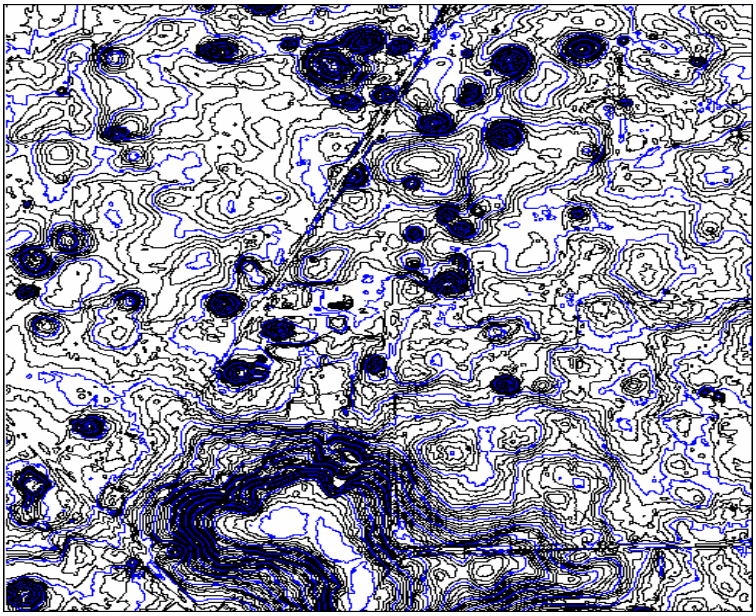

Figure 5-24. Contour Map of area. Note that these are 1 foot contours.

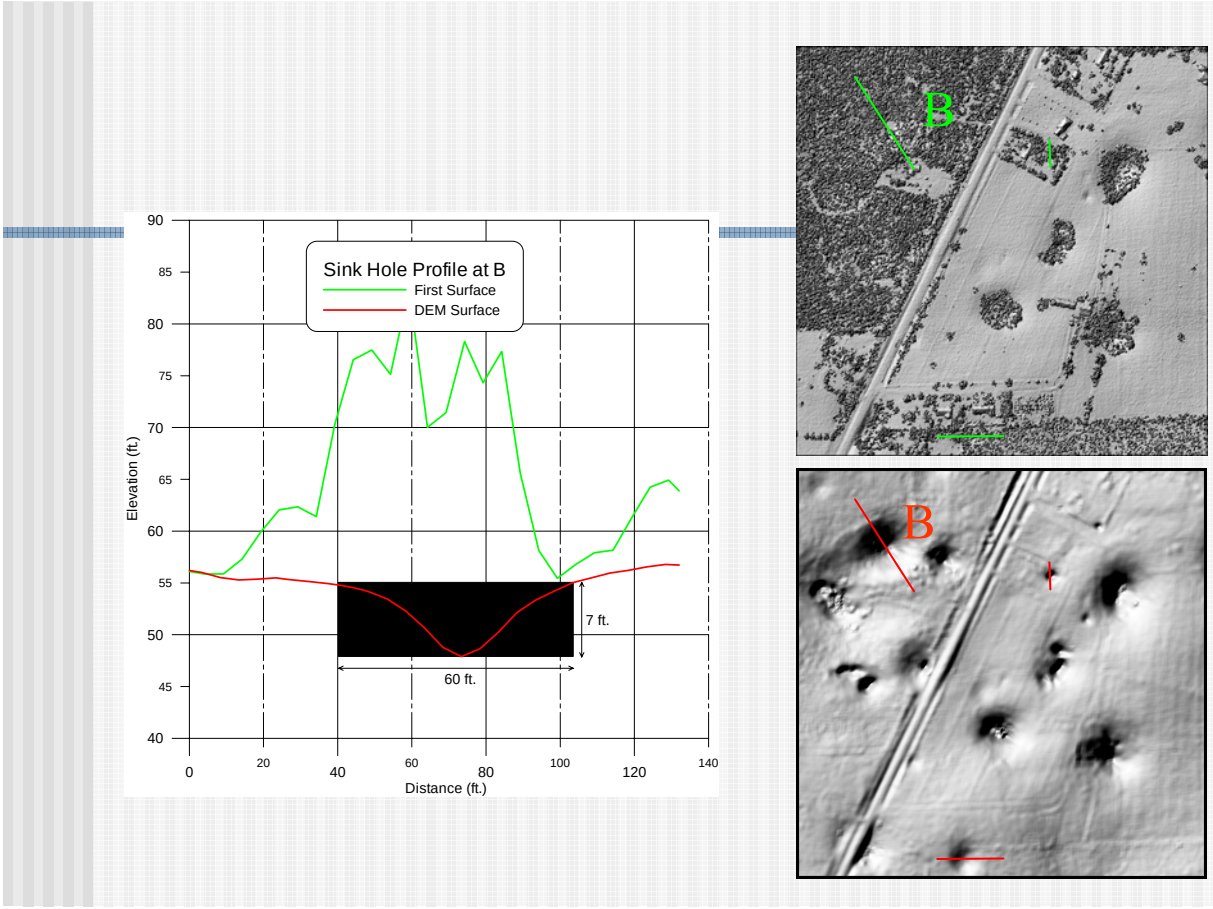

Figure 5-25. Cross Section of a depression. The green line indicates tree branches/leaves.

Summary of ALSM Collection/Processing

Based on the multiple overflights and data analysis (over 800 hours), it is apparent that the level of detail necessary to monitor quantifiable temporal topographic events via ALSM is not feasible at the current state of technology. As was pointed out, there are several variables that have a tremendous affect on the output and hence confidence interval.

For example, GPS satellite orientation, known as PDOP (Position Dilution of Precision) often varies during a flight and can corrupt the collection data, hence the final product's accuracy.

The instability of the atmosphere – especially during the summer months – creates up and down drafts that alter the trajectory of the aircraft. Any violent motion of the airplane overwhelms the IMU (inertia measurement unit) making it unable to adequately correct and account for the orientation of the laser pulses.

Vegetation, especially thick under brush prevents pulses from reaching the ground surface. This condition translates into an incorrect DEM and greatly complicates comparisons amongst successive flights.

Finally, how a particular data processor processes the information will affect the results.

However, the effort expended did yield valuable information. That is to say, it did point out that it can serve as a preliminary assessment tool to locate suspect areas of interest. Then, investigators can employ other geotechnical tools in order to conduct further research.

CHAPTER 6: NON-DESTRUCTIVE EVALUATION AND DETECTION USING INFRARED THERMOGRAPHY

Background

While airborne laser comparisons did not yield sufficient resolution to observe geometric changes of a suspect karst-derived feature, it nevertheless provided valuable baseline data for further research. Based on a suggestion from the FDOT technical coordinator, Peter Lai, the research focus shifted to IR usage to see if this technique would prove to be a viable complement. This chapter provides a review of infrared thermography, including other potential uses for civil engineering applications. The various ASTM approved tests are included, since it is possible that this research may be the stepping stone for a future ASTM standard for sinkhole detection. A UF PhD student, Jeff Brown, was the operator of the IR camera for the sinkhole overflights and provided the background information on IR technology.

Introduction

Infrared thermography is a non-destructive evaluation technique (NDET) that attempts to characterize the properties of a material or the behavior of a structure by monitoring its response to thermal loading. This technique is currently being used to assess a broad array of structures and materials ranging from carbon fiber reinforced polymers (CFRP) to human teeth. For sinkhole identification, the thermal loading is provided by the sun. Due to this widespread area of applicability, the field of IR thermography has grown considerably in recent decades. As improvements are made in the areas of IR cameras, data acquisition, image processing, and methods of applying controlled thermal loads, researchers in all areas of engineering are identifying new uses for this technology. Veterinarians at Sea World use IR cameras to aid in health monitoring of whales and walruses while engineers at NASA use identical cameras to detect blockages in cooling systems on the space shuttle. In fact, the astronauts are using an IR camera to observe damage on the Shuttle's heat dissipating tiles.

The purpose of this chapter is to provide an overview of the IR thermography technique and to summarize several applications in civil engineering, including the novel use for the detection of sinkholes.

History

The term "infrared" refers to a specific portion of the electromagnetic spectrum containing waves with frequencies just less than those of red visible light (*infra*red means *less than* red, see Figure 1). Another term that we are all familiar with is "ultraviolet" radiation. This refers to the portion of the electromagnetic spectrum containing waves with frequencies higher than the visible color violet. A brief discussion of how infrared waves were first discovered will help to clarify this definition as well as lay the groundwork for how IR cameras function.

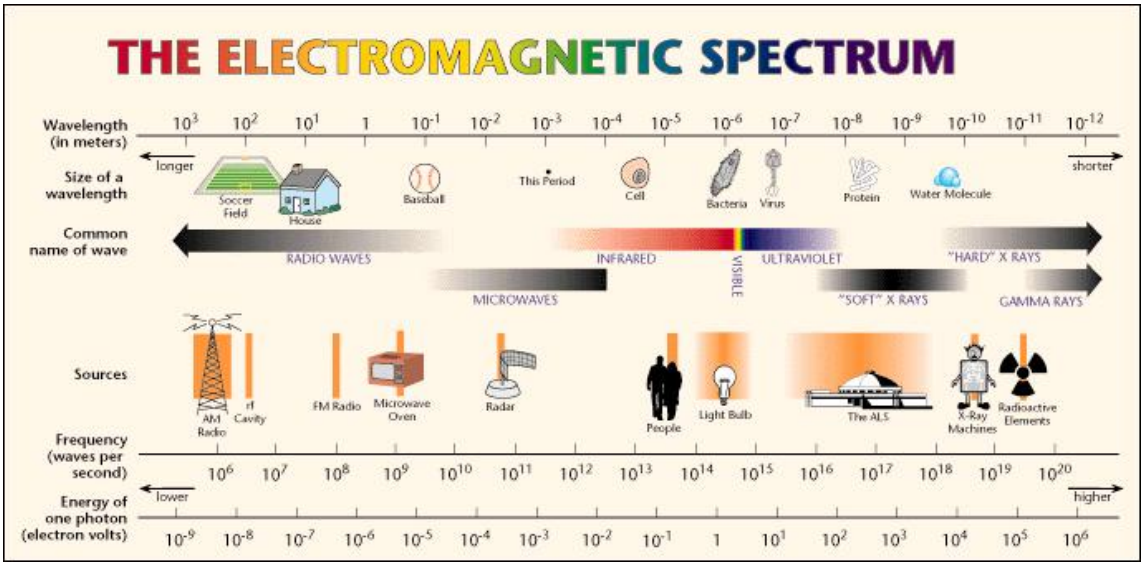

Figure 6-1: The electromagnetic spectrum

Sir William Hershel (1738-1822) was the first person to perform an experiment revealing the presence of IR waves (see Figure 6-2). The relationship between visible light and heat had long been recognized since sunlight had an obvious effect on the temperature of an object. The important observation in Hershel's experiment was that objects could still be heated if they were placed beyond the visible spectrum using a beam of light passing through a prism. It was obvious, that something was responsible for generating the heat, but it could not be observed with the naked eye.

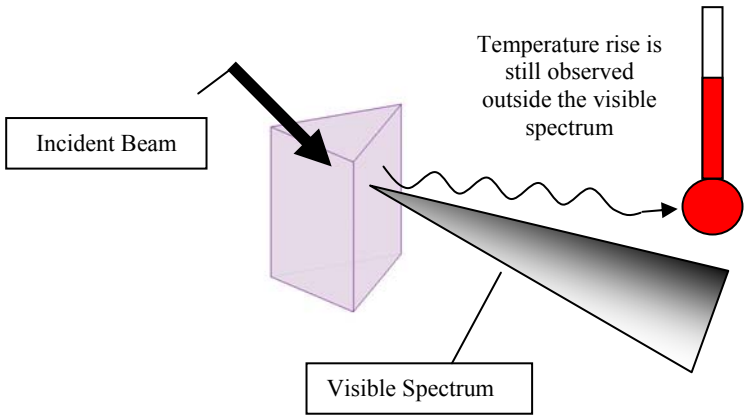

Figure 6-2: Hershel's experiment identifying the presence of IR waves

A similar experiment was performed in 1800 by William Herschel (royal astronomer to King George III of England). What Herschel noticed was that even though heating occurs due to light across the entire visible and IR spectrum, there is a specific wavelength at which the amount of heating is maximized. Herschel's son, Jon, expanded his father's work and created the first thermal image in 1840 using an evaporograph. This device consists of a thin film of oil onto which an image is projected. Due to the variations of heating across the film (as a result of the various temperatures contained in the "subject"), the oil is evaporated differentially and a "thermal" image is created.

The first person to formally quantify this phenomenon was Max Plank. Planck's theory of radiation can be summarized as follows:

- All objects emit quantities of electromagnetic radiation
- Higher temperature objects emit greater quantities of radiation.
- The electromagnetic radiation emitted from a body consists of a "broadband" signal in that it contains radiation with a spectrum of wavelengths.

- The particular wavelength containing the peak intensity of radiation varies with the temperature of the object (see Figure 6-3). This is best summarized by the Wien Displacement Law (for black body emissions):

$$\lambda_m = \frac{2898}{T}$$

where:

λ_m = wavelength corresponding to peak radiation intensity (μm)

T = temperature of object emitting radiation (K)

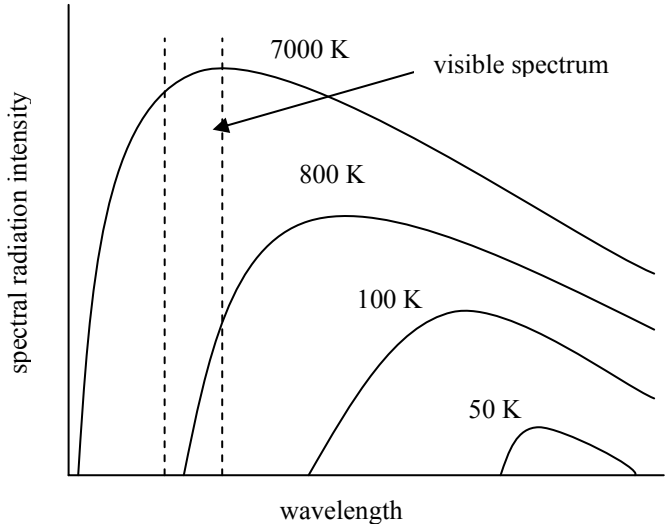

Figure 6-1: Spectral radiance of a blackbody per Planck's Law

Notice that the peak wavelength for an object at 7000 K is in the range of the visible spectrum. The sun, whose surface temperature is around 6250 K, is a good example of an object emitting radiation that falls within the visible spectrum. Other objects at lower temperatures also emit radiation that falls within the visible spectrum. A stovetop heating element near 800 K will appear to glow red even though the wavelength with peak intensity lies outside of the visible spectrum. As the temperature of the object decreases below 800 K, all of the emitted radiation lies in the IR spectrum. Thus, the earth's surface temperature, during the day and especially at

night, is dissipated or absorbed primarily in the IR regime. This signifies that using an IR camera could sense the differences in temperature between dissimilar soil/moisture conditions.

Thermal and Photonic Detectors

Prior to Max Planck's formulations regarding radiation emissions, several devices (in addition to the traditional thermometer) had been invented to measure the temperature of an object. The first thermocouple was invented in 1829 by Leopoldo Nobili. This device is a contact sensor that produces a differential voltage proportional to the temperature difference between the contact point and a reference point. Macedonio Melloni improved this concept and developed a thermopile (basically a group of thermocouples arranged in series to increase the sensitivity) capable of detecting the heat radiating from a human at a distance of 10 m. This device relied on a direct increase in temperature on the detector surface as a result of the incoming radiation. The bolometer, invented in 1880, works on a similar principal except that the increase in temperature on the detector surface results in a change in the electrical conductivity of the detector surface.

After Max Planck's theoretical formulation, the relationship between the electromagnetic spectrum and the IR phenomenon was heavily utilized in the development of photonic detectors. Previous detectors relied on a direct heating of the detector surface. Photonic detectors rely on a direct interaction between the IR photons and the detector surface (see Figure 6-4). This technology can be combined with standard video camera scanning and optics in order to form 2-dimensional infrared images.

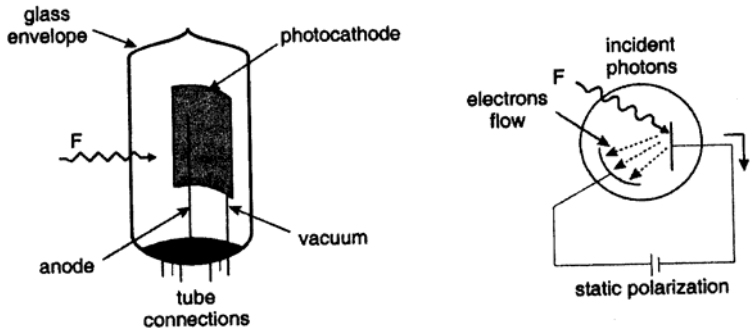

Figure 6-2: Schematic of photoemssive detector (from Maldague, 2001)

One final advancement that bears mentioning is the development of scanning radiometers. These devices are capable generating 320 x 240 pixel digital images containing the exact temperature data for each pixel. The precise temperature data is obtained by comparing the IR image signal to the signal generated by an internal reference object. Depending on the data acquisition system employed, thermal images containing 76,800 unique temperature values can be obtained at a rate of 50 to 60 frames per second (see Figure 6-5).

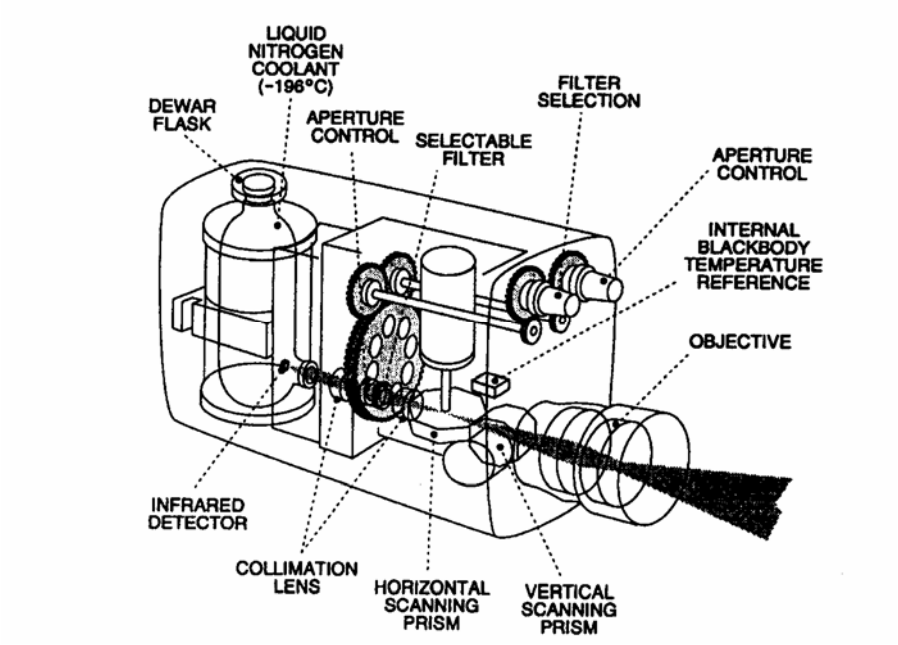

Figure 6-3: Schematic of scanning radiometer IR camera (from Maldague, 2001)

Fortunately, the newer cameras (as was used in this research) eliminate the cold reference datum (liquid nitrogen) which greatly reduces the cost and operational difficulties. The currently available IR cameras are typically purchased for a specific inspection task. Hence, there are three basic parameters to consider:

- Spectral Range
- Field of View
- Minimum Resolvable Temperature Difference

Spectral range refers to the region of the IR spectrum that the camera is designed to detect. The IR spectrum is divided into three loose regions based on the wavelength of the radiation: near IR (0.7 to 5 microns), mid IR (5 to 25 microns), and far IR (25 – 200 microns). As a general rule, hotter objects emit radiation with shorter wavelengths and colder objects emit radiation with longer wavelengths. The human body, at normal temperature, emits radiation most strongly near 10 microns. IR camera detectors and optics are designed to function in a specific IR range, so it is important to know the temperature range of the object you are trying to measure. ASTM provides guidelines for choosing spectral range depending on the particular application. For example, thermal insulation inspection of buildings requires a camera that operates in the range between 2 and 14 microns (ASTM C1060-90). It bears mentioning that terrestrial radiation (the IR signature of the earth's surface, is in the 4 μm (micron) range.

Field of View (FOV) is shown in Figure 6-6. In order to maximize the size of the object under consideration in the thermal image, it is useful to know the size of the object and from what distance the object will be inspected. For the case of wet insulation detection in roofing systems, ASTM C1153-97 provides information on how to determine the minimum required FOV for walkover surveys (given as 0.21 rad H x 0.10 rad V) and elevated vantage point surveys (FOV_h = 1.0/d , FOV_v = 0.5/d), and aerial surveys (0.10 rad H x 0.05 rad V). The latter specs are relevant for sinkhole examination.

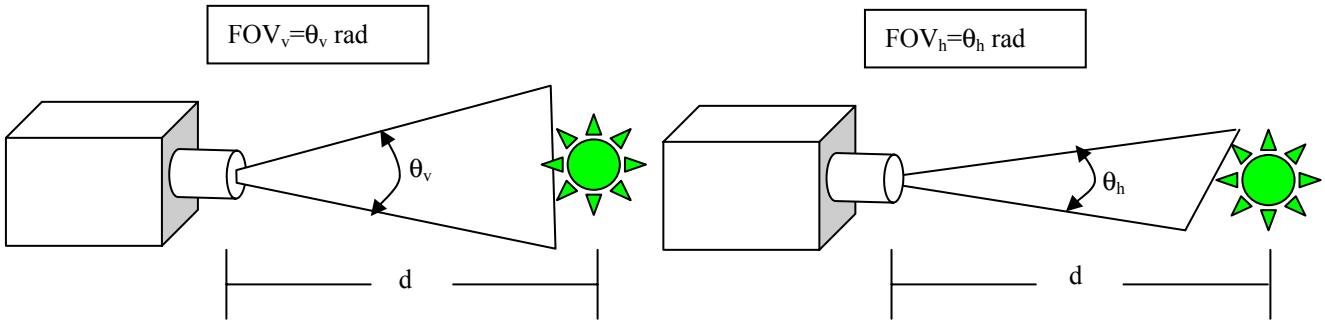

Figure 6-4: Field of View for typical IR camera

Minimum resolvable temperature difference (MRTD) is a measure of the smallest detectable change in temperature between adjacent pixels on the output image. Higher quality cameras usually have lower MRTDs, however, there is a trade off in cost and spectral range capabilities. The particular application usually dictates the required MRTD. For qualitative passive thermography applications, temperature changes are usually very slow and cover a large range. As a result, higher MRDT values are acceptable. On the other hand, laboratory experiments that involve rapid application of heat and slight variations in temperature require lower MRDTs. Once again, ASTM provides information on the minimum allowable MRDT for particular tests. ASTM D4788-88 specifies a MRDT of 0.2 K for detecting delaminations in bridge decks using IR thermography. However, for measuring the slow cooling or heating of the ground, the MRDT can be much higher. What was required for this project was an additional lens (akin to a telephoto camera lens) to provide the correct FOV for aerial work.

Emissivity

Since IR waves are essentially the same as visible light waves, it is important to understand how they interact with the surface (the soil) being measured. For example, if an infrared camera is pointed at a mirror that is reflecting the image of a person's hand, a traditional camera will accurately portray a photograph of the hand. Hence, if IR waves are the same as visible light waves, an IR camera should also produce an accurate thermograph depicting the surface temperature data of the hand. But the mirror's temperature is most likely cooler than a person's hand, so what is the temperature one is recording? This quandary exists when taking IR readings of surface waters that are calm and act like the above mirror. Fortunately, the water of interest in this project is below ground and does not contribute to the uncertainty produced by this condition.

For IR thermography images to contain *the desired* temperature data, it is important to distinguish between the radiation emitted from an object (which is related to its temperature) and radiation that is reflected off of the object from other sources. Emissivity (ε) is the quantity used to describe a particular surface's ability to absorb and emit radiation. For the case of a "blackbody", the emissivity is assumed to be 1. This means that all of the incident radiation falling on the surface is absorbed and results in an increase in temperature of the object. This

increase in temperature then results in increased radiation by the object. For the case of a mirrored surface (a perfect reflector), the emissivity is assumed to be zero. This implies that none of the radiation being emitted by the surface was actually generated by the object.

Emissivities for common engineering materials are provided in Table 6-1. Note that materials with a low emissivity are not particularly well suited for inspection by IR thermography. However, it is possible to increase the emissivity of shiny objects by treating the surface with flat paint.

Another interesting point involves the emissivity of glass. The relatively high value of .94 indicates that glass is essentially opaque to IR waves. As a result, an IR camera pointed at a glass window will provide temperature information for the glass surface as opposed to the temperature of any visible objects on the other side. This phenomenon is of significant

importance when considering which materials are suitable for use in IR camera lenses and associated optics.

Table 6-1: Emissivities of Common Civil Engineering Materials

Material	Emissivity
Steel Buffed	0.16
Oxidized	0.80
Concrete	0.92
Rock	0.93
Soil	***0.92***
Graphite	0.98
Wood	0.95
Window Glass	0.94

Soil and Minerals exhibit stronger spectral features. The "restralen" bands of quartz sand cause strong spectral features between 8 and 10 microns that depend on the grain size. The signature in the 3 to 5 µm region depends strongly on the water and organic content. The dryer, purer soils have lower emissivities. (UCSB Library)

Water has very high emissivities, ranging from 0.98 to 0.995. This attribute can help identify high water content soils such as one might encounter in a clay rich environment. This is especially true during periods of dry weather. As can be seen in the graph below, even a "dry" hardpan retains sufficient adsorbed (as opposed to absorbed) water to generate a high IR signature. (UCSB Library). Thus, based on the information gleaned from the literature, the most efficacious conditions for locating sinkholes would occur during mid afternoon in the summer and with a lack of rain preceding the data collection. This would also help reduce any vegetation influences, since they also emit high IR energy. However, it would be reasonable to assume that during periods of drought, vegetation growing in well drained soils would lose more water than their clay/silt neighbors.

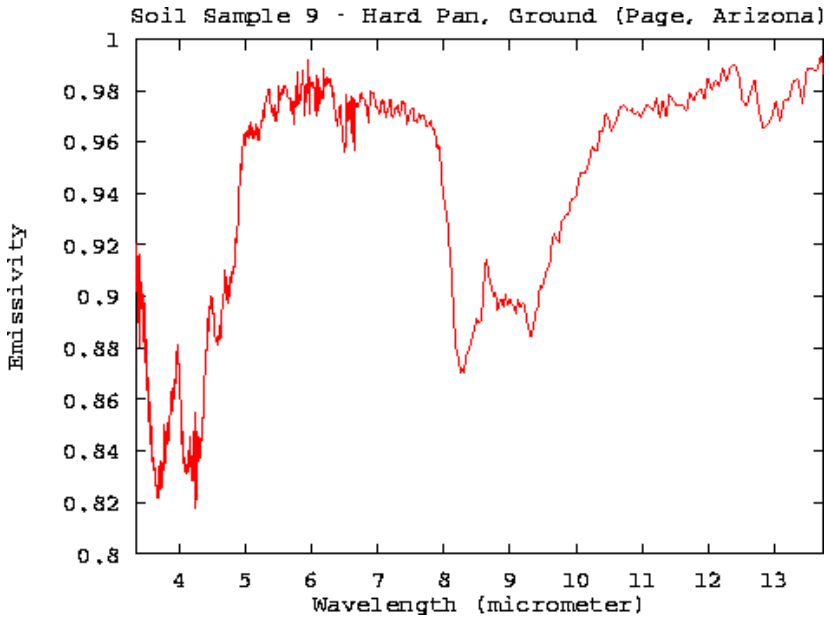

Figure 6-7: Emissivity versus Soil Particle Size (as a function of wave length)

ASTM C1371-97 outlines a standard test method for determining the emissivity of a material at room temperatures. A portable emissometer (shown in Figure 6-8) is used to compare the emittance of a specimen to the emittance of two objects with known emissivity (one high and one low). The heat sink ensures that the temperatures of all three objects are the same while the thermopile temperature sensor in the emissometer provides an output voltage proportional to the amount of heat radiated by each object. The emissivity of the test specimen can then be obtained by linear interpolation.

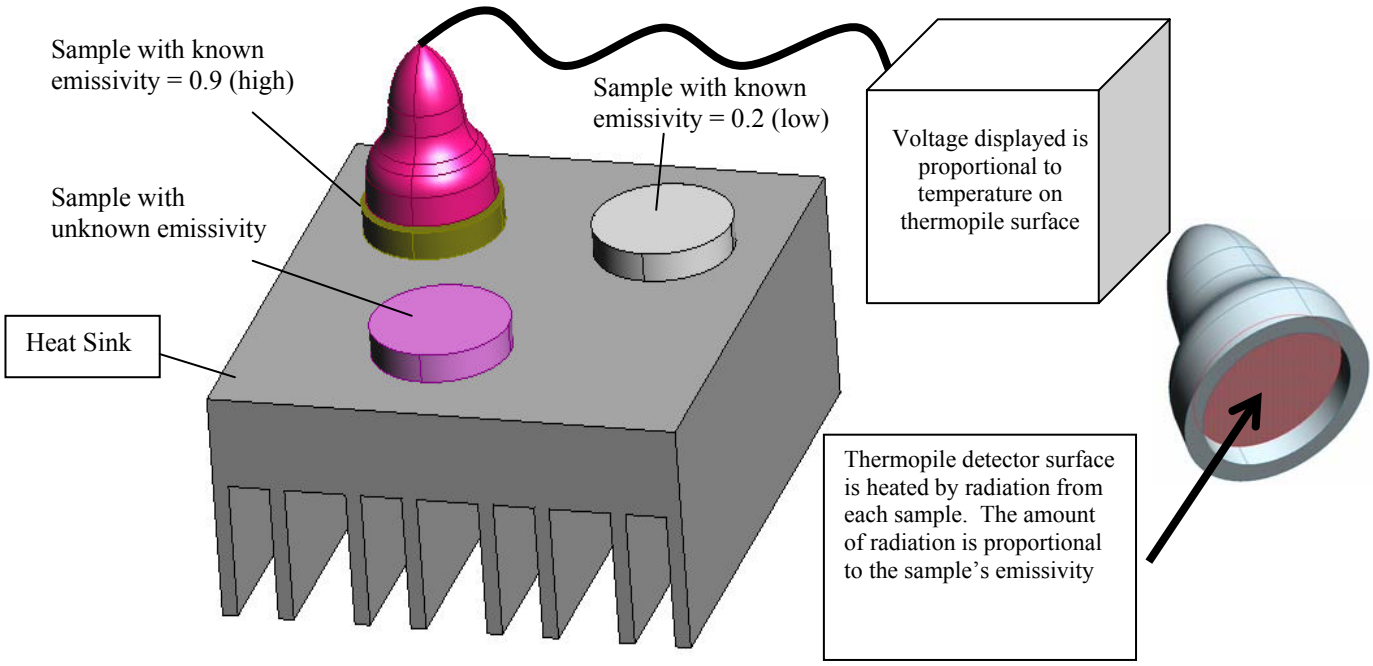

Figure 6-8: Test setup for determining emissivity using portable emissometer

IR Thermography and Material Assessment

IR thermography was first used as a non-destructive evaluation technique for civil engineering materials. That is because sound and damaged materials have different thermal conductivity properties. If a constant heat flux is applied to the surface of a uniform homogeneous material, the increase in temperature on the surface of the object should be uniform. If, however, the material is non-homogeneous, the temperature along the surface will vary (see Figure 6-9).

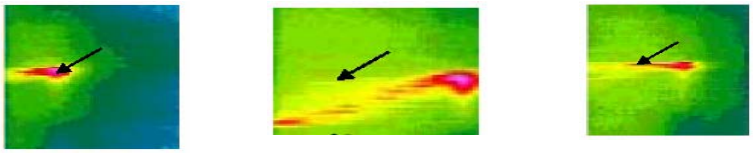

Figure 6-9: Typical thermograph revealing defects

Since the ground surface (and below) is rarely homogeneous, it should provide the necessary contrast in temperature to distinguish at least qualitatively the boundaries of the soil horizons. This was the idea on attempting to use IR to remotely identify anomalous patterns of temperature differences, even though they may appear, from the surface, to be made up of the same soil type.

Passive Thermography

Passive IR thermography is the most convenient process to perform and involves collecting temperature data from a scene or object without applying an external heat source. Of course, the sun does heat up the earth's surface, but if the data collection occurs at night, it does not classify as an external source since the entire area of interest, i.e., the sinkhole and surrounding soil is being cooled. This method provides qualitative information about a location and can be used to quickly determine if a problem might exist. For example, in the construction industry, passive IR thermography has been used for many years to evaluate thermal insulation in buildings and moisture infiltration in roofs (ASTM C1060-90 and ASTM C1153 – 97, respectively). Passive thermography is also used to detect delaminations in reinforced concrete bridge decks (ASTM D4788-88). While this research project attempts to use IR thermography for locating sinkholes, to our knowledge this has not been attempted in the past. However, illustrating how the technique is used in other civil engineering applications can provide clues extracting pertinent information for sinkhole detection.

ASTM D4788-88: Delaminations in RC Bridge Decks

In this test, a vehicle mounted IR imaging scanner is driven slowly over the bridge deck under consideration. If the evaluation is performed during daylight hours, the delaminated areas will appear as "hot spots". During the evening as the bridge is cooling down, the delaminated areas will appear "cooler" relative to the sound bridge deck. The IR scanner can also be incorporated with an electronic distance measuring device so the resulting thermographs can be overlaid onto scaled CAD drawings. If any areas of concern appear in the thermographs, a more detailed inspection of the suspect area can be performed (usually by coring or ultrasonics).

For the delaminations to be detected, there must be a minimum temperature difference between the delaminated area and sound areas of 0.5 °C (the IR scanner must have a MRTD of 0.2 °C). The test standard indicates that roughly three hours of direct sunshine is sufficient to develop this temperature differential.

It is also specified that the bridge deck should be dry for at least 24 hours prior to testing. Windy conditions should also be avoided and care must be taken when interpreting results in areas where shade may have influenced the surface temperature distribution.

This is the likely reverse analog to the sinkhole scenario. That is to say, lack of excess moisture in the surround soil will act similar to the delaminated concrete by producing more IR energy during the daytime. Strata or zones of soil that retain moisture (clayey materials) should be cooler due to evaporation and evapotranspiration from vegetation. Alternatively, at night, the moisture rich soils will retain their latent heat and appear hotter than the cooler surrounding soils.

ASTM C1060-90: Inspection of Insulation in Buildings

This test standard describes the recommended procedure for evaluating insulation in frame walled buildings. Energy loss due to poor insulation is both costly and can also lead to structural deficiencies. Particularly in cold climates, poor insulation can lead to moisture build-up in walls and roofs that will result in damage to wood or other metals prone to corrosion.

The thermal difference between the inside and outside of the structure being examined is typically generated by the building's heating or cooling system. The standard recommends a minimum temperature difference of 10 °F for a period of at least four hours prior to the test. Special care should also be taken when monitoring the exterior surface of a building due to solar radiation and wind. No direct solar radiation should fall on the surface under consideration for a period of 3 hours for light frame construction and 8 hours for heavy masonry veneer construction. It is also specified that the wind speed be less than 15 mph across the surface being inspected.

If the above conditions are satisfied prior to the inspection, thermograph results for well-insulated buildings should contain vivid vertical lines indicating the presence of framing studs. If the exterior is cooler than the interior, the studs will appear as "hot spots" on the thermograph (the theory being that the stud provides a heat transfer corridor between the interior and the exterior). If there is any missing or damaged insulation, a warm or cool spot will appear in the thermograph.

Interpreting the thermograph is usually subjective and requires previous experience. If the surface being inspected contains different materials with varying emissivity values, the IR camera may report a thermal gradient that does not exist. Another consideration is that interior rooms may be at different temperatures. The resulting exterior temperature gradients may or may not indicate a problem.

As in the previous discussion, valuable information can be inferred from this standard as well. That is to say, in order to reduce the effects of temperature fluctuations during data collection, scans should be acquired during the day when the ambient temperature is not changing. This would mean taking readings around noon or early afternoon.

ASTM C1153-97: Inspection of Wet Insulation in Roofs

This is the situation that most closely resembles the sinkhole situation. The basic theory behind this test is that wet roofing insulation retains more heat due to the higher specific heat of water. As the sun sets in the evening, it is natural to expect a roof surface to begin cooling. If the roof has become damp, the moisture will take a longer time to cool down than the surrounding sound roof. This temperature gradient can easily be detected using an IR camera.

The ASTM standard for this test contains information that is similar to the tests for bridge deck delaminations and insulation inspection: imaging system requirements, weather conditions, and the presence of material differences in the roof construction. Separate guidelines are also provided for walkover and aerial surveys. One interesting limitation that is pointed out in the standards is that wet applied roofing insulation systems (lightweight concrete or gypsum) are not well suited to this method since they typically retain large quantities of construction moisture. Care must also be taken when attempting to assess roof systems finished with low emissivity materials.

Other details regarding environmental conditions include:

- No precipitation events within 24 hours of the inspection
- Wind speed should be less than 15 mph
- Roof surface should be free of ponded water, ice, snow, etc…

Passive Thermography Summary

Passive thermography is a non-destructive testing technique that provides qualitative information about a particular situation. Once potential problem areas have been identified, further testing (usually destructive in nature) can be conducted in the suspect areas. In geotechnical vernacular, this would consist of CPT or SPT soundings. The primary advantage of this technique is that large areas can be surveyed relatively quickly and without disruption to the users of a structure. Some typical thermographs showing defects in large structures are provided in Figure 6-10.

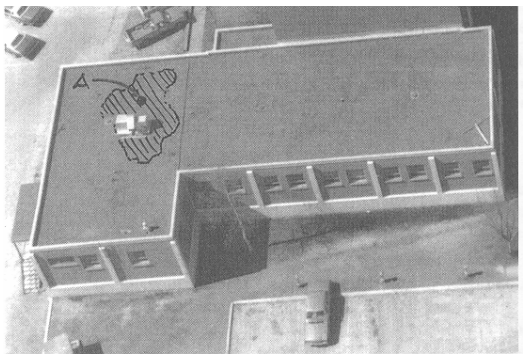

(a) Visual image of roof

(b) IR thermograph showing moisture

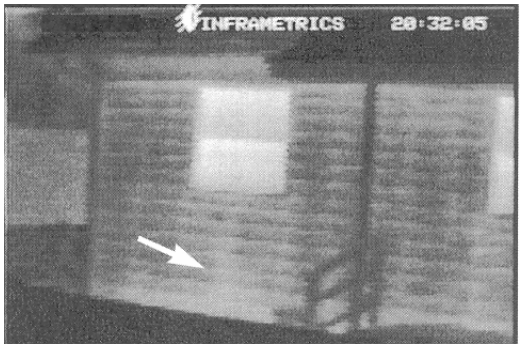

(c) Poorly insulated frame wall

Figure 6-10: Passive IR thermography examples

Active Thermography

In active thermography, heat is applied (by the inspector) to the surface of the object under investigation while an IR camera monitors the temperature variations on the surface. The advantage of active thermography over passive is that a quantitative analysis of the data collected can reveal important defect characteristics (size and depth). This type of IR thermography is not usually employed in civil engineering structures for overall health assessment since the required energy inputs would be large. It should be noted, however, that thermal input from the sun or a building's heating/cooling system and subsequent IR measurements is a form of active thermography.

Since IR thermography is only capable of monitoring the surface temperature of an object, the technique is usually limited to situations where defects are located near the surface. As defect depth increases and defect size decreases, assessment becomes more difficult. Fortunately, the near surface moisture retained in fine-grained soils, should meet this requirement. In addition,

capillary action in silt size material signifies that the IR technique indeed can be used to penetrate deeper into the surface. This is yet another possible usage of this technology. Over flight of an area (again without recent rains) could identify zones of different types soils simply by their temperature. If there is a supply of subsurface water/moisture, capillary rise would maintain a constant migration of water upwards. Hence during subsequent evaporation as it nears the surface would translate into a cooler image.

The active IR thermography technique also involves more elaborate test setups than are encountered in passive thermography. The required MRTD of IR camera equipment is smaller and heating of the specimen surface must be carefully controlled. As a result, most applications of active IR thermography are performed in a laboratory or a well controlled manufacturing environment. Current applications of active IRT include the evaluation of composite structures for delaminations, coating thickness evaluation, and the integrity of coating-substrate bonds. With the increased use of advanced composites in civil engineering structures, active IR thermography is under investigation by several researchers as a potential means of evaluating the quality of installation and long-term durability of the composite strengthening system.

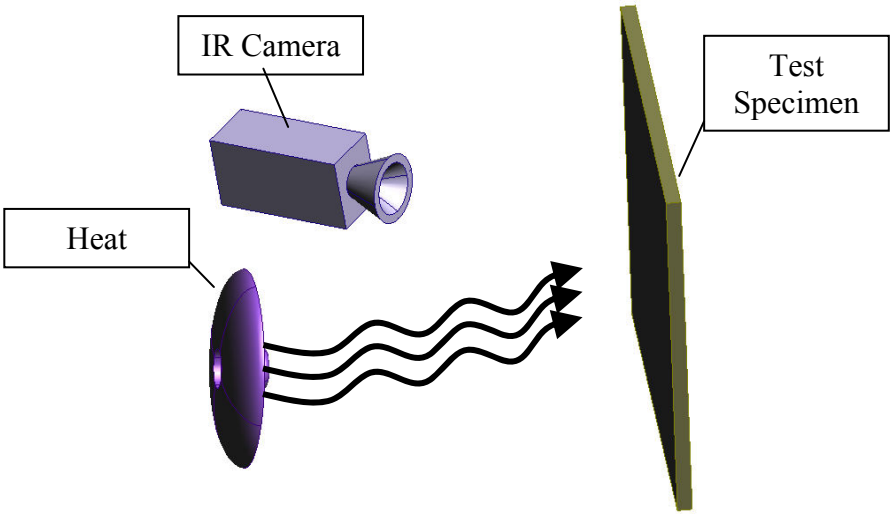

Figure 5: Active IR thermography test setup

Heat Transfer Theory

In active IRT, incident radiation on the surface of the specimen has two fundamental results: an increase in the surface temperature and the propagation of a thermal front normal to surface. If the heat flux applied to the surface is uniform and the material is homogeneous, the temperature variation in the specimen reduces to a one-dimensional heat transfer problem governed by the following differential equation:

$$\frac{d^2}{dz^2} T(z,t) - \frac{1}{\alpha} \cdot \frac{d}{dt} T(z,t) := 0$$

where:

T = temperature

z = depth (measured normal to surface)

t = time

α = thermal diffusivity

Figure 6-12 shows a graph of T (z = 0, t). In this graph, it is assumed that T (0,0) = $T_{ambient}$ (temperature at the surface is equal to ambient air temperature when t = 0) and a constant heat flux is applied from t = 0 to t = t_{hf}. During the interval when the heat flux (the sun) is applied, the temperature of the surface rises. Once the heat flux is ceases, the surface will begin to cool (following a pattern of exponential decay) as a result of convection and heat diffusion normal to the surface.

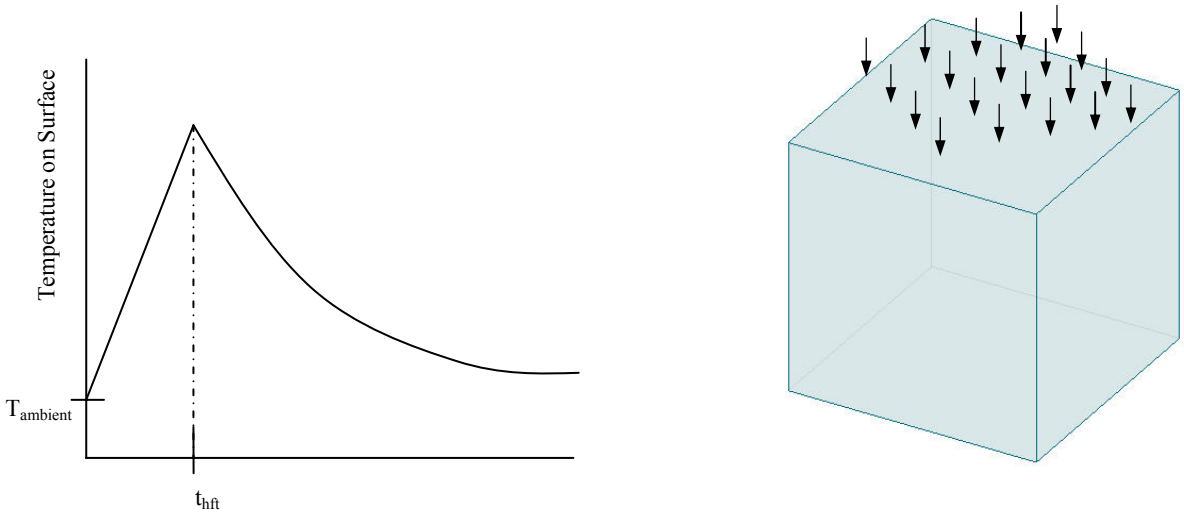

Figure 6-12: Surface temperature as a function of time for homogenous material

Now consider a case in which the area of interest contains a defect at some depth z_d below the surface. Immediately after the heat flux is applied to the surface, the thermal wave front will propagate in the same fashion as was observed in the homogeneous sample. Once the thermal front reaches the defect, however, the governing differential equation changes to the following:

$$T_{,,jjj} - \frac{1}{\alpha}\frac{dT}{dt} = 0$$

where:

$T_{,,jjj}$ = gradient of T (x,y,z,t)

Since the thermal properties of the defect are different than the surrounding sound material, the thermal front will either be absorbed more rapidly or be deflected and forced to travel around the defect. Either scenario will have some effect on the surface temperature in the area directly above the defect (assuming the defect is of sufficient size and not too deep). This phenomenon is illustrated in Figure 6-13.

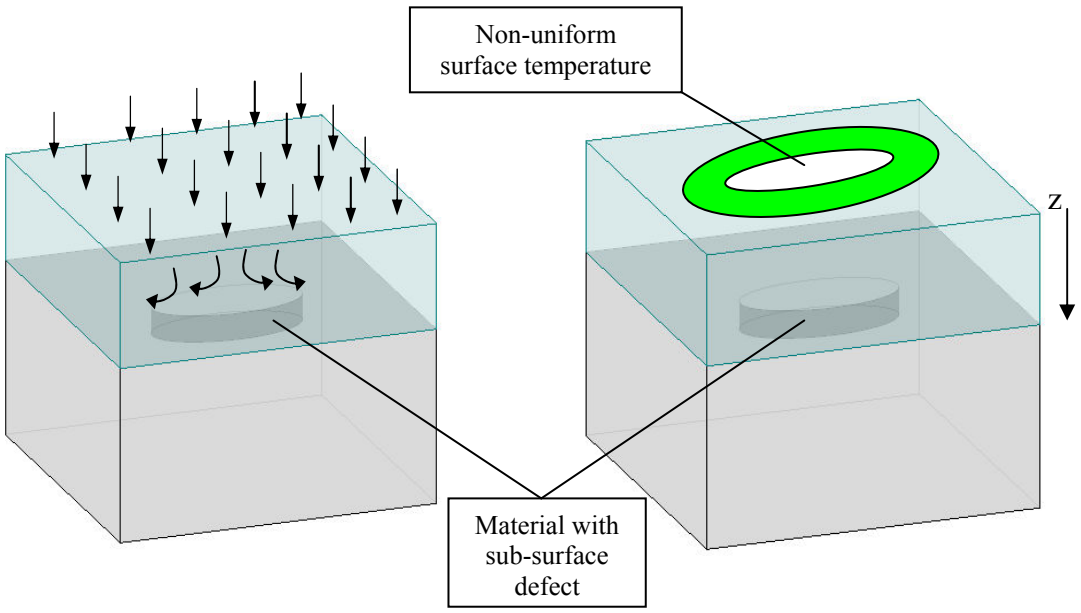

Figure 6-13: Surface temperature variation due to subsurface defects

This scenario is analogous to that of a change in soil type/moisture content

Active IR thermography can be divided into three basic categories: pulsed heating thermography, step heating thermography, and lock-in thermography. The major distinctions are in regards to how the heat is applied to the specimen and the subsequent monitoring of surface temperatures.

Pulsed Heating Thermography

This technique involves applying a short burst of energy to the specimen and then carefully monitoring the temperature decay on the surface. The most common equipment used for applying the heat is high powered photographic or cinematographic flashes. Quartz infrared line lamps or laser heaters can also be used. The objective of the pulse heating is to deposit as much heat on the surface as possible in the shortest period of time. The limiting factor, however, is keeping the surface temperature below any level that may cause damage to the specimen. An example of the type of flash and the generated heat pulse are shown in Figure 6-14.

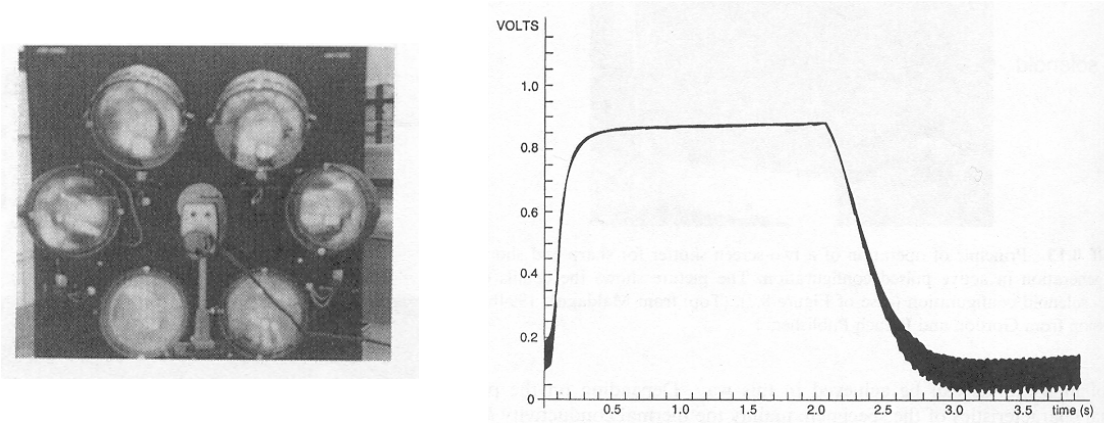

Figure 6-14: Typical lamps used in pulse thermography

Once the heat has been applied to the specimen, surface cooling will proceed as is shown in Figure 6-12. If a defect is encountered, there will be a slight perturbation as shown in Figure 6-15. The first important parameter to note is the time required for the perturbation to begin (t_p). Since the thermal front will travel uniformly through a sound homogeneous medium, t_p is proportional to the defect depth (z_d). The second important parameter to note is the size of the perturbation or observed thermal contrast (ΔT_p). This value is related to the size (in z-direction) and the thermal properties of the defect. Mathematically, the relationships between t_p, ΔT_p, and z_d are as follows:

$$t_p \approx \frac{z_d^{\,2}}{\alpha} \text{ and } \quad \Delta T_p \approx \frac{1}{z_d^{\,3}}$$

where:

t_p = time required for perturbation to begin

z_d = defect depth beneath surface

ΔT_p = Thermal contrast on surface above defect

α = thermal diffusivity of the material

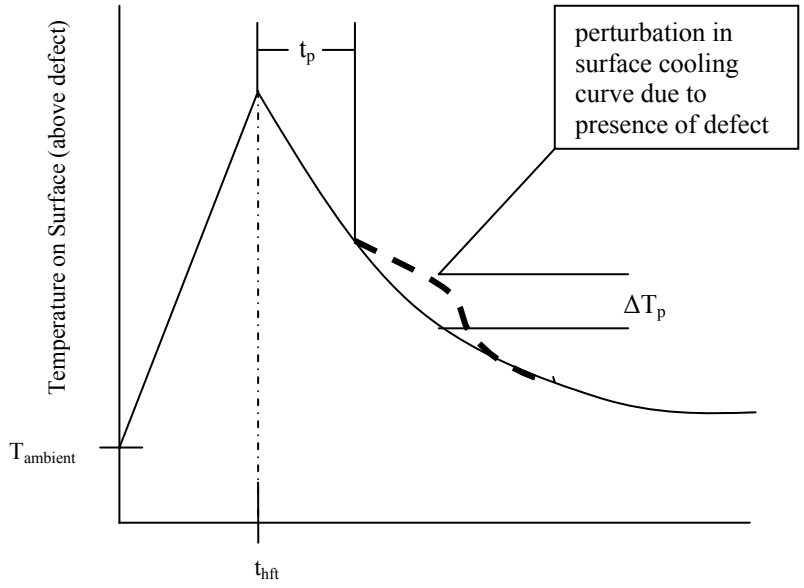

Figure 6-15: Surface temperature above defect vs. time

In order to use this technique, it is first necessary to establish more precise relationships between t_p, ΔT_p, and z_d. These relationships are usually obtained using a combination of analytical and experimental techniques. Finite element or finite difference methods can be useful in helping to determine the optimal heating conditions to maximize the thermal contrast on the surface. It is also possible to gain a better understanding of the maximum depth and maximum size defect that can detected. To better explain this method, Maldague (2001) presents the results of finite difference modeling for graphite epoxy specimens (see Figure 6-16). As long as the basic thermal properties (conductivity, density, and specific heat) are known for a material and a defect type, this type of analysis can be applied to a broad array of problems. Once the basic mechanics of the heat transfer are understand, experimental procedures can be developed to capture the desired results. After the data collection scheme has been validated, it is possible to proceed with "production mode" testing.

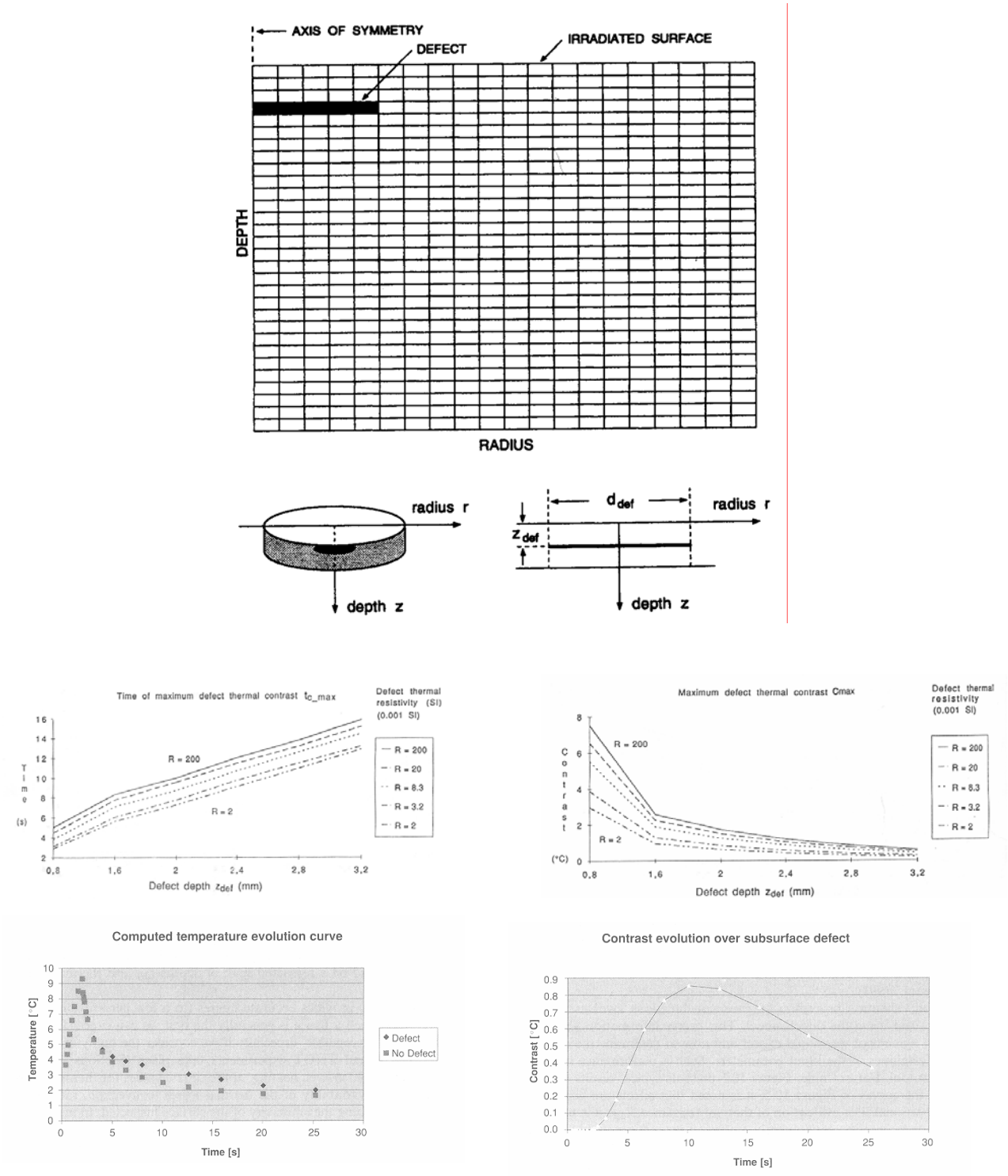

Figure 6-16 : Finite difference model and results for simulated pulsed thermography evaluation of carbon graphite epoxy laminates (from Maldague 2001)

Shepard (2001) reported experimental data from pulsed thermography tests on carbon graphite epoxy laminates with built-in defects. Two sample types were constructed from 30 layers and 10 layers of CFRP pre-impregnated composite material with a thickness of .007 in. and .0135 in, respectively. Defects were simulated by cutting slits of various sizes and depths (measured in number of plies removed) on one side of the sample. The opposite side was then subjected to heat from a 12 kJ flash lamp and the resulting temperature variations on the surface were monitored for around 15 sec. One pixel was selected directly above the defect and another 25x25 pixel area was selected in the region free of defects. Figure 6-17 shows the specimens and the relationship that was observed between the square of defect depth and the time to the first observed thermal contrast.

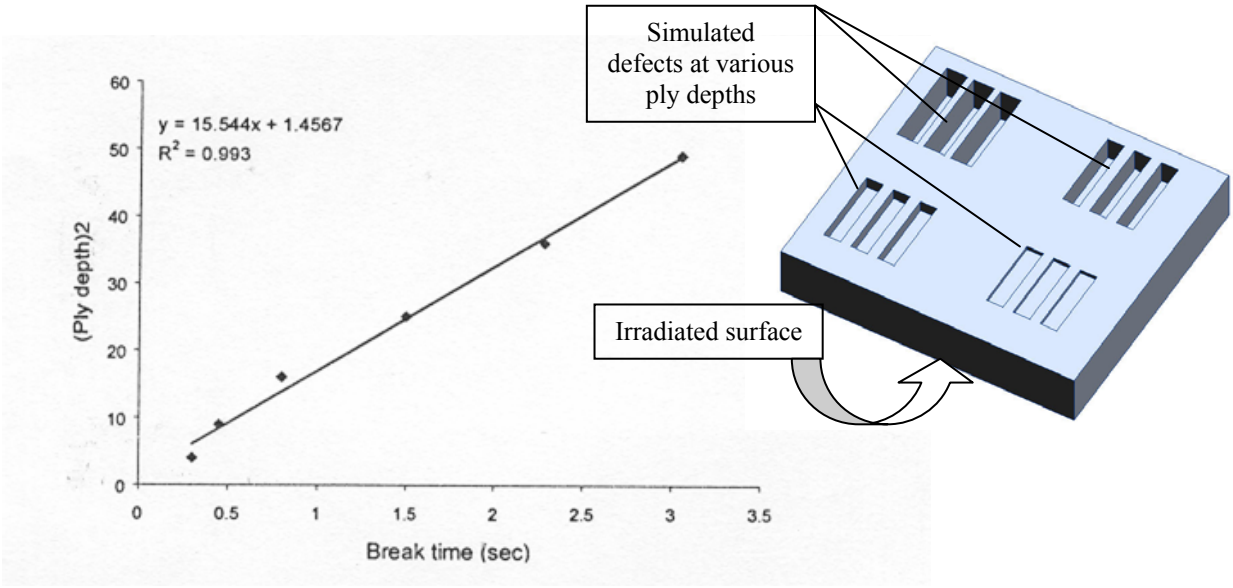

Figure6-17: Experimental results for CFRP composite (Shepard, 2000)

It is important to note that the resulting curves are only applicable to the same material subjected to the same thermal loading. However, once the baseline analysis and experiments have been performed for a particular component, the subsequent "production mode" mode testing becomes very automatic. Predetermined threshold values for thermal contrast can be established and utilized in digital image analysis algorithms. Parts moving off of an assembly line can then be quickly heated by a flash and the resulting thermograms can be analyzed to identify defects.

Step Heating Thermography

The major distinction between step heating and pulsed thermography is that step heating involves a longer duration, low energy heat input. Also, during step heating, the temperature response of the specimen's surface is monitored throughout the heating process. Pulse thermography relies solely on post-heating temperature decay. This technique is better suited for evaluating materials with deeper defects. The concept is illustrated in Figure 6-18.

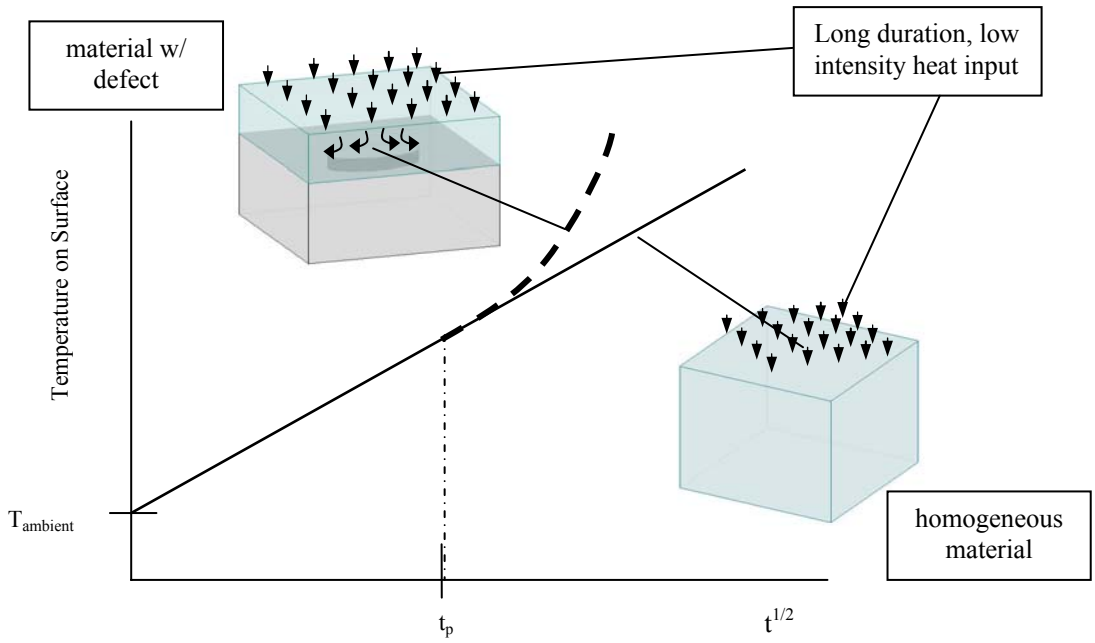

Figure 6-18: Step heating thermography concept

Though the fundamental concept behind the experiment is different from pulsed thermography, the data analysis portion is very similar. Defect depth is related to the time at which a perturbation from the surface heating curve experienced by sound material is observed (t_p). The magnitude of the perturbation also contains information about the defect's thermal properties.

Another area where step heating is commonly employed is the evaluation of coating thickness and coating- substrate bond. Consider a composite material consisting of two distinct layers subjected to a constant heat flux as shown in Figure 6-18. How much interruption the thermal

front feels when it encounters the internal material interface is described by a thermal mismatch factor, Γ:

$$\Gamma = \frac{e_2 - e_1}{e_2 + e_1}$$

where:

e_i = thermal effusivity of material i

$e = \sqrt{k\rho C}$

k = thermal conductivity

ρ = density

C = specific heat

If the thermal effusivity of e_2 is much less than that of e_1 (as would be the case for a solid material interfaced with an air void), the value of Γ approaches -1. This situation would result in the presence of a "hot spot" above the defect. If the thermal effusivity of e_2 is much greater than that of e_1 (as would be the case for a ceramic coating on top of a metal), the value of Γ approaches +1. This situation would result in a decreasing rate of increase for the surface temperature once the thermal front reaches the interface. The other quantity that will effect the rate of change of surface temperature is the thickness of layer 1.

A very interesting experiment was presented in Maldague, 2001. Step heating thermography was applied to a 1 mm thick fiberglass-epoxy coating that was overlaid onto several different materials. The resulting temperature evolution on the surface of the specimen varied greatly between the regions directly above the various materials (see Figure 6-19). As was the case with pulse thermography, the step heating thermography technique is capable of providing information about defect depth and its thermal properties. If the type of defect that is commonly encountered in a particular situation can be characterized beforehand and its thermal signature established during experiments, the application of the procedure can be easily automated.

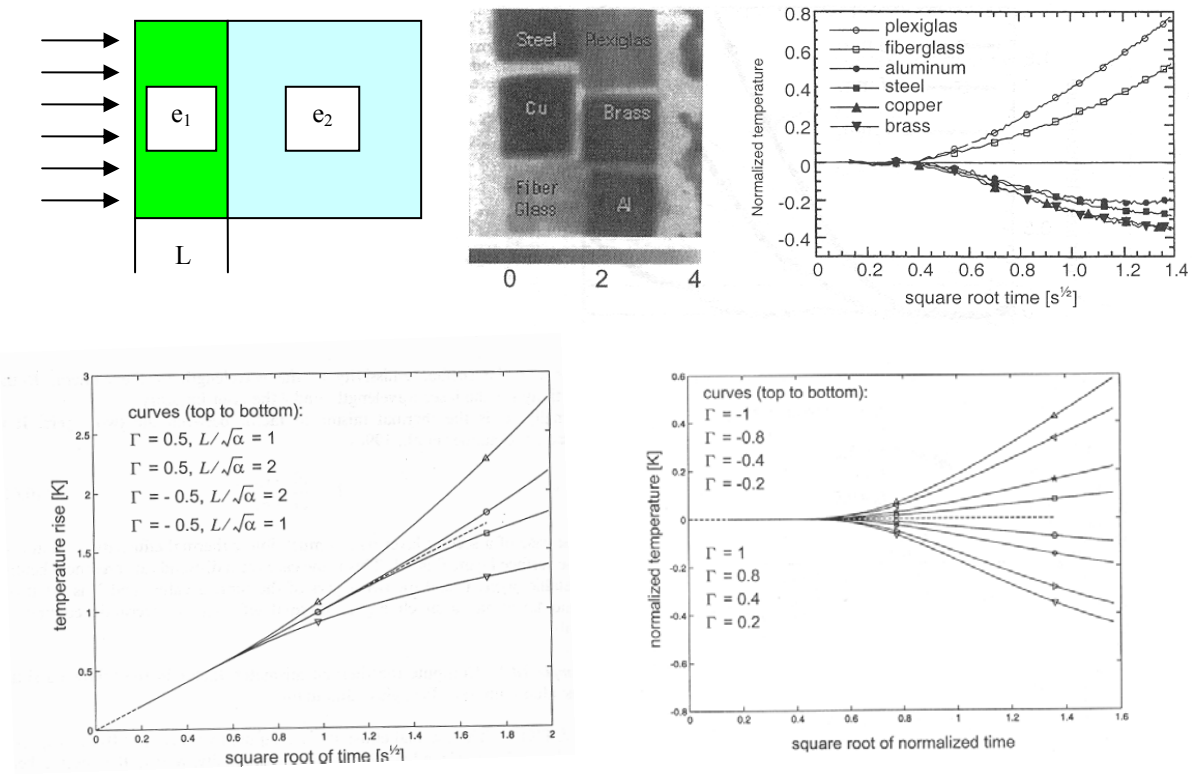

Figure 6-19: Effect of surface coating thickness and substrate effusivities on surface temperature for step heating thermography (Maldague, 2001)

While the pulse heating is not amenable to geotechnical investigations, the step heating might be a viable technique. If a particular area is identified in an over flight, then the area could then be tested using an IR camera set up on a tripod mounted on a CPT rig for example. The camera would be set to take images every 5 minutes during morning and throughout the day as the soil heats up. This is analogous to step heating of the test specimen. By observing any perturbations that may result from unequal heating could verify the existence of subsurface anomalies.

Lock-in thermography

One final form of active thermography is termed lock-in thermography. One of the major shortcomings of all IR thermography techniques is that materials with different emissivity values will appear as having different temperatures in a thermal image even if the temperatures are the same. Another shortcoming, especially in field applications, is the difficulty encountered in

applying a uniform heat flux to a surface. The combination of these effects can result in thermographs that are difficult to interpret and may contain false information.

Lock-in thermography seeks to remedy this phenomenon by applying a modulated heat source. Both the heat source signal and the resulting local response on the surface of the specimen are fed through a lock-in amplifier capable of monitoring the magnitude and the phase of the response (Carlomagno, 2001).

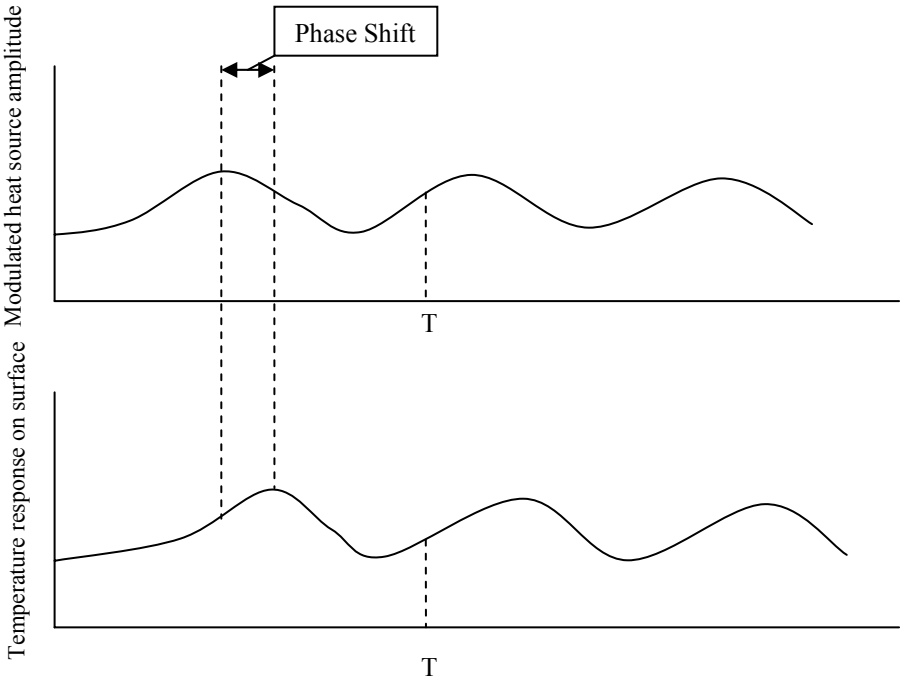

Figure 6-20: Lock-in thermography concept

Rather than monitoring the temperature data at every pixel in a thermograph, Lock-in thermography focuses on the phase shift of every pixel. The advantage of this scheme is that the value of the phase shift is relatively independent of the surface temperature and the surface emissivity. Phase shift will, however, be affected by the presence of subsurface defects. This technique results in "cleaner" thermal images and is also capable of detecting subsurface defects at greater depths than can be obtained with pulse or step heating IRT. Figure 6-21 (a) shows a standard thermal image indicating the presence of subsurface defects. Figure 6-21 (b) shows the

same image except that each pixel contains the phase shift data (after some signal processing) instead of the temperature.

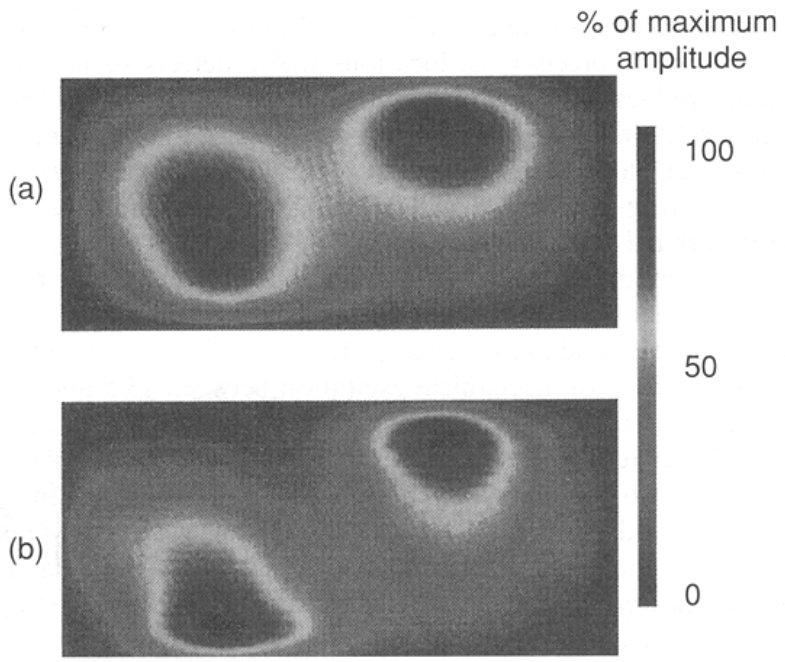

Figure 6-21: Comparison of thermal images created by step heating and lock-in thermography (Maldague, 2001)

Preliminary sinkhole identification using IR thermography

To see if an IR signature could be used to locate areas of geotechnical interest, i.e., possible sinkholes, several flights were performed during 2005 using a ThermaCam SC 2000. The specifications for it are provided below.

SPECIFICATIONS

THERMAL

Field of view/min focus distance	24°x18° /0.3m
Spatial resolution (IFOV)	1.3 mrad
Thermal sensitivity	0.1°C at 30°C
Image frequency	50/60 Hz non-interlaced
Focus	Automatic or manual
Electronic zoom function	4X continuous
Detector type	Focal Plane Array (FPA), uncooled microbolometer 320 x 240 pixels
Spectral range	7.5 to 13μm
Digital image enhancement	Standard

VISUAL

Built-in digital video	640 x 480 pixels, black and white, or full color
Remote-control options	Remote focus (standard), RS-232 (standard) Remote control panel (optional)
Operating temperature range	-15°C to +50°C (5°F to 122°F)
Storage temperature range	-40°C to +70°C (-40°F to 158°F)
Humidity	Operating and storage 10% to 95%, non-condensing
Encapsulation	IP 54 IEC 359 (metal casing)
Shock	Operational: 25G, IEC 68-2-29
Vibration	Operational: 2G, IEC 68-2-6
Type	High capacity PC-Card, ATA compatible (160MB min)
File formats - THERMAL 1	4-bit radiometric IR digital image (IMG), includes header file with all radiometric data 8-bit standard bitmap (BMP), image only or image w/screen graphics. Every image stored in both formats
File formats - VISUAL	Standard bitmap (BMP); visual images(s) linked with corresponding thermal images(s)
Voice annotation of images	30 sec. of digital voice “clip” stored together with the image
Text annotation of images	Predefined text selected and stored together

	with the image
Field of view/min focus distance	7°x5.3°/6m • 12°x 9°/2m • 45°x 34°/0.2m • 80°x 60°/0.2m • 200µm close-up (64mm x 48mm/150mm) •106µm close-up (34mm x 25mm/80mm)
Lens identification	Automatic
Type	Internal rechargeable nickel metal hydride (NiMH) battery, field replaceable
Operating time	2 hours continuous operation
Charging system	4 bay intelligent charger 110/220 volt
Temperature range	-40°C to +1500°C (-40°F to 2732°F) Up to +2000°C (3632°F), optional
Accuracy	±2°C, ±2%
Atmospheric transmission correction	Automatic, based on inputs for distance, atmospheric temperature and relative humidity
Optics transmission correction	Automatic, based on signals from 5 internal sensors
Automatic emissivity correction	Variable from 0.1 to 1.0 or select from listings in pre-defined materials list

The area targeted for over flight was located in High Springs Florida. Based on the ALSM Laser data, this area is rich in surface expressions, most notably sinkholes. On the following page is the USGS quad map of the area with the laser DEM (Digital Elevation Model) shown immediately thereafter.

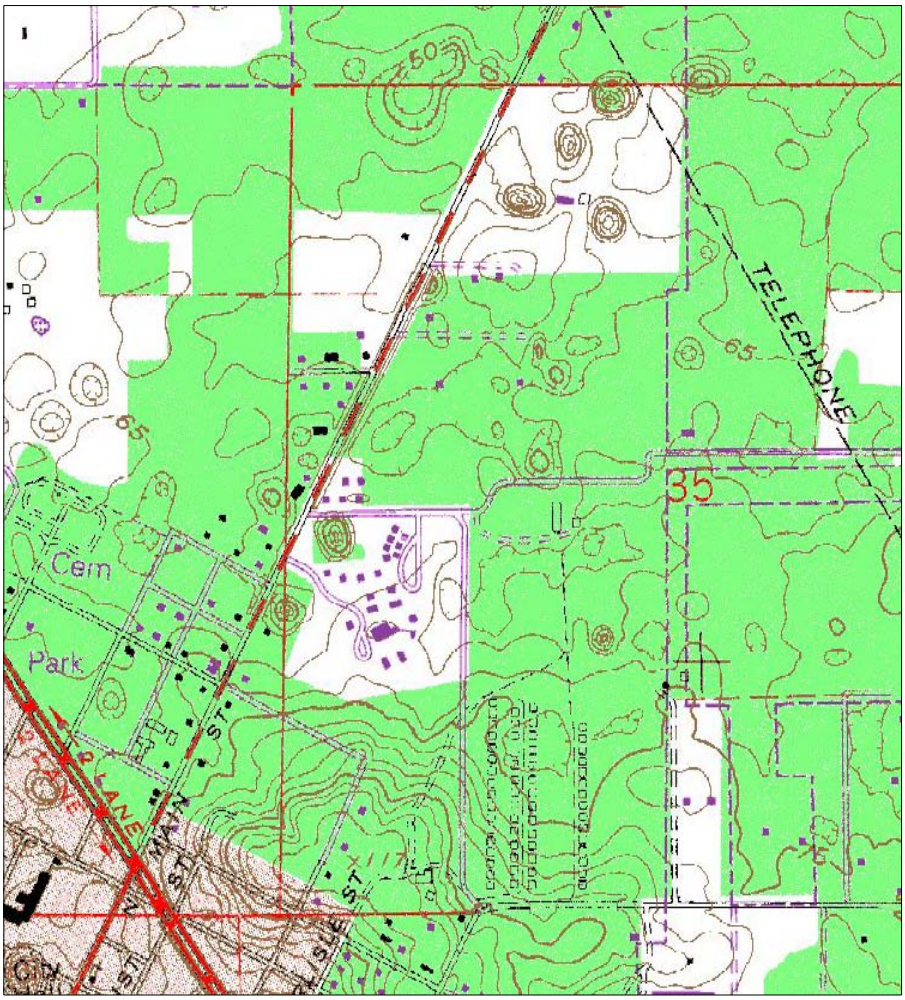

Figure 6-22. High Springs Florida Quad Map

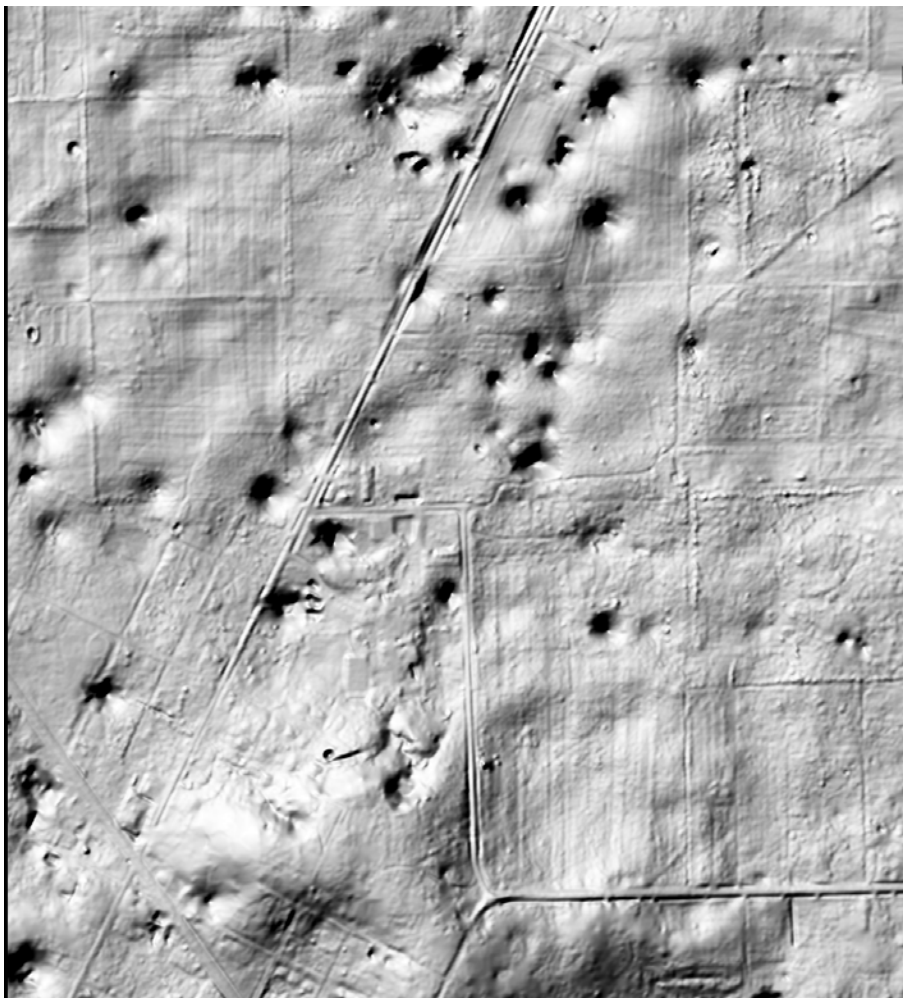

Figure 6-23. ALSM Bare earth DTM

Of particular interest are the numerous depressions located in the upper area. This area was reflown several times during both warm and cool days.

Images Taken on 3/13/05 (Warm Day)

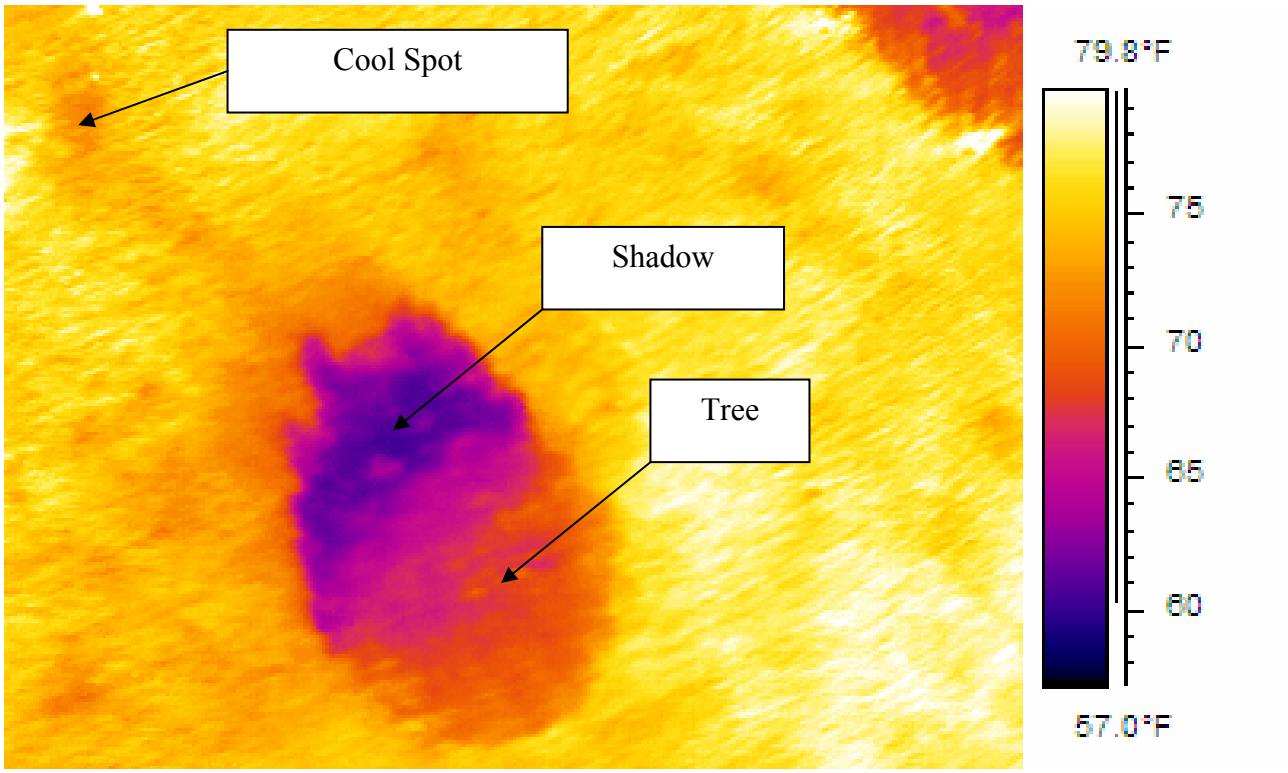

Figure 6-24. IR Results

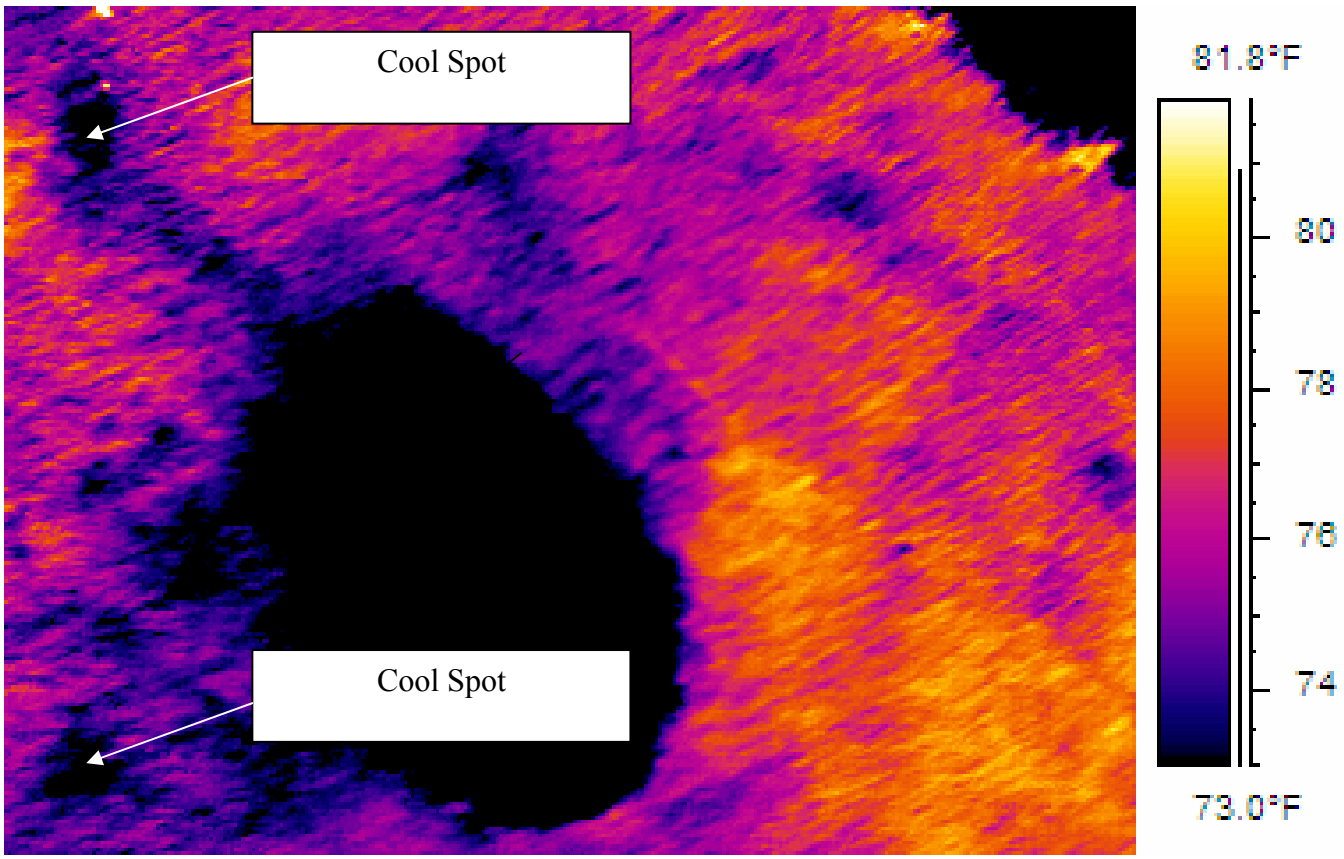

Figure 6-26: Images Taken on 12/20/04 (Cold Day)

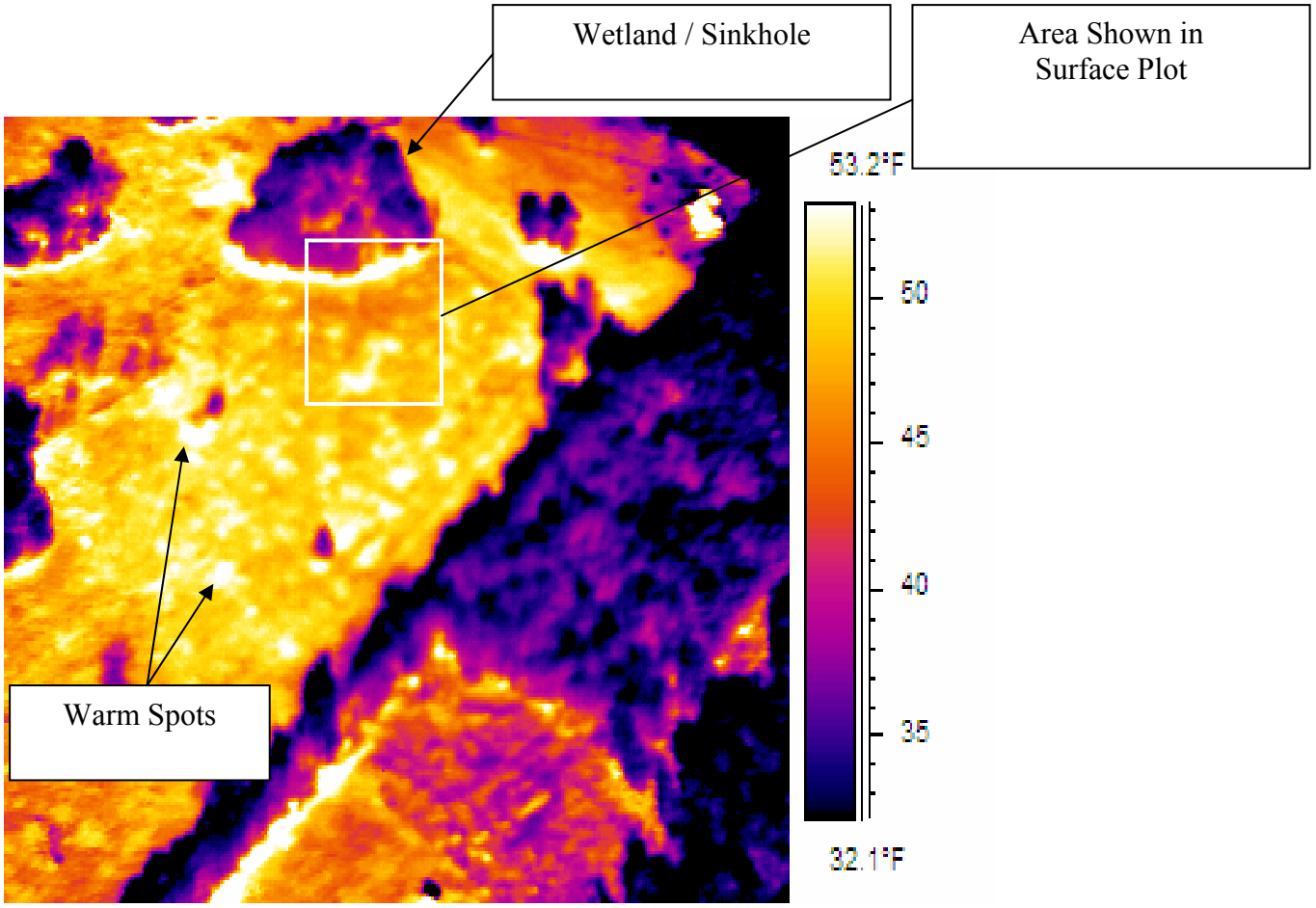

Figure 6-27 Surface Plot of Temperature adjacent to wetland/sinkhole

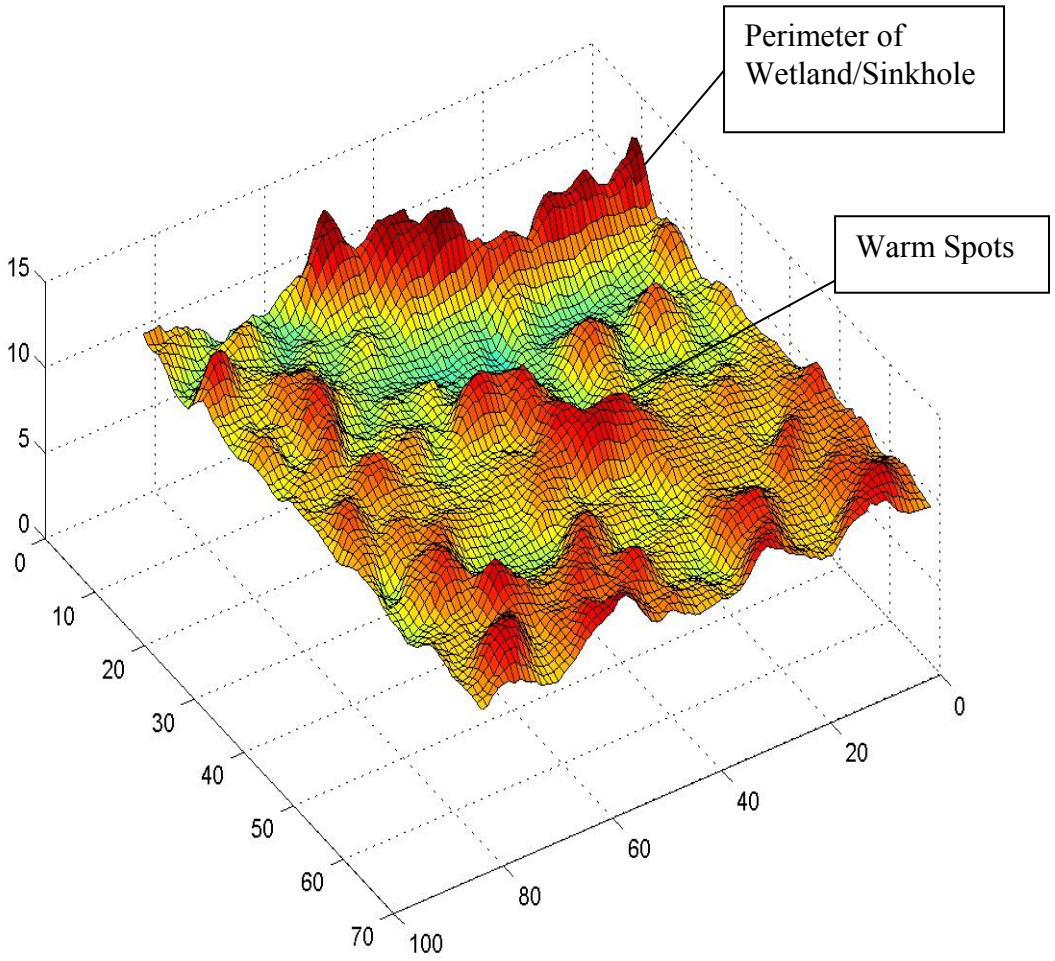

Figure 6-28: Temperature in degrees C and Length in meters.

Conclusions

IR thermography appears to possess great potential as a non-destructive evaluation technique civil engineering . Research that has already been conducted by CE material researchers with regards to advanced composite materials and hence can be quickly adapted to CFRP strengthened civil infrastructure. There is, however, still a need for conducting baseline experiments to establish thermal signatures with a high degree of confidence. Field application will also prove difficult (especially for active thermography), so new techniques must evolve before widespread use becomes feasible.

The exciting feature of this test method is that as long as materials have different thermal properties based on heating/cooling, the only limitation to using IR thermography is the current level of IRT technology. As detectors become more accurate and further advances are made in the realm of data acquisition and image processing, new test procedures are almost certain to evolve. This should improve the capabilities of correlating topographic features to subsurface conditions, vis-à-vis sinkhole detection.

As seen in the previous thermographs, it appears that IR technology can be used to assess potential surface anomalies. While more data collection/analysis remains, it is encouraging that this cost effective technique ($40K versus $1.5M for ALSM) has shown promise. Hence, while this research project has concluded, the authors are continuing to test the methodology for FDOT. Due to the accessibility of the IR camera as well as two aircraft (Cessna 172 and RAF2000 Gyroplane), numerous data collection flights are scheduled for 2006. This will result in a Update Report to FDOT for distribution to the various Districts.

References

ASTM C1060-90, “Thermographic Inspection of Insulation Installations in Envelope Cavities of Frame Buildings”, Annual Book of ASTM Standards, v 04.06.

ASTM C1153-97, “Location of Wet Insulation in Roofing Systems Using Infrared Imaging”, Annual Book of ASTM Standards, v 04.06.

ASTM C1371-97, “Determination of Emittance of Materials Near Room Temperature Using Portable Emissometers”, Annual Book of ASTM Standards, v 04.06.

ASTM D4788-88, “Detecting Delaminations in Bridge Decks Using Infrared Thermography”, Annual Book of ASTM Standards, v 04.03.

Carlomagno G and Meola C, “Infrared Thermography in the Restoration of Cultured Properties”, Proceedings of SPIE, v 4360, 2001, p 203-216.

Maldague X., Theory and Practice of Infrared Technology for Nondestructive Testing, John Wiley and Sons, Inc., 2001.

Sakagami T, “Development of a New Diagnosis Method for Caries in Human Teeth Based on Thermal Images Under Pulsed Heating”, Proceedings of SPIE, v 4360, 2001, p 504-510.

Shepard S, “Quantitative Infrared Defect Detection in Composite Aerospace Structures”, International SAMPE Symposium and Exhibition (Proceedings), v 45, 2000.

InnovMetric, “PolyWorks,” *http://links.umen.ca/innovmetric/english/home.html*, accessed June 2004.

Optech, “ILRIS-3D Benefits and Features,” *http://www.optech.on.ca/ilrisfeatbens.htm*, accessed June 2004.

Applanix, *POSProc User Manual Version 2.1*, Applanix Corporation, Revision: 2, March 1997.

Carter, W.R.; R. Shrestha; G. Tuell; D. Bloomquist; and M. Sartori, “Airborne Laser Swath Mapping Shines New Light on Earth’s Topography,” *Eos, Transactions, American Geophysical Union,* Vol. 82, No. 46, Nov. 2001, Pages: 549-555, 2001.

Golden Software, *Surfer Version 8.03 – User Guide*, Golden Software, Inc., May 2003.

Mader, G.L., "Rapid Static and Kinematic Global Positioning System Solutions Using the Ambiguity Function Technique," *Journal of Geophysical Research*, 97, 3271-3283, 1992.

NOAA, “National Geodetic Survey – What is CORS?” *http://www.ngs.noaa.gov/CORS/cors-data.html*, accessed June 2004.

NOAA, “OPUS – What is OPUS?” *http://www.ngs.noaa.gov/OPUS/What_is_OPUS.html,* accessed June 2004.

Optech, *REALM Survey Suite Data Processing Manual - ALTM,* Optech Inc., Document No.: 195-090-06, Release: 3.1, Oct. 2002.